



US 20180323016A1

(19) **United States**(12) **Patent Application Publication****El-Kady et al.**(10) **Pub. No.: US 2018/0323016 A1**(43) **Pub. Date: Nov. 8, 2018**(54) **CAPACITOR WITH ELECTRODES MADE OF AN INTERCONNECTED CORRUGATED CARBON-BASED NETWORK**(71) Applicant: **The Regents of the University of California**, Oakland, CA (US)(72) Inventors: **Maher F. El-Kady**, Los Angeles, CA (US); **Veronica A. Strong**, Portland, OR (US); **Richard B. Kaner**, Pacific Palisades, CA (US)(21) Appl. No.: **16/029,930**(22) Filed: **Jul. 9, 2018****Related U.S. Application Data**

(63) Continuation of application No. 15/612,405, filed on Jun. 2, 2017, which is a continuation of application No. 14/382,463, filed on Sep. 2, 2014, now Pat. No. 9,779,884, filed as application No. PCT/US13/29022 on Mar. 5, 2013.

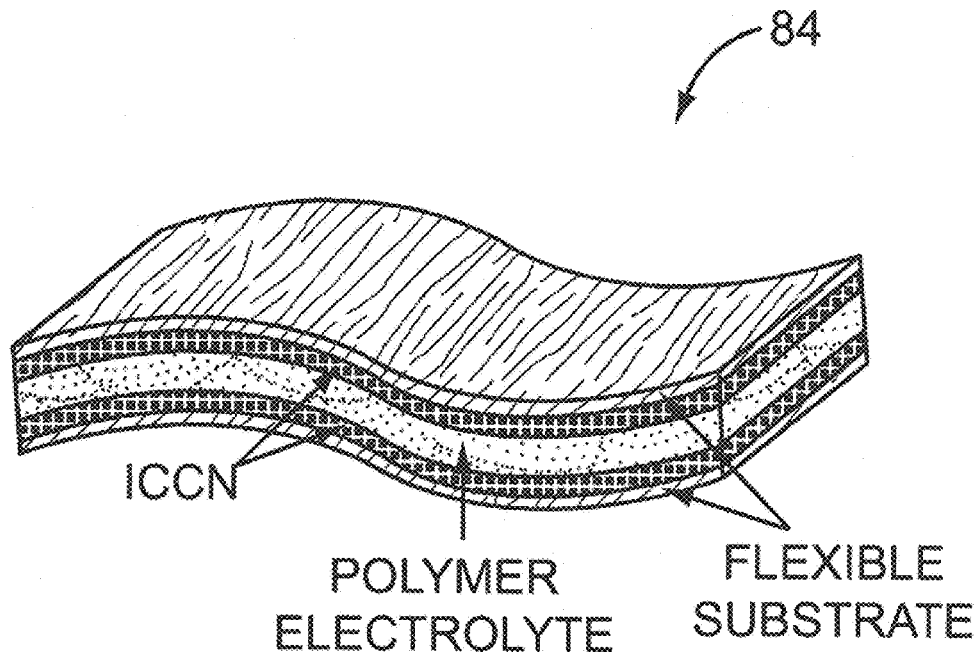
(60) Provisional application No. 61/606,637, filed on Mar. 5, 2012, provisional application No. 61/757,077, filed on Jan. 25, 2013.

Publication Classification(51) **Int. Cl.****H01G 11/32** (2006.01)**H01G 11/36** (2006.01)(52) **U.S. Cl.****CPC** **H01G 11/32** (2013.01); **H01G 11/36** (2013.01); **H01G 11/56** (2013.01)

(57)

ABSTRACT

Capacitors having electrodes made of interconnected corrugated carbon-based networks (ICCNs) are disclosed. The ICCN electrodes have properties that include high surface area and high electrical conductivity. Moreover, the electrodes are fabricated into an interdigital planar geometry with dimensions that range down to a sub-micron scale. As such, micro-supercapacitors employing ICCN electrodes are fabricated on flexible substrates for realizing flexible electronics and on-chip applications that can be integrated with micro-electromechanical systems (MEMS) technology and complementary metal oxide semiconductor technology in a single chip. In addition, capacitors fabricated of ICCN electrodes that sandwich an ion porous separator realize relatively thin and flexible supercapacitors that provide compact and lightweight yet high density energy storage for scalable applications.



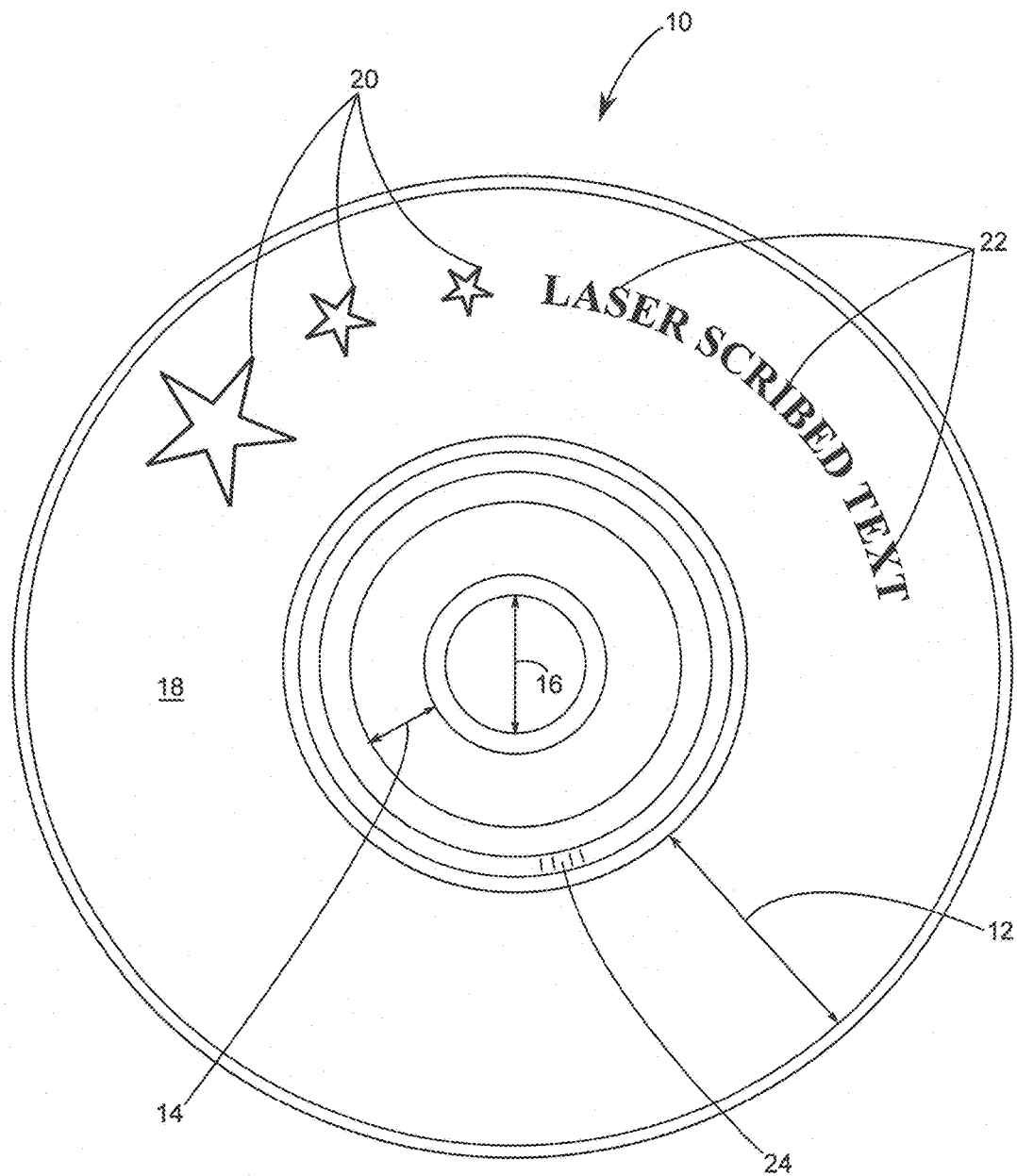


FIG. 1
(PRIOR ART)

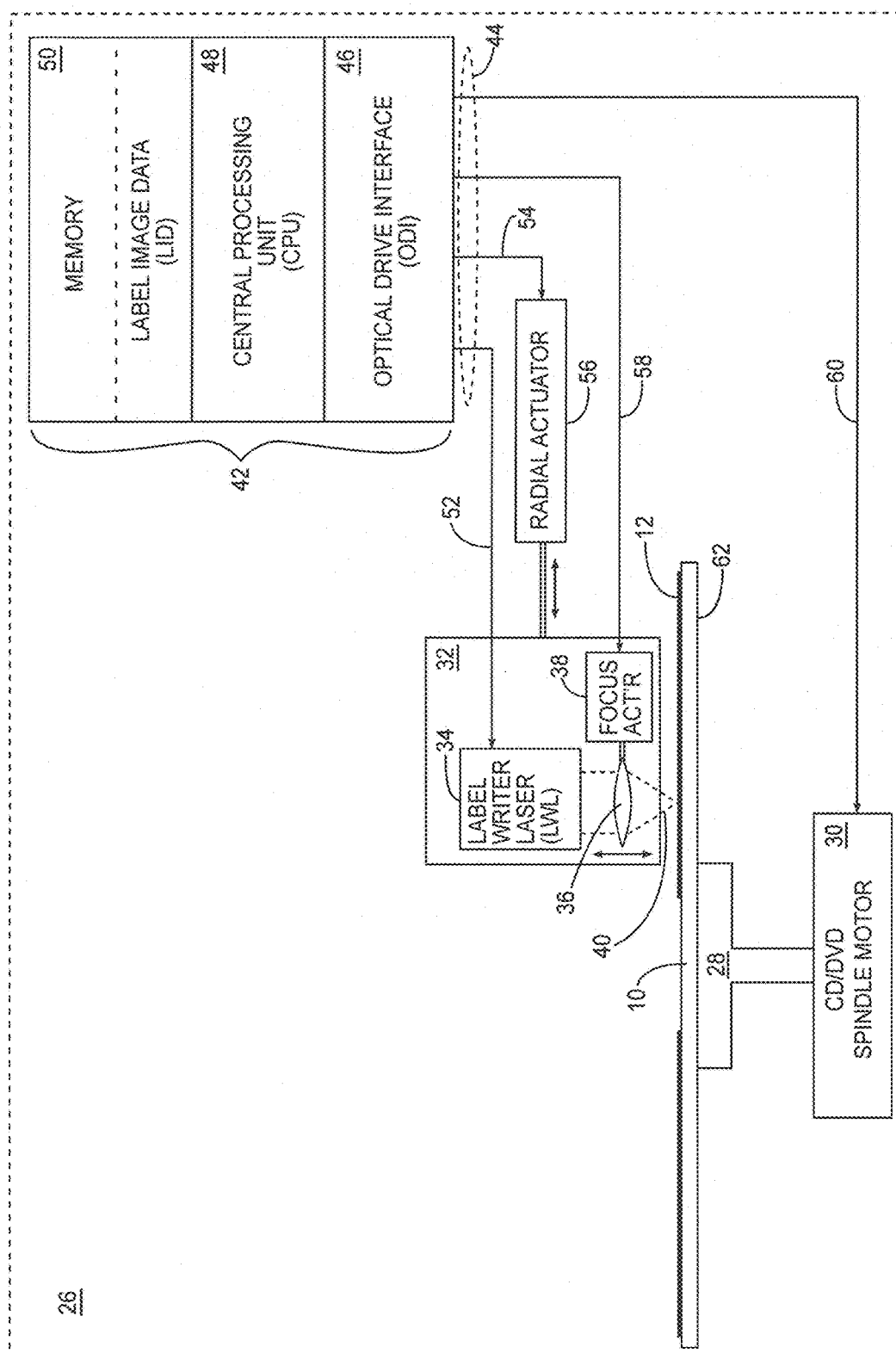


FIG. 2
(PRIOR ART)

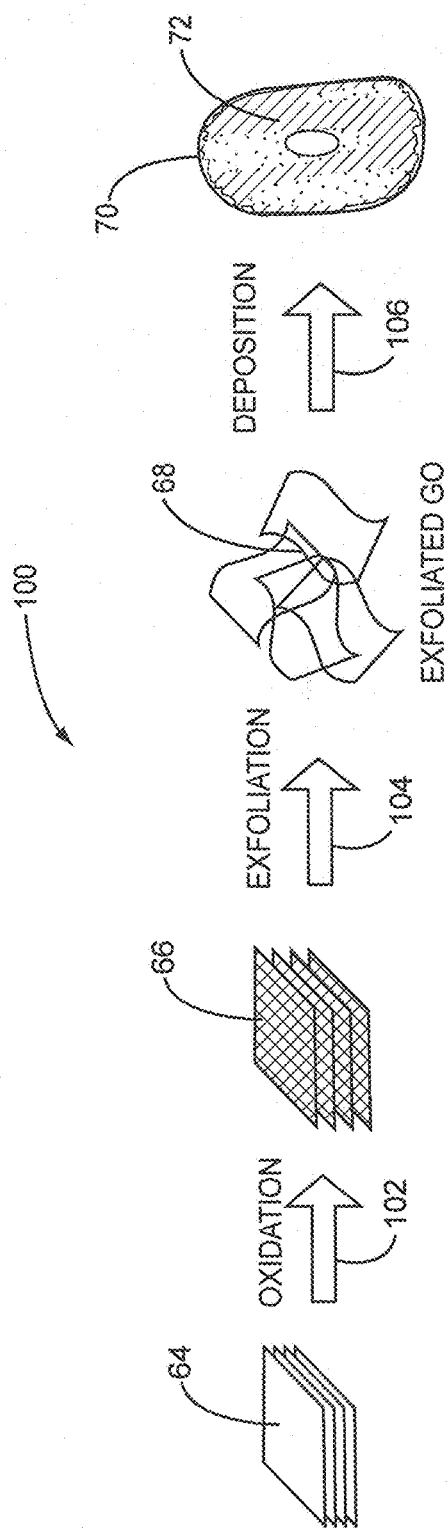


FIG. 3

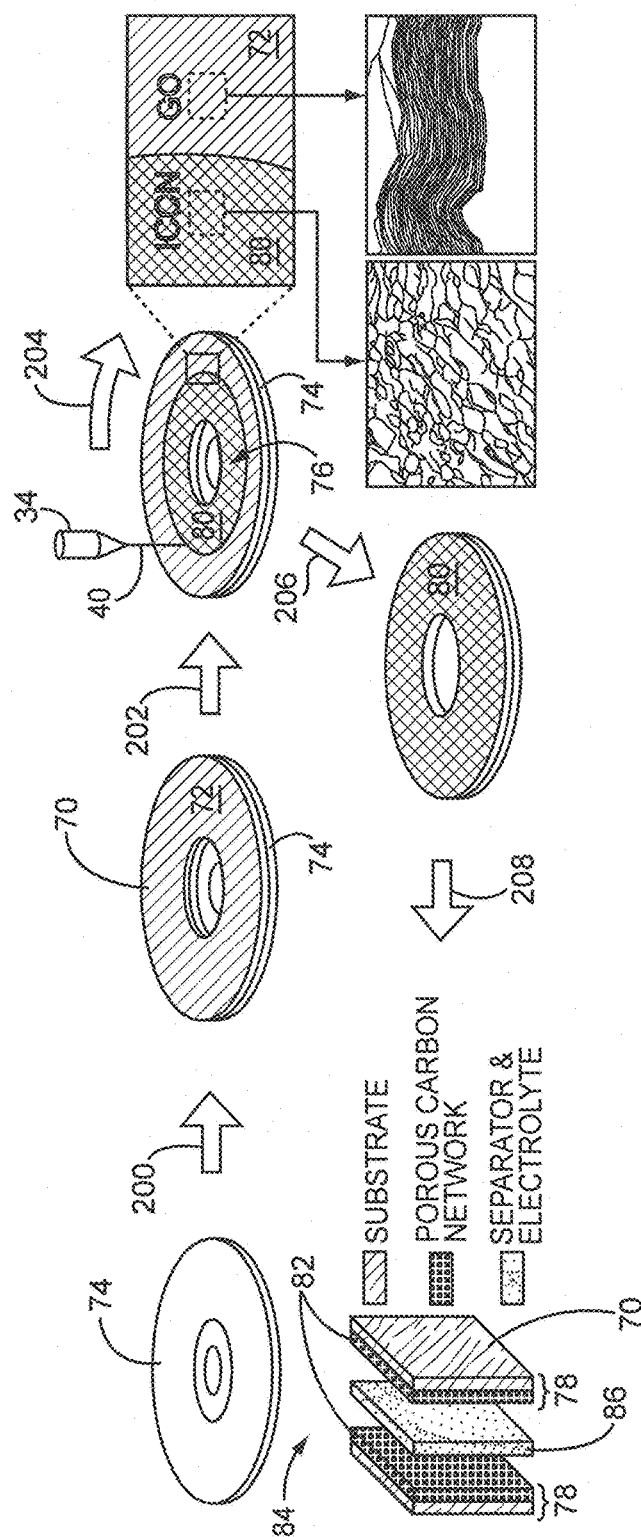


FIG. 4

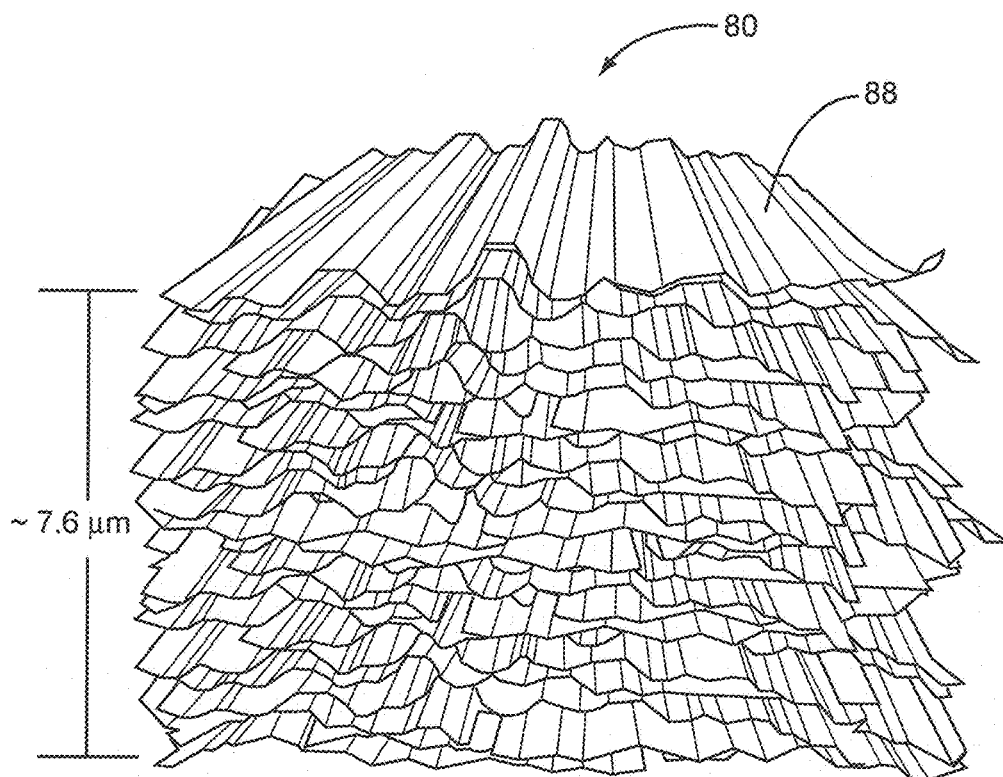
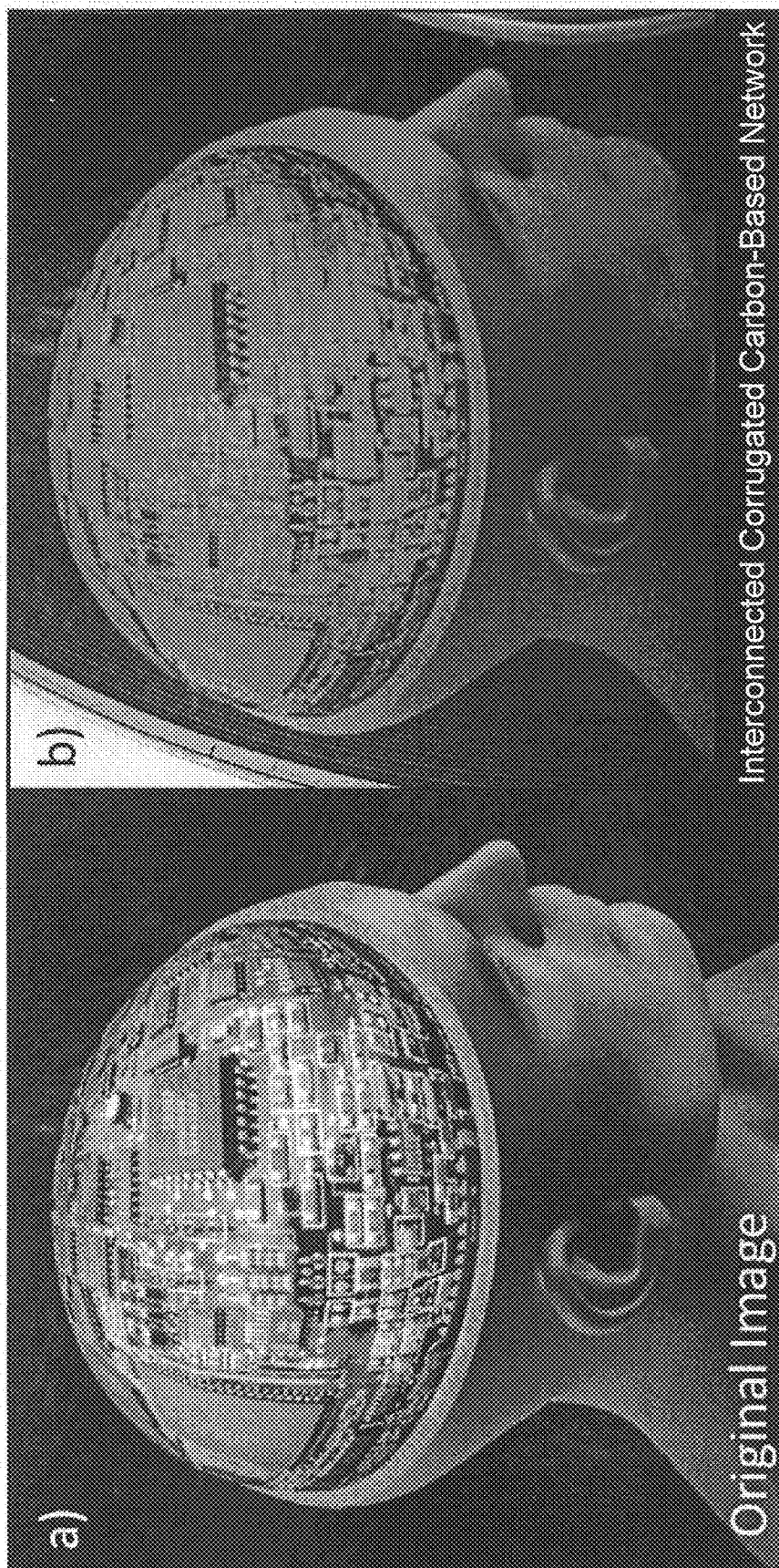


FIG. 5



Original Image

Interconnected Corrugated Carbon-Based Network

FIG. 6A

FIG. 6B

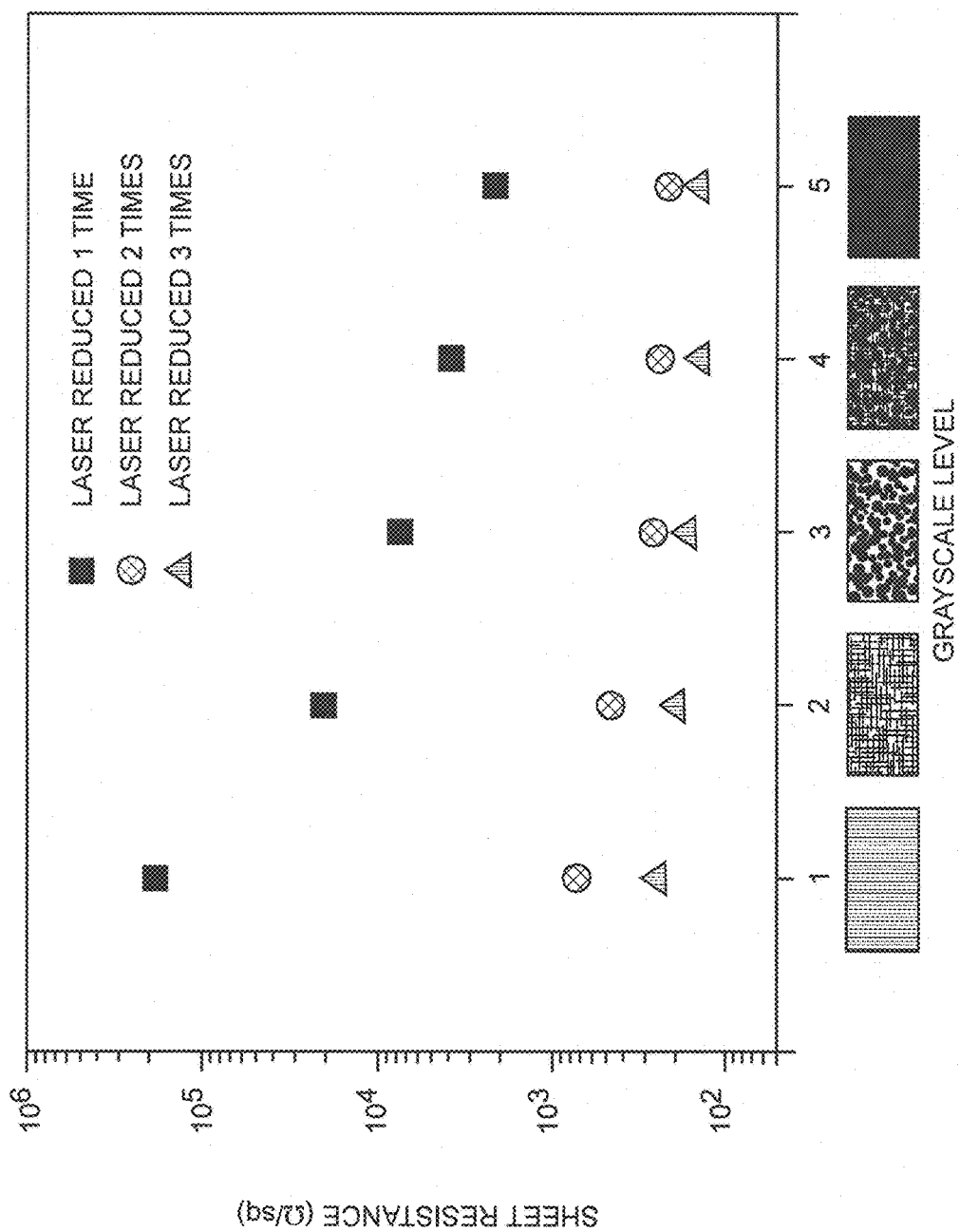


FIG. 7

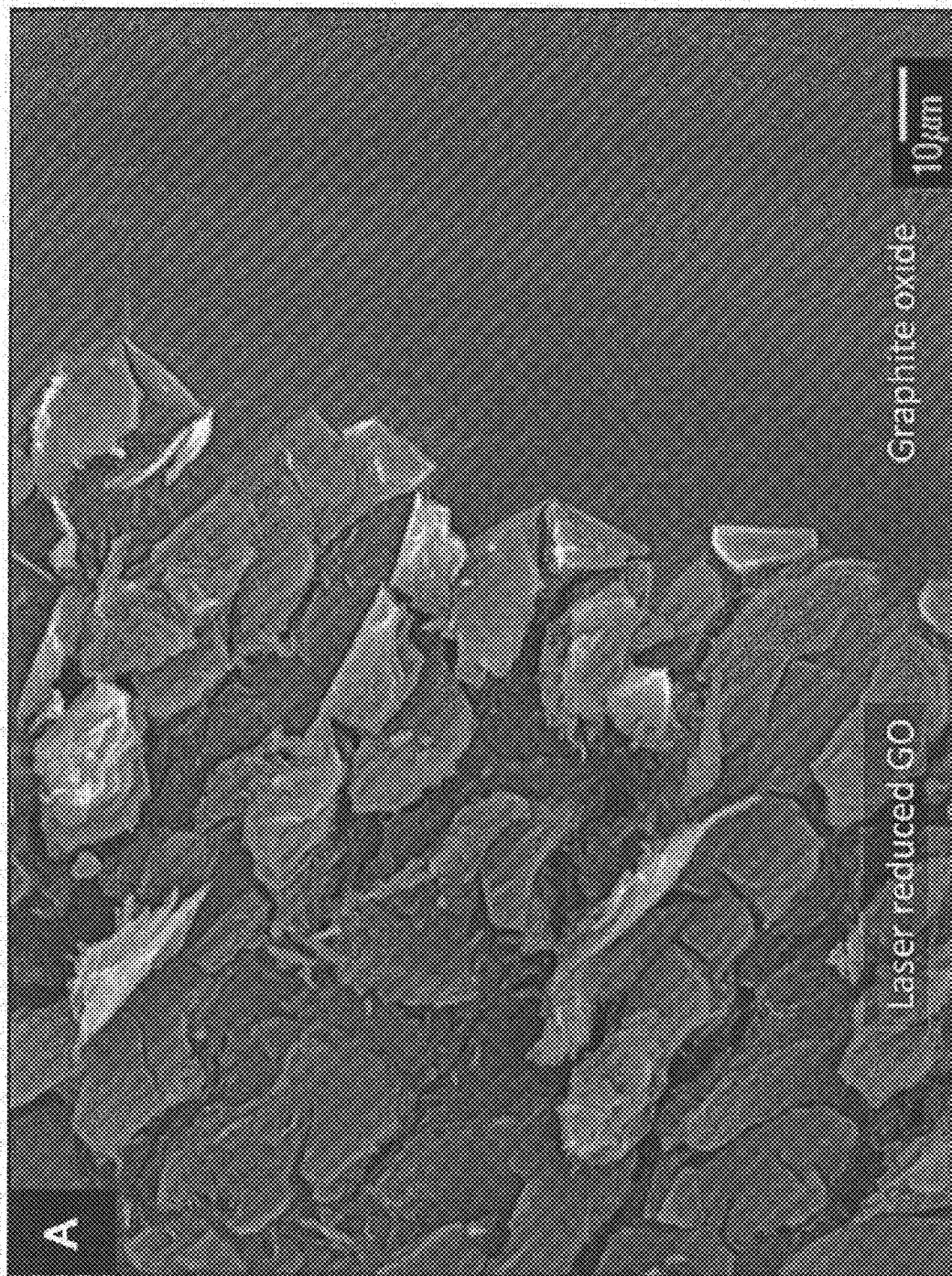


FIG. 8A

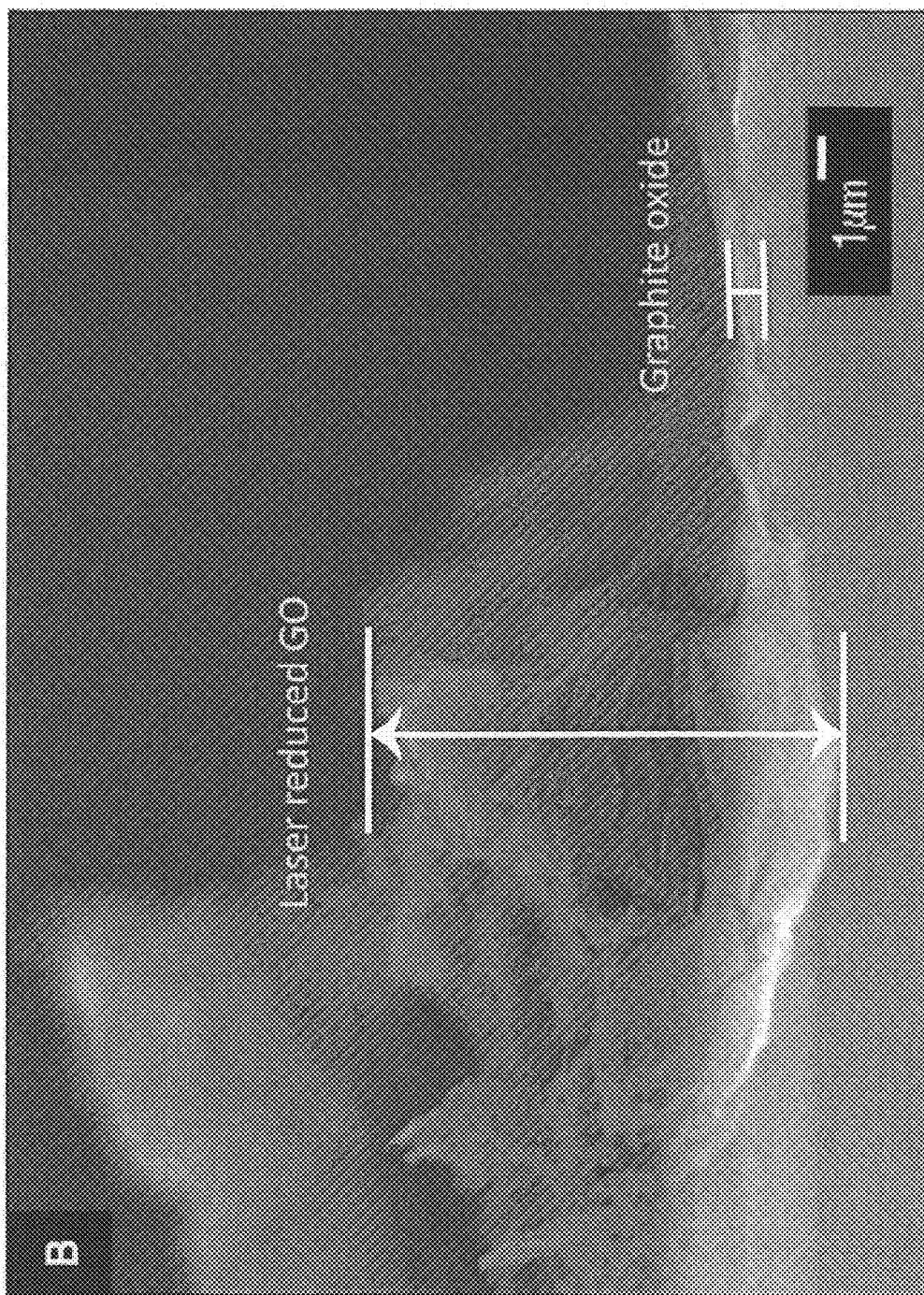


FIG. 8B

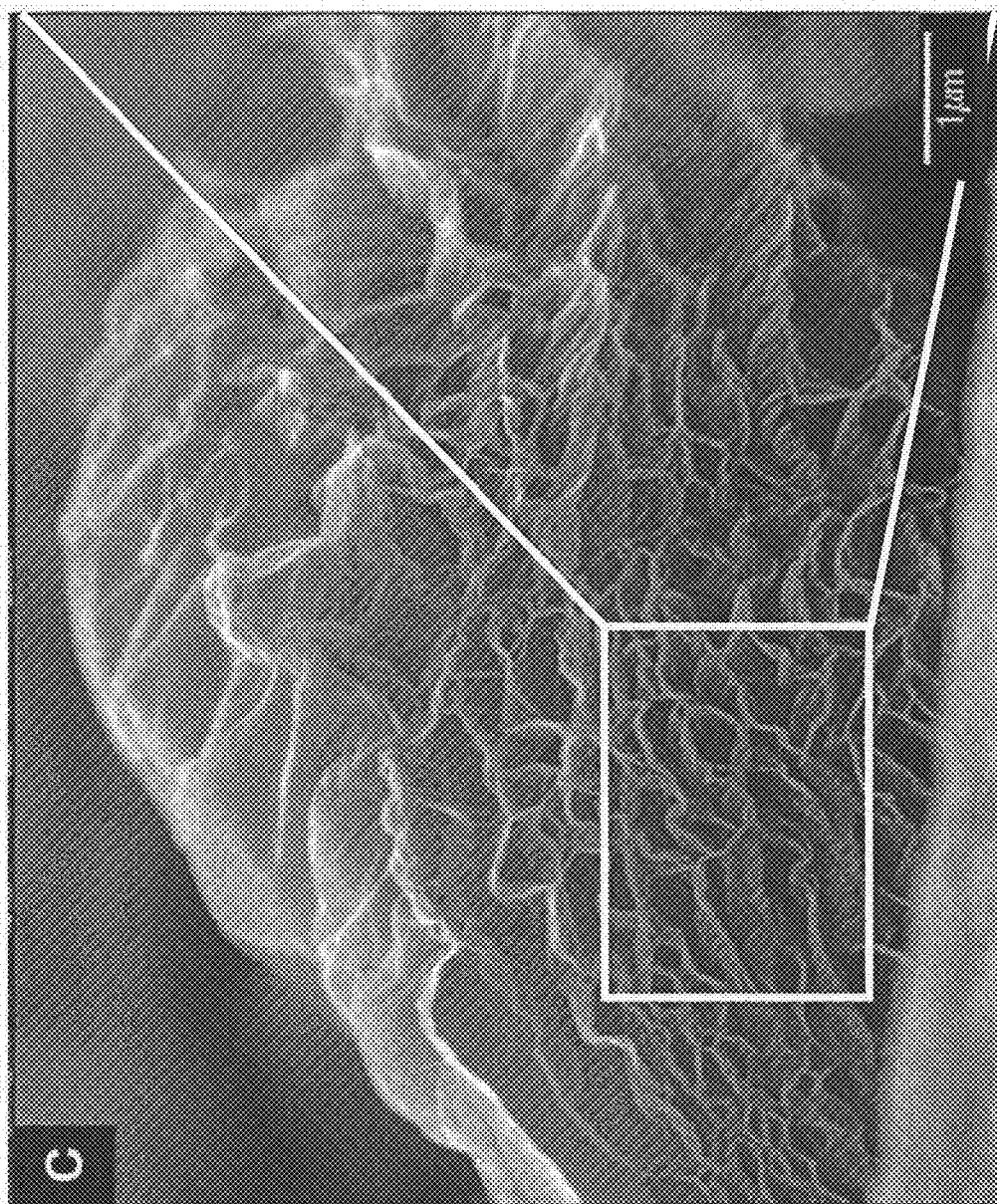


FIG. 8C

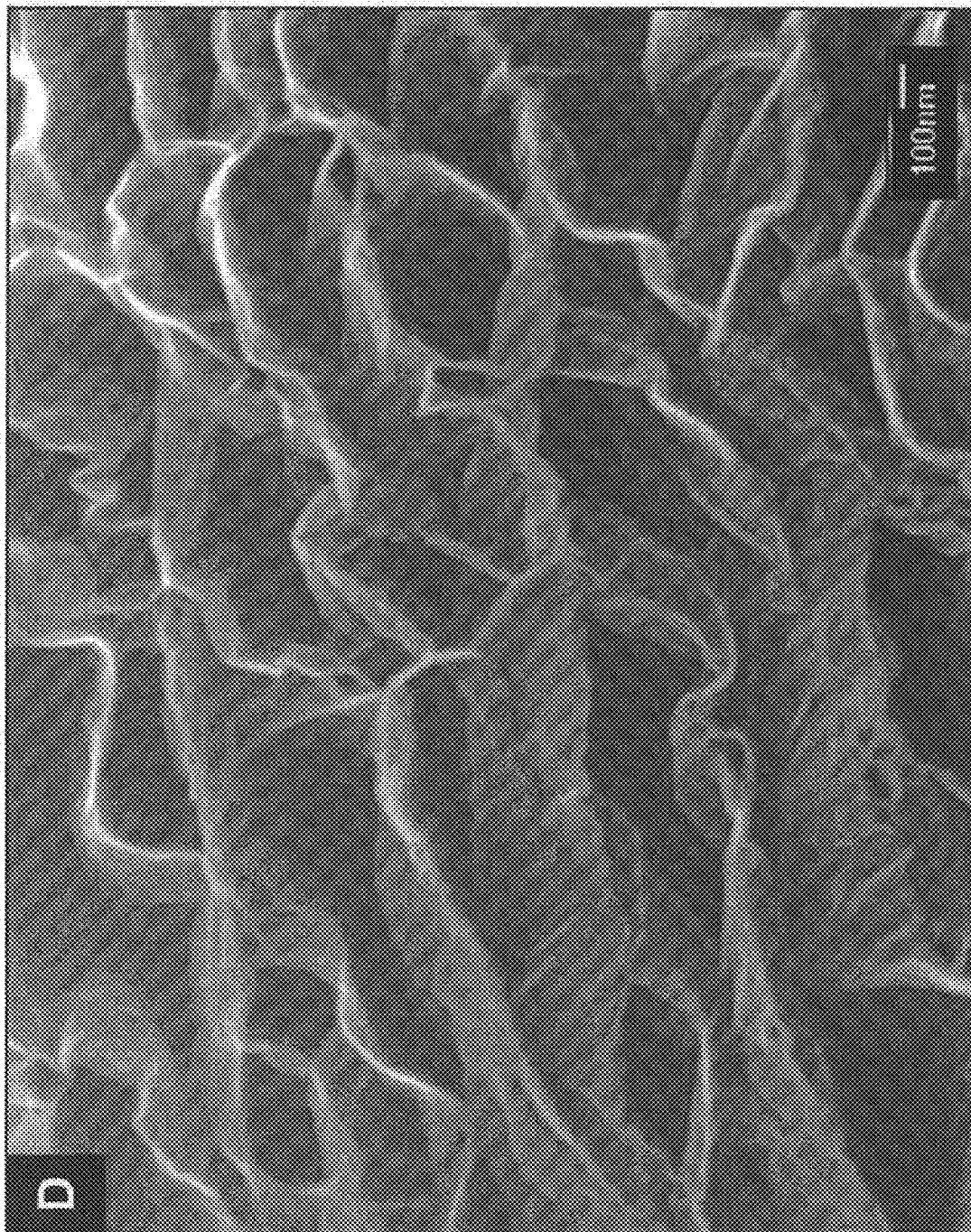


FIG. 8D

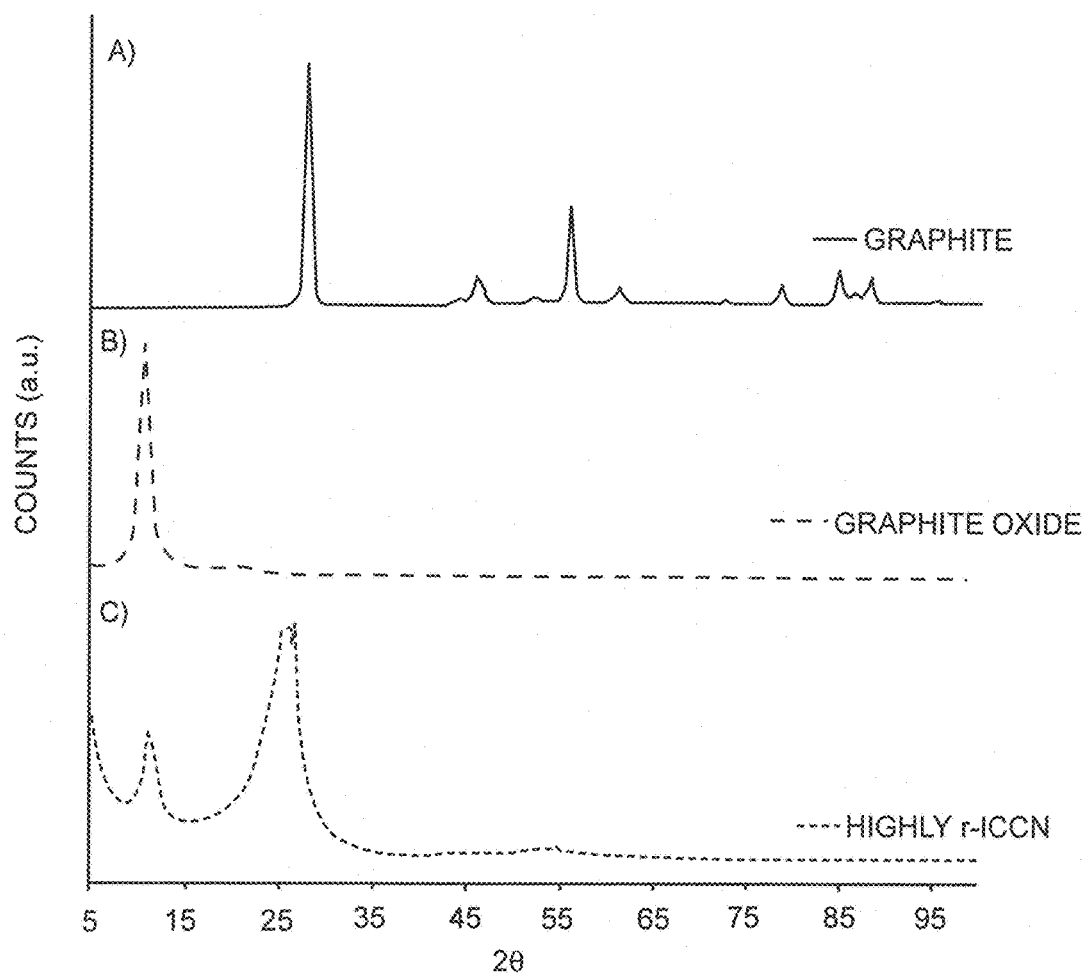


FIG. 9

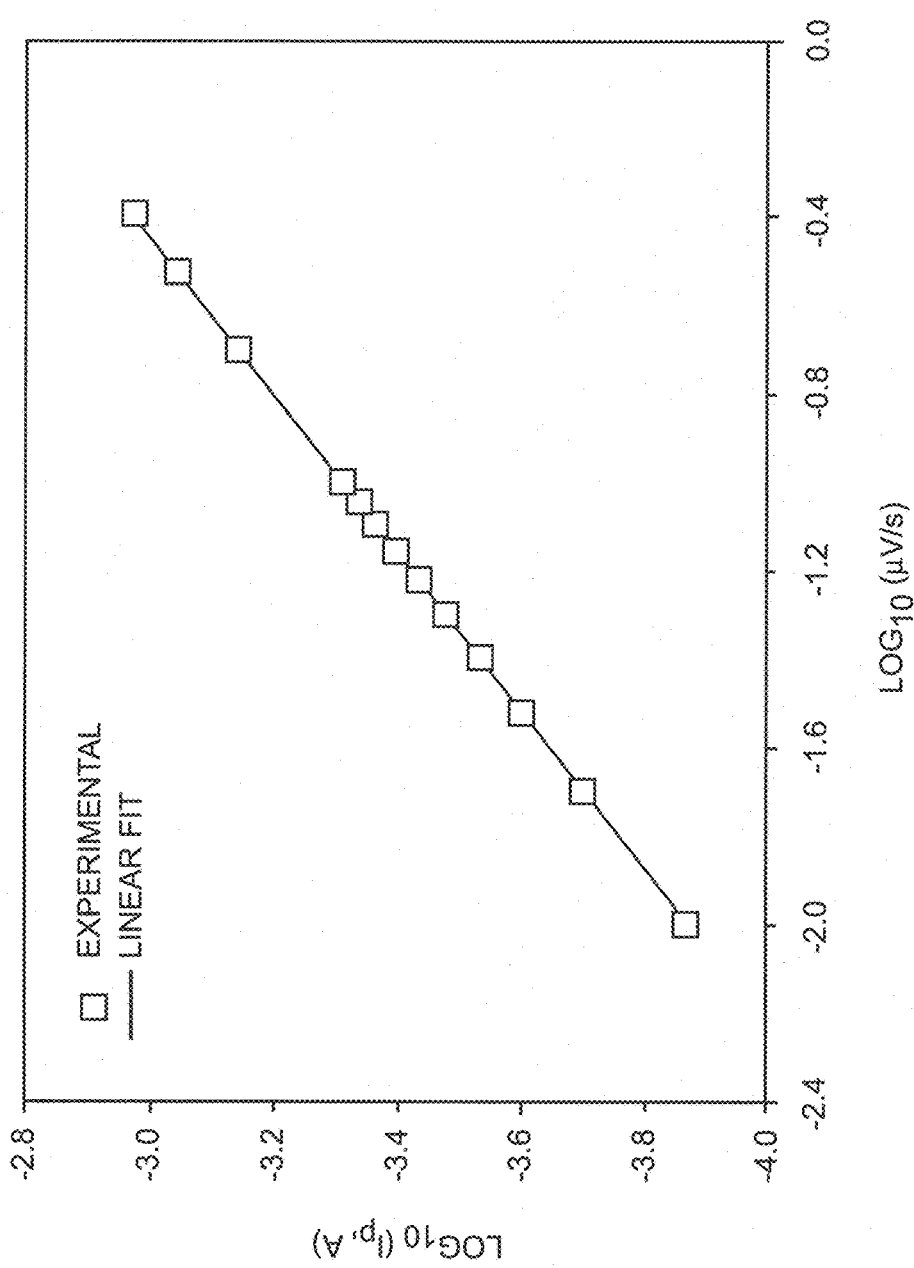


FIG. 10

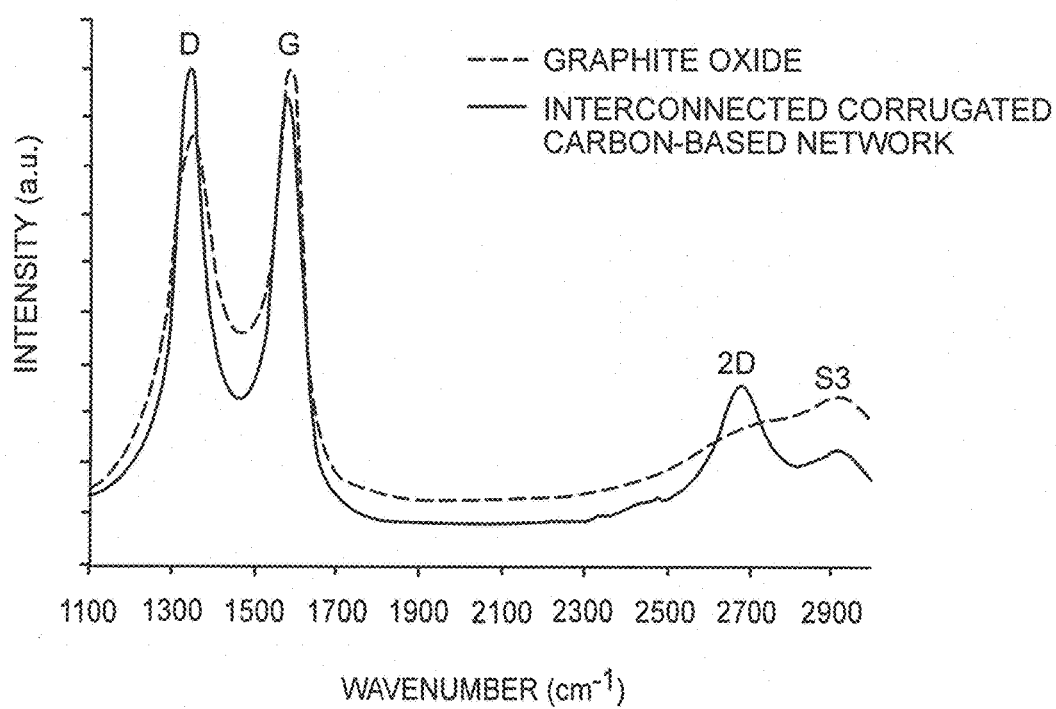


FIG. 11A

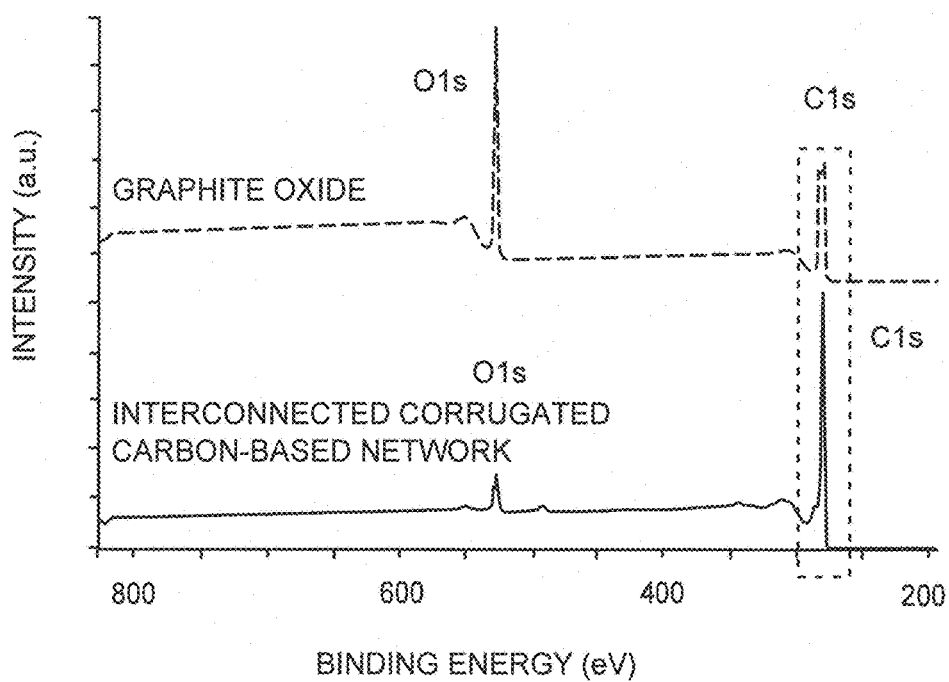


FIG. 11B

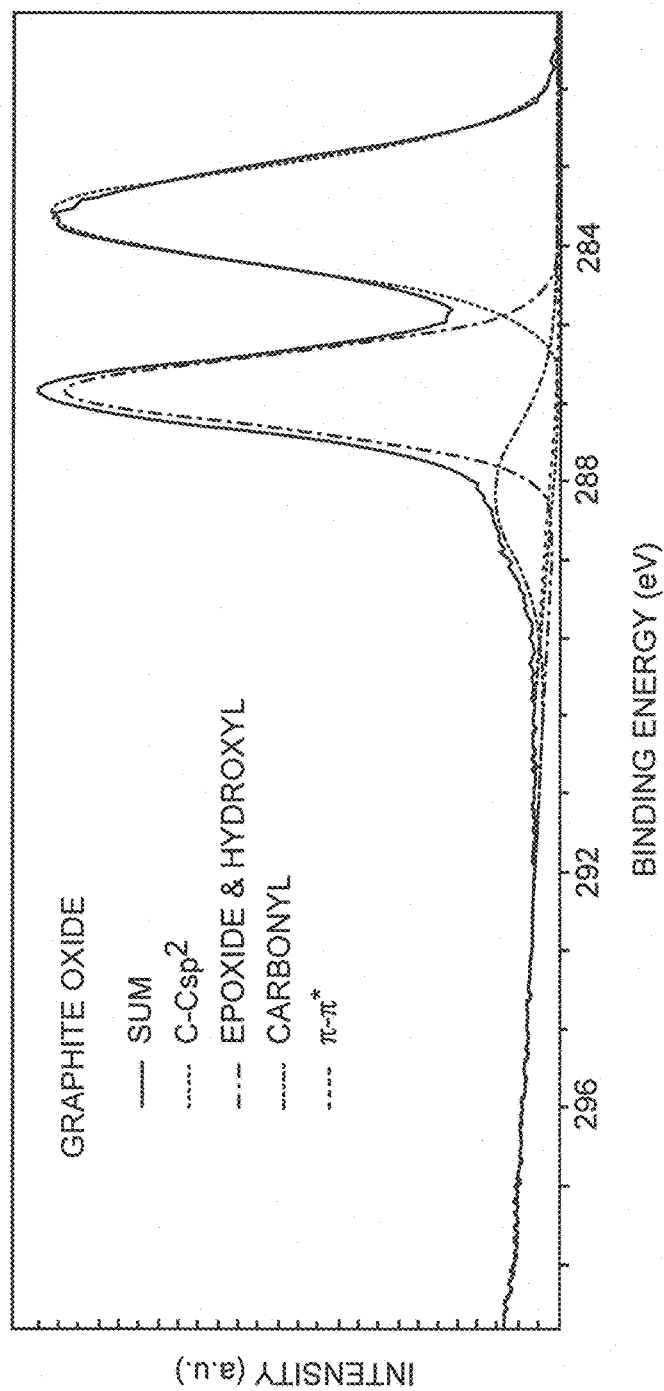


FIG. 11C

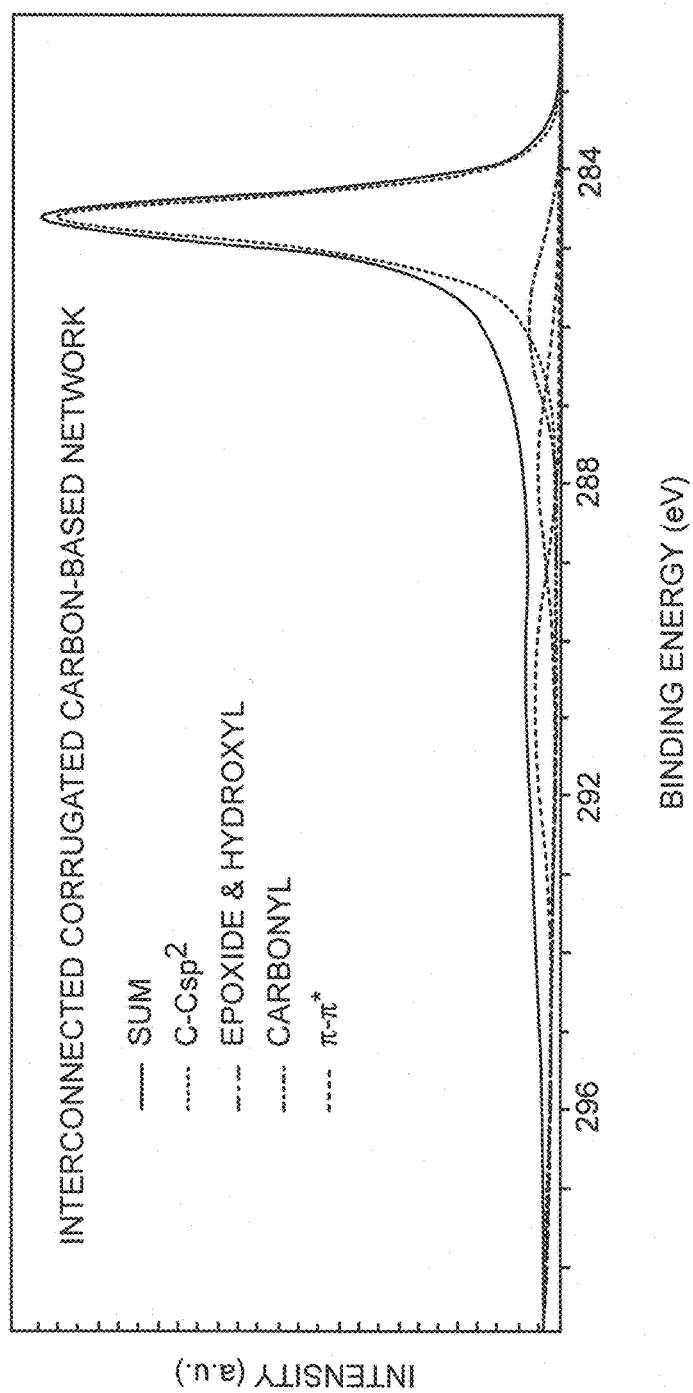


FIG. 11D

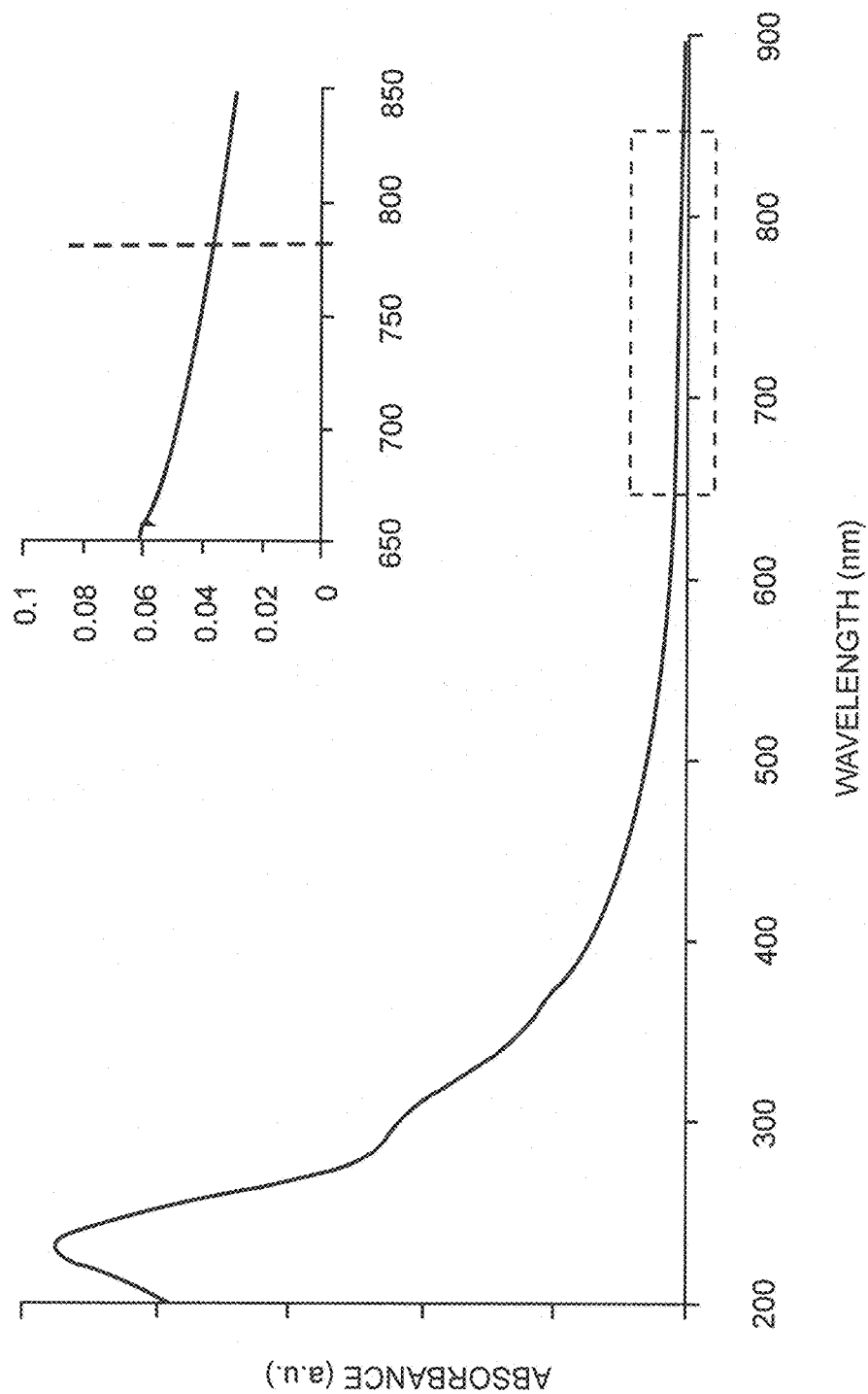


FIG. 11E

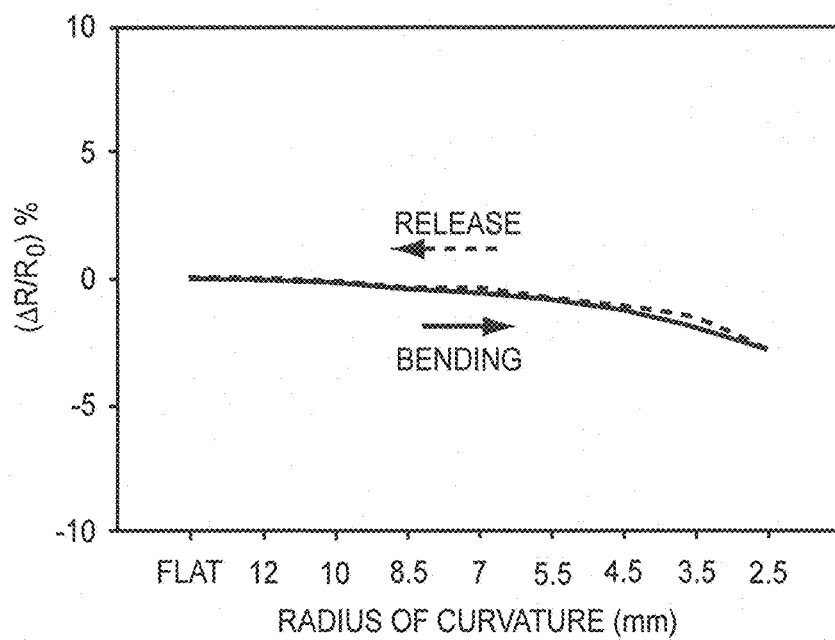


FIG. 12A

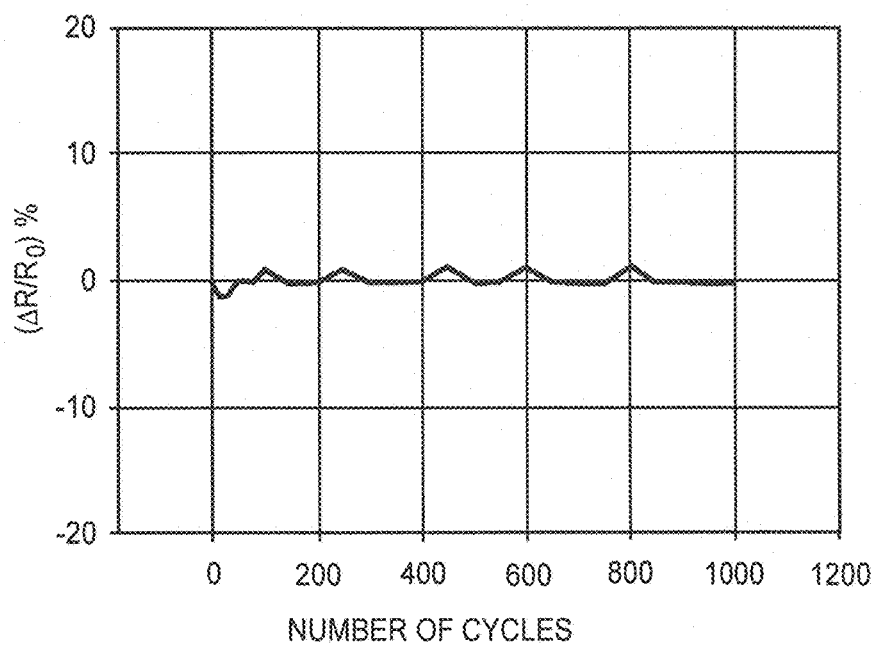


FIG. 12B

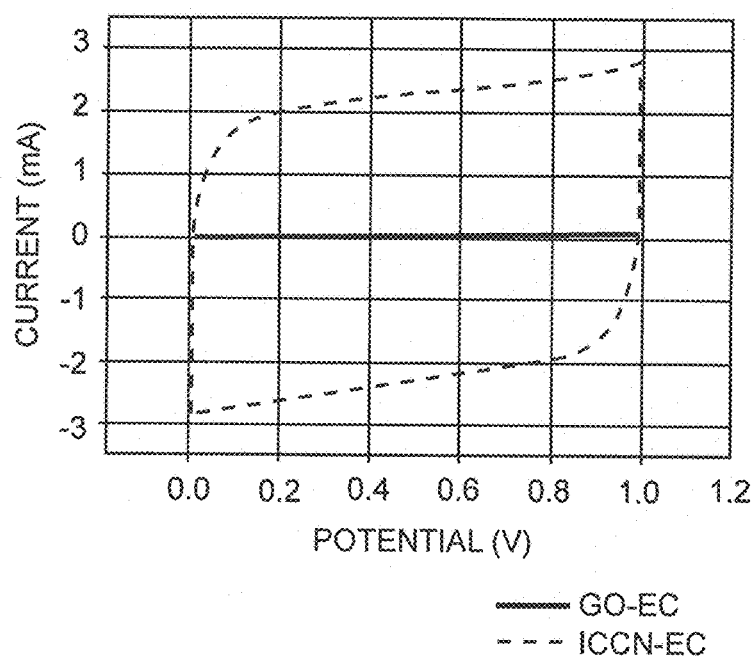


FIG. 13A

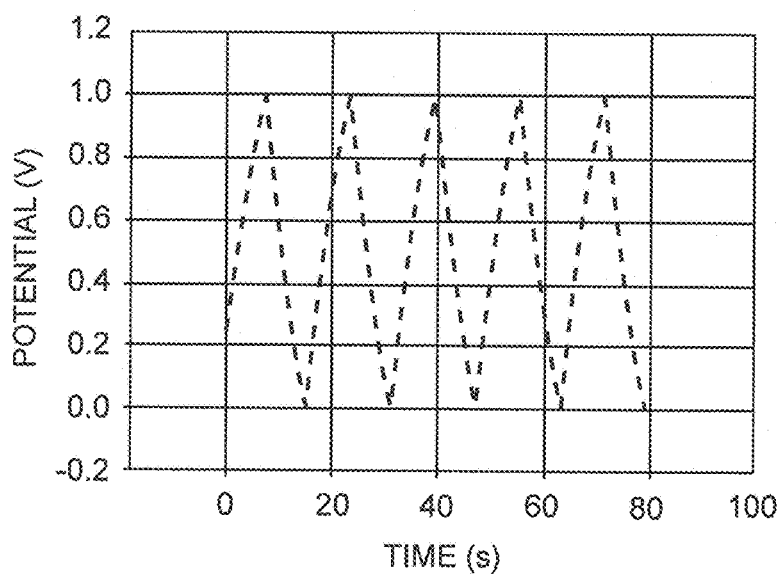


FIG. 13B

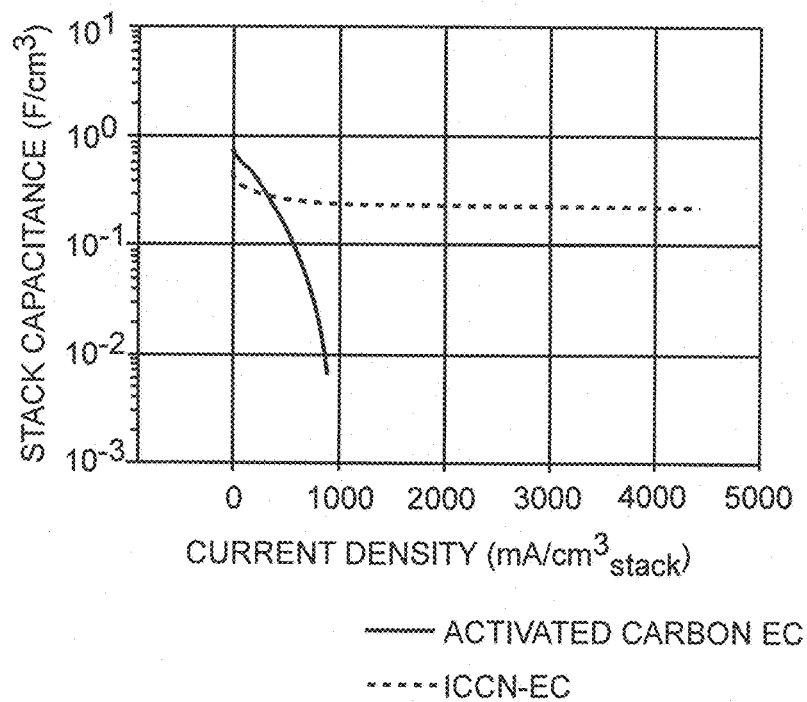


FIG. 13C

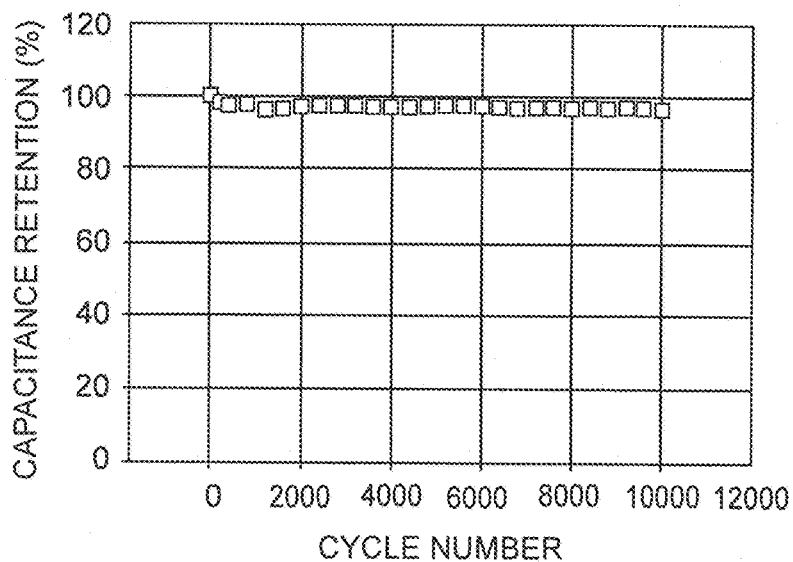


FIG. 13D

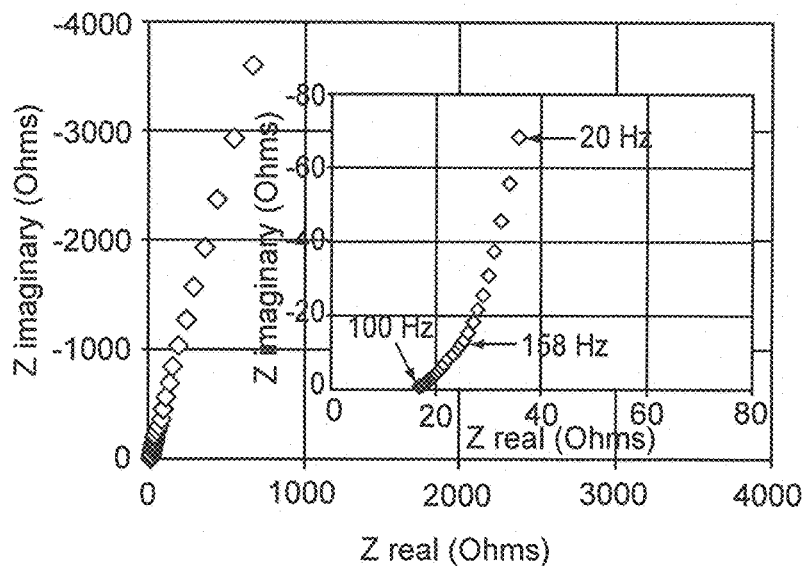


FIG. 13E

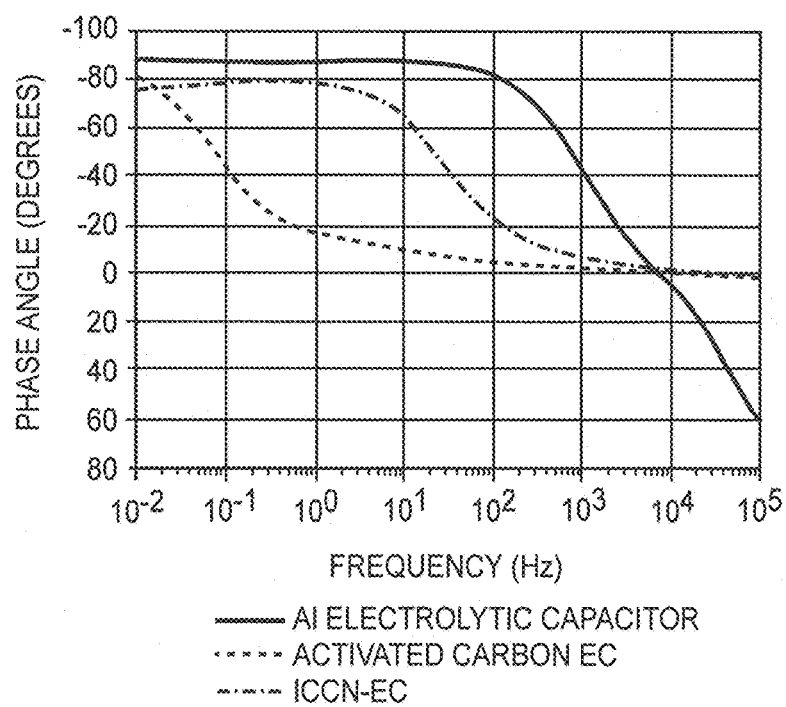


FIG. 13F

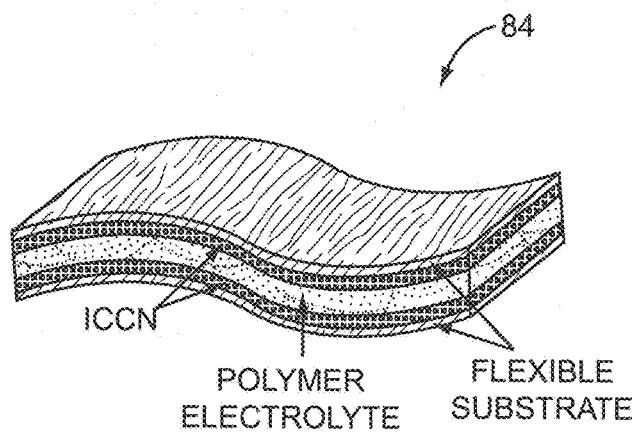


FIG. 14A

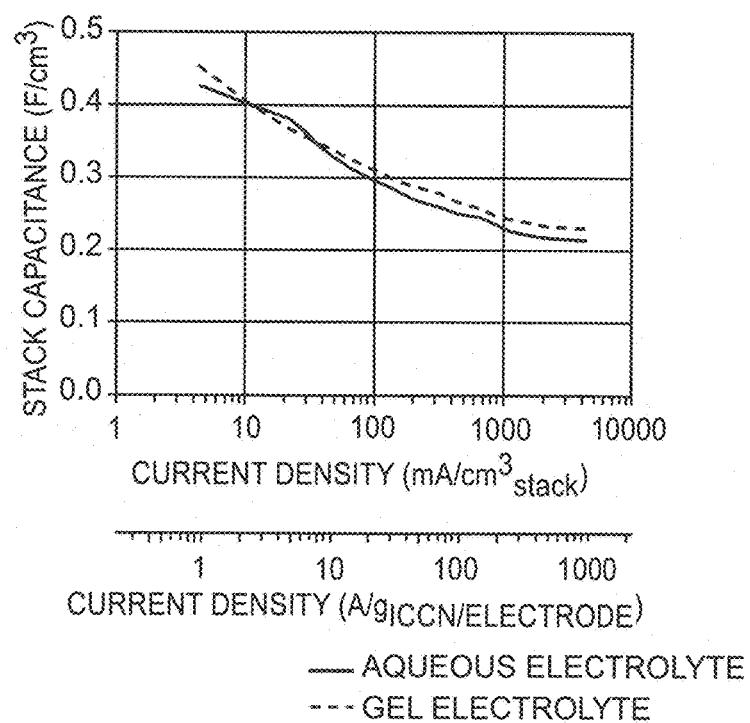


FIG. 14B

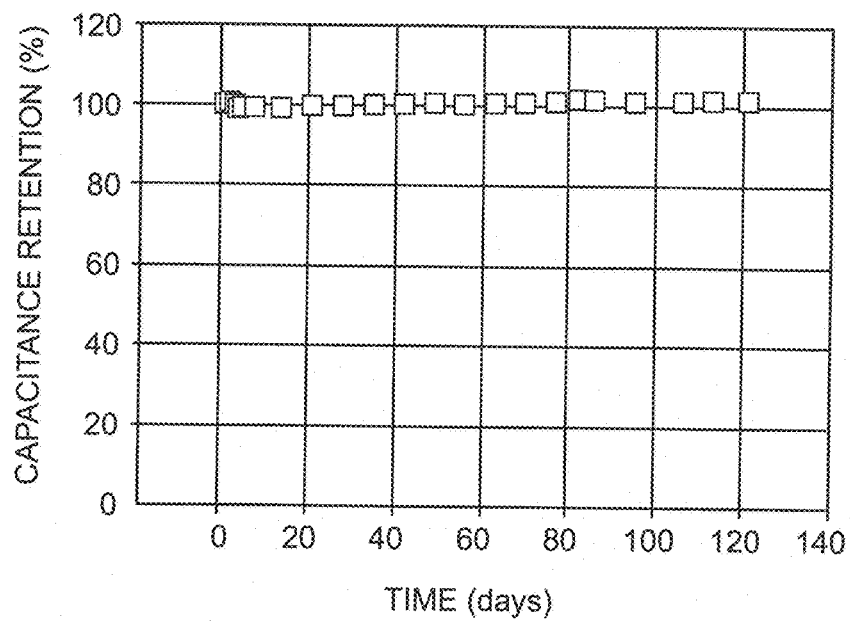


FIG. 14C

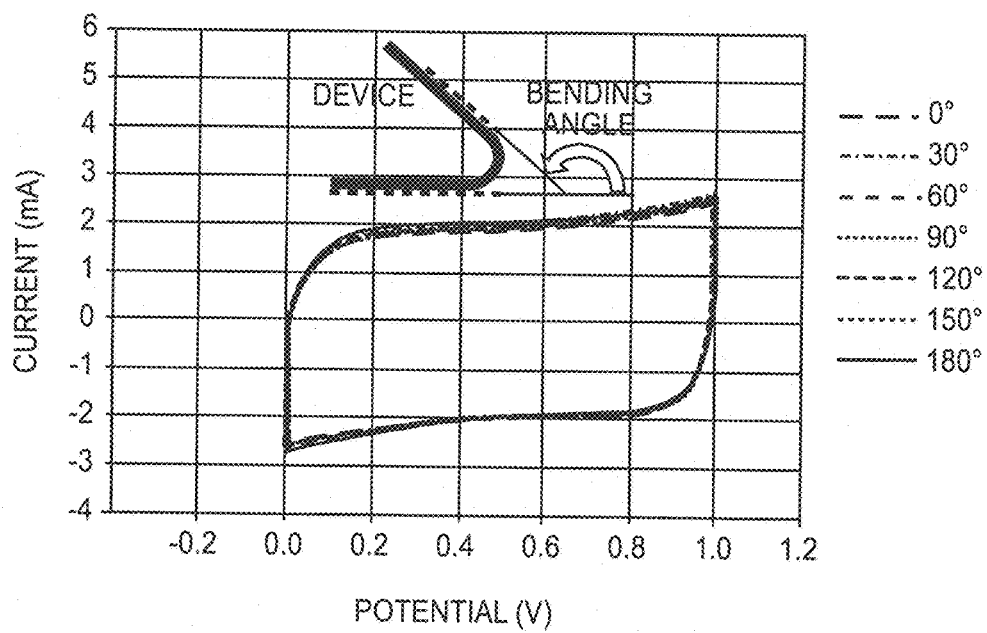


FIG. 14D

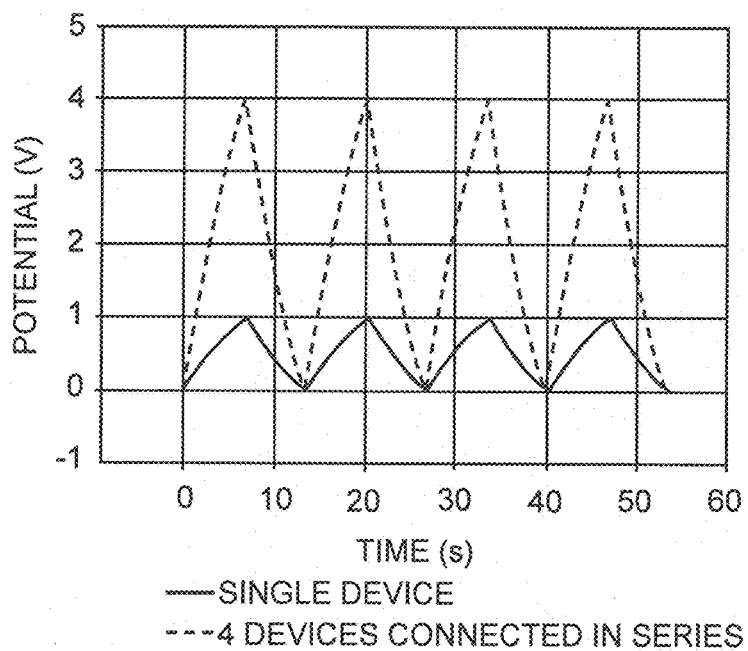


FIG. 14E

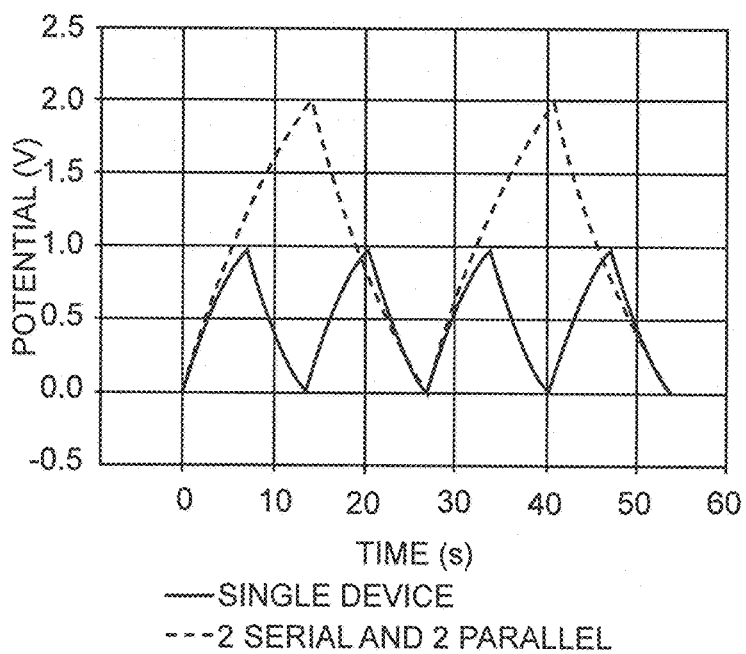


FIG. 14F

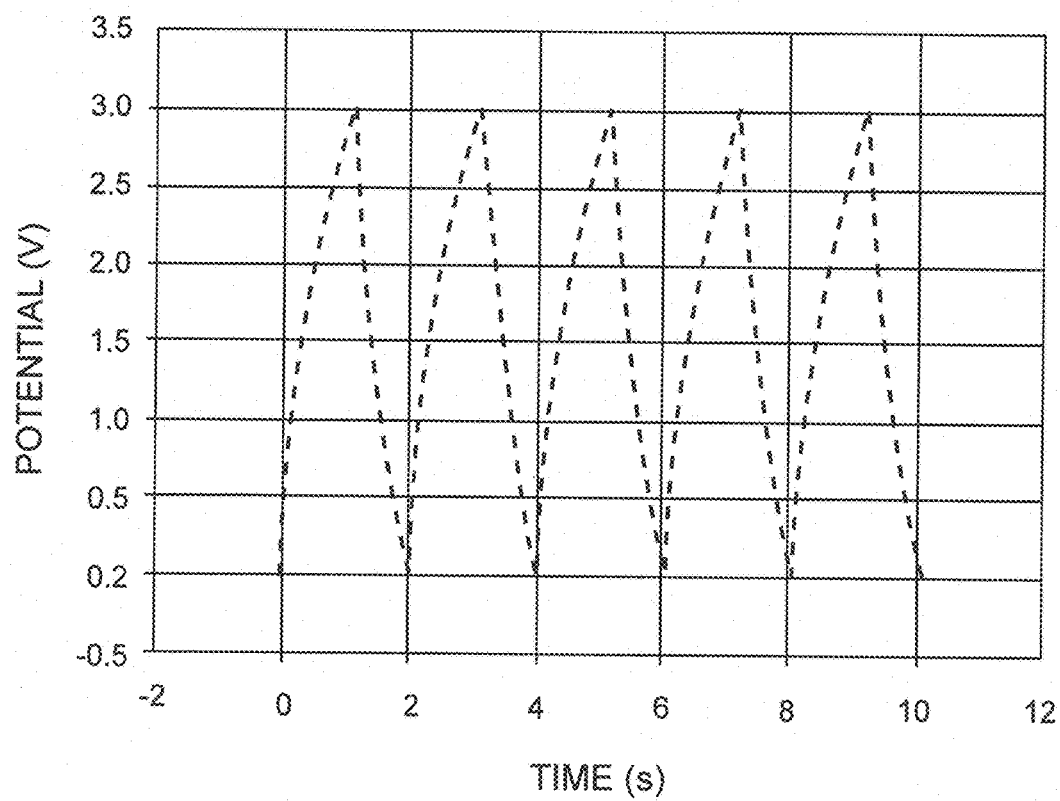


FIG. 15

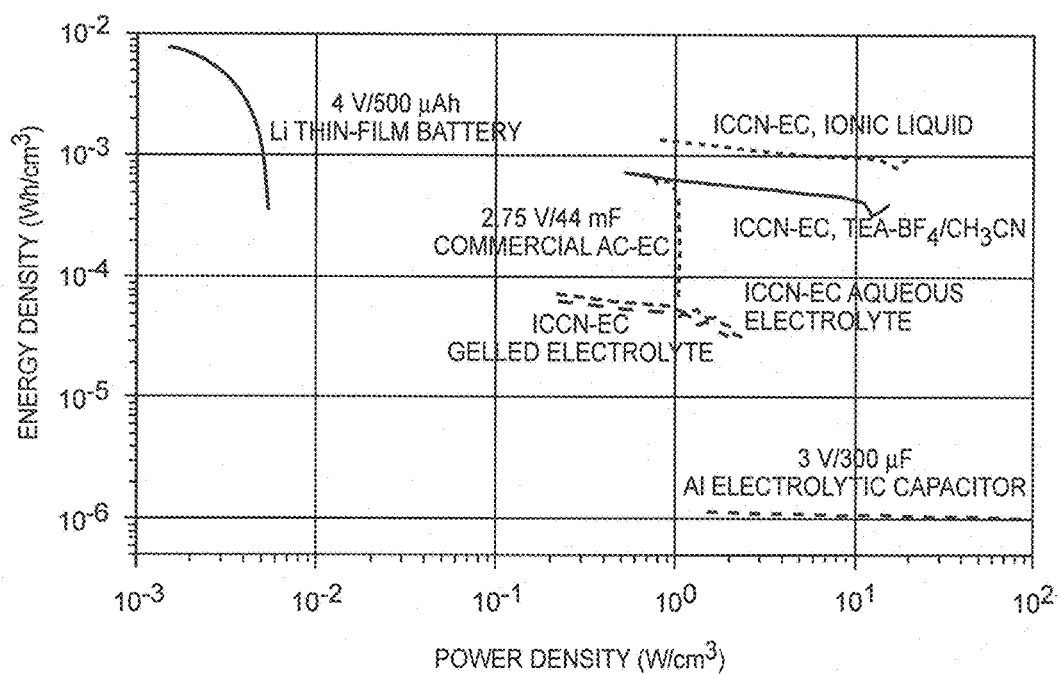


FIG. 16

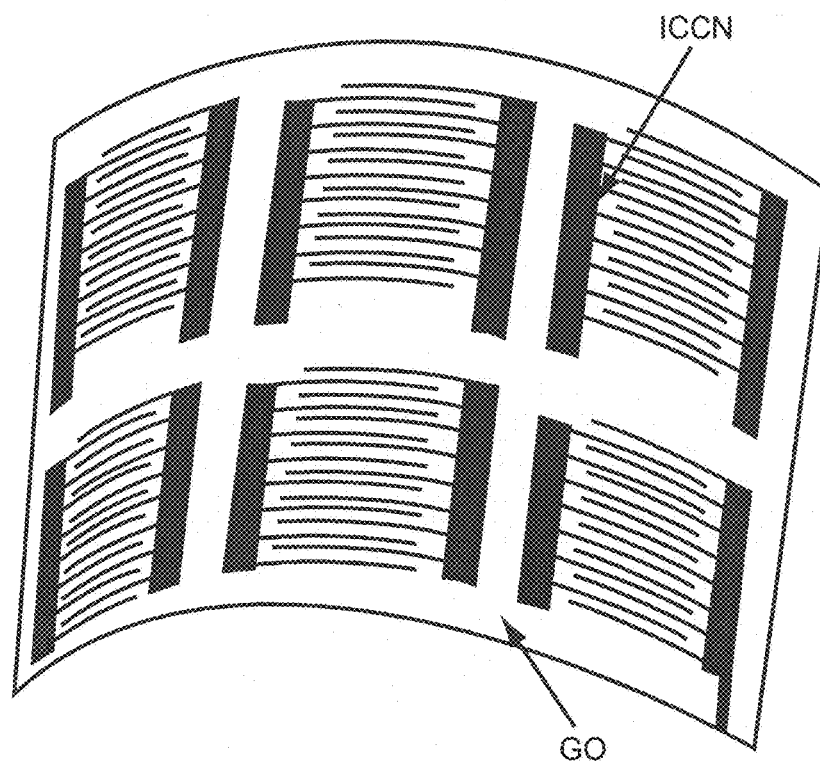


FIG. 17A

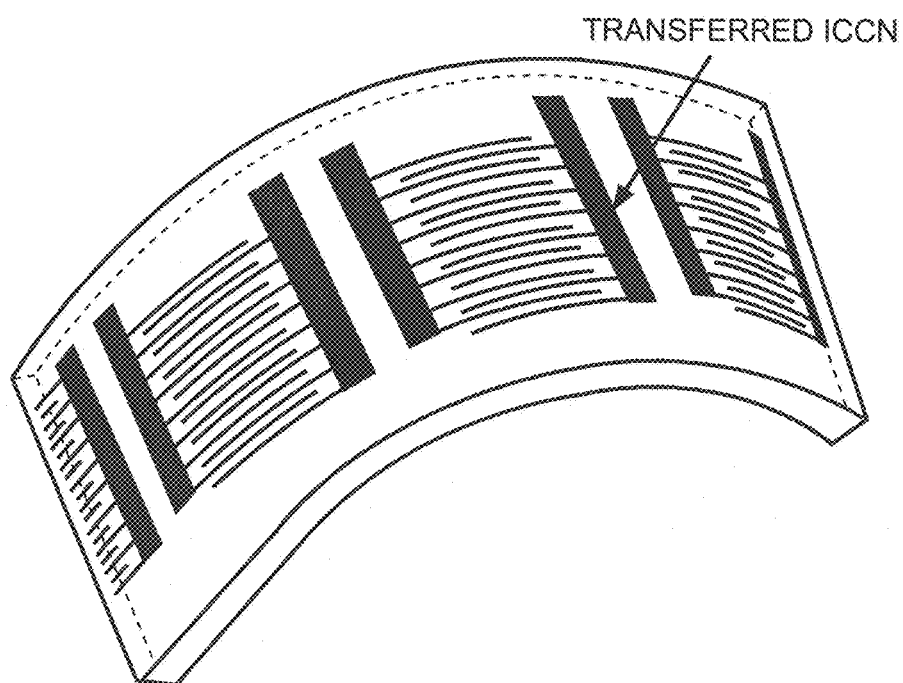


FIG. 17B

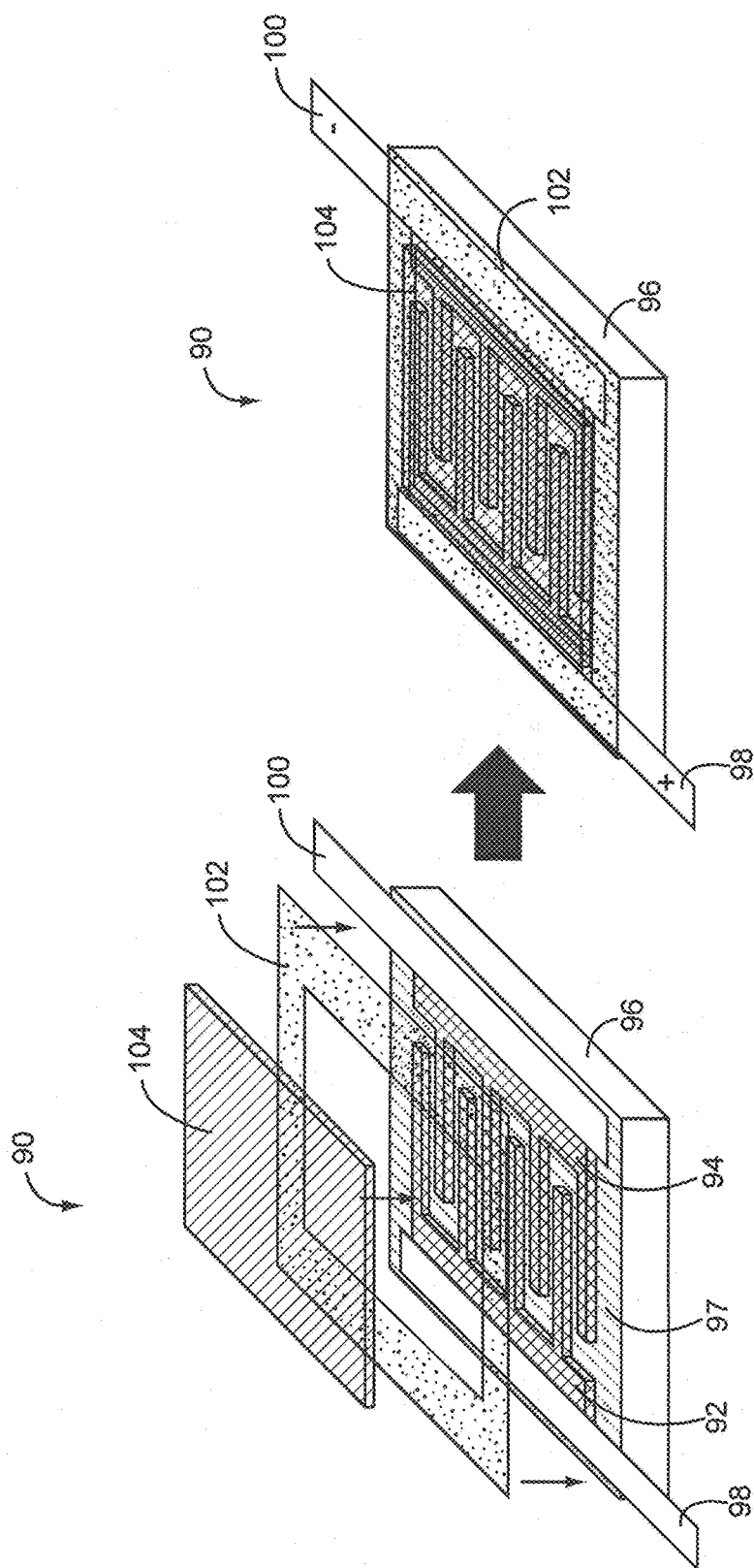
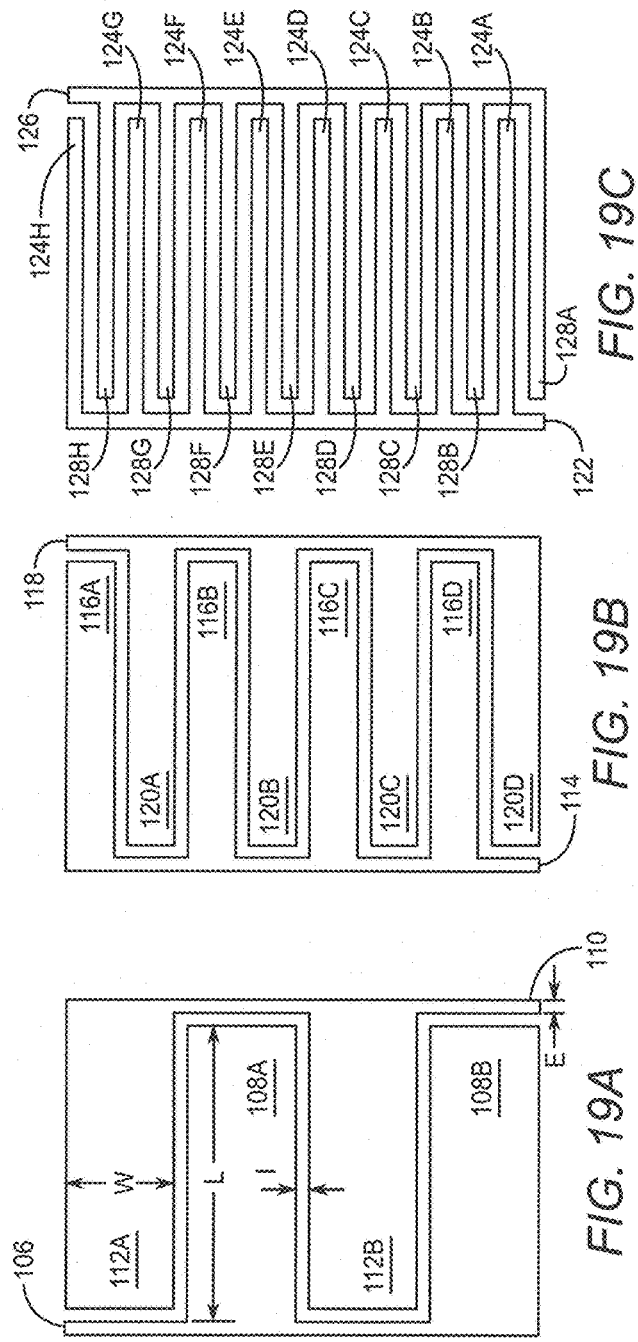


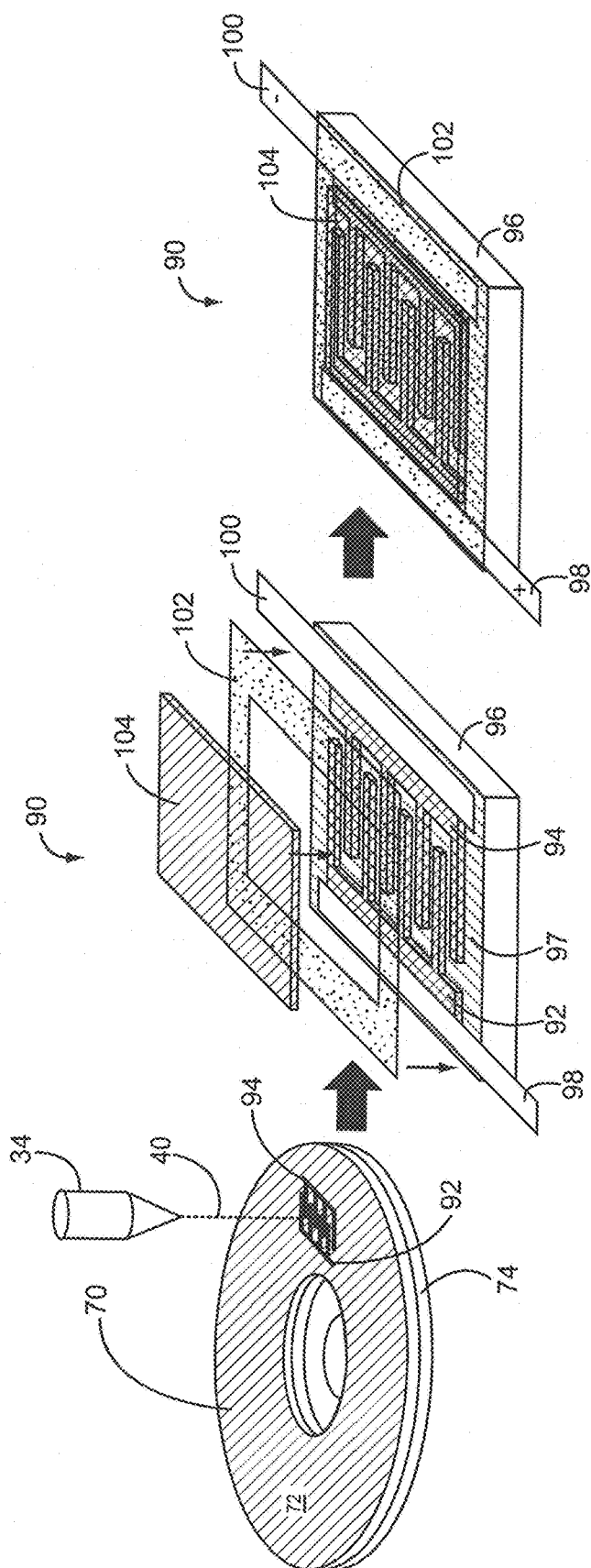
FIG. 18B

FIG. 18A



NUMBER OF ELECTRODE DIGITS	4	8	16
WIDTH, W (μm)	1770	810	330
LENGTH, L (μm)	4800	4800	4800
INTERSPACE, I (μm)	150	150	150
EDGE, E (μm)	200	200	200
TOTAL AREA, (mm^2)	40	40	40

FIG. 20



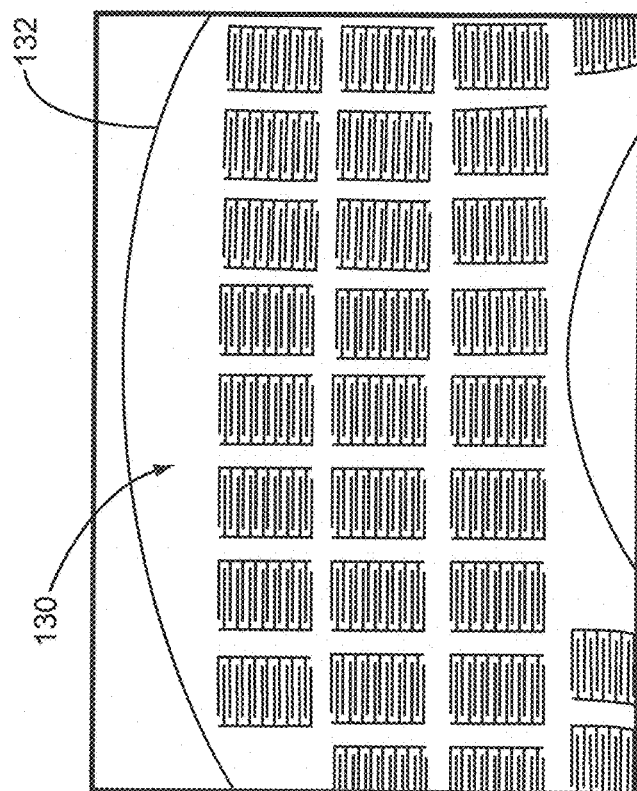


FIG. 21E

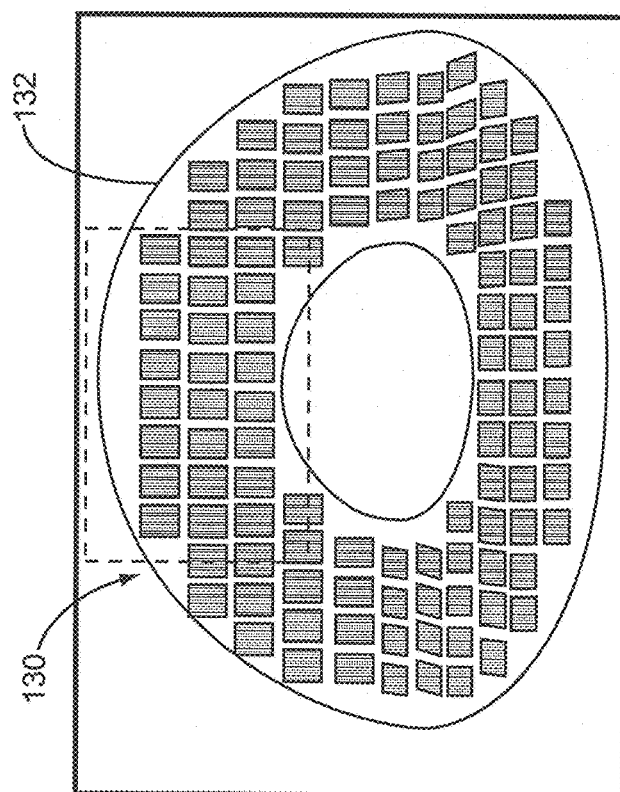


FIG. 21D

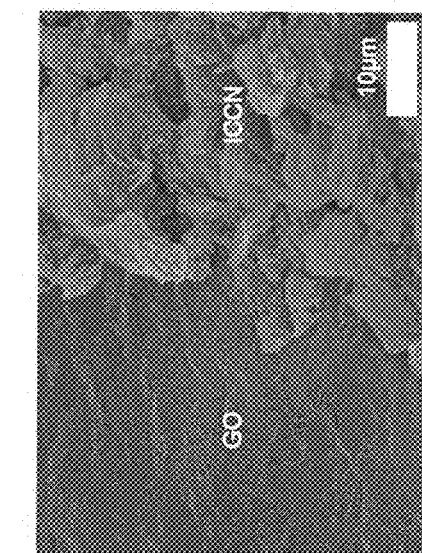


FIG. 22C

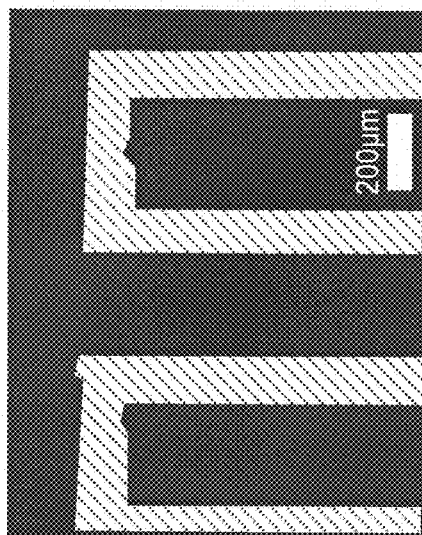


FIG. 22B

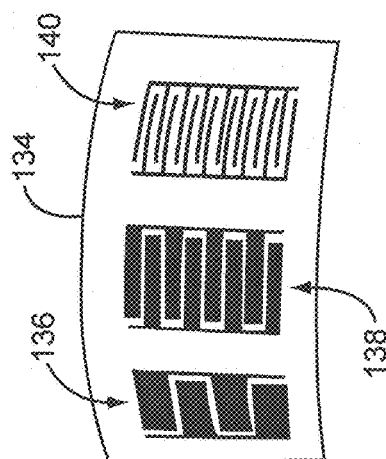


FIG. 22A

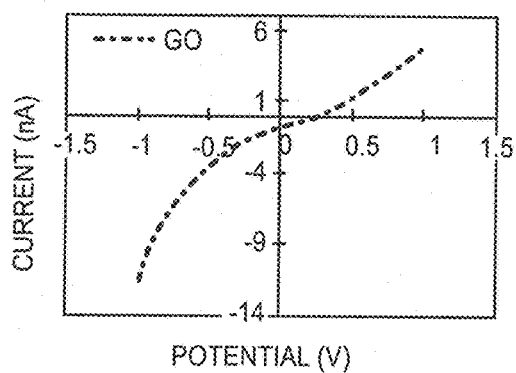


FIG. 22D

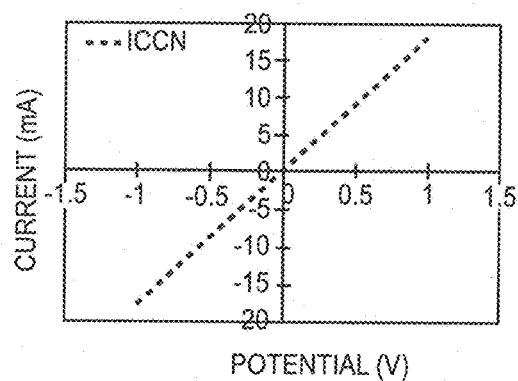


FIG. 22E

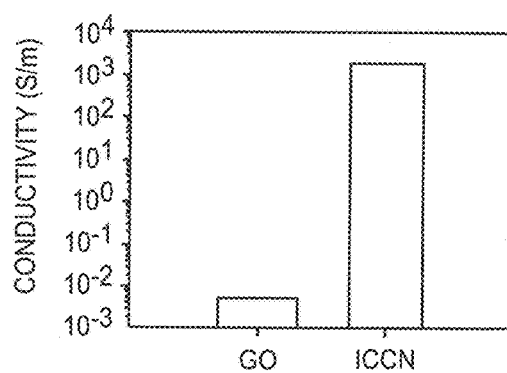


FIG. 22F

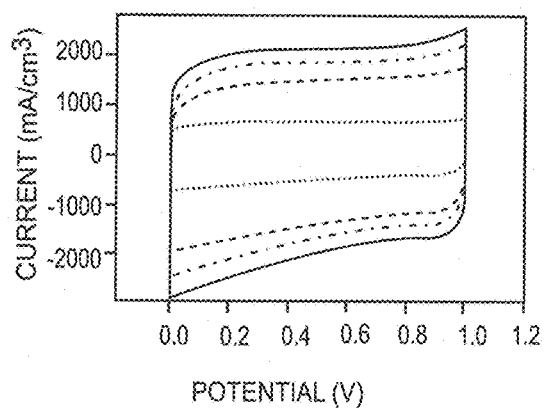


FIG. 23A

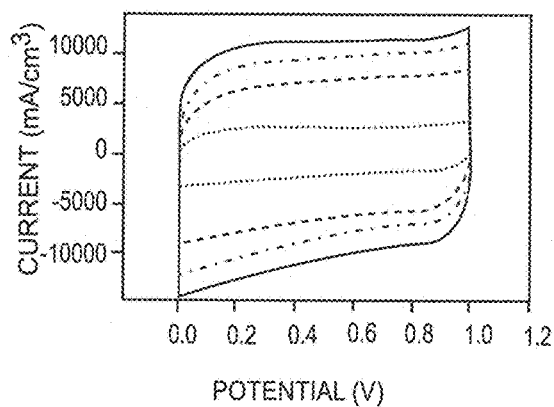


FIG. 23B

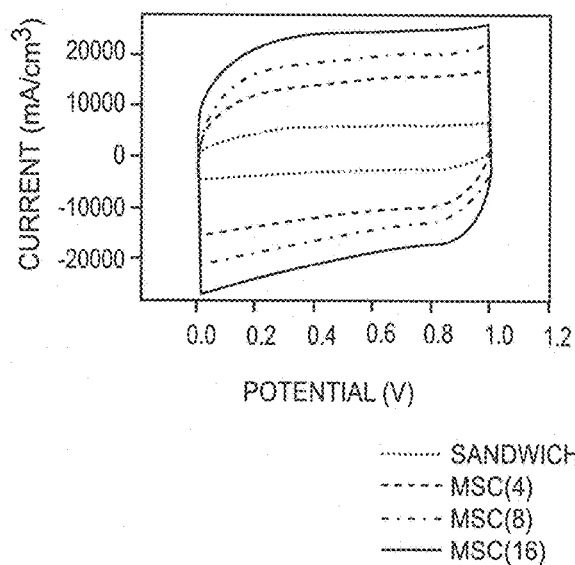


FIG. 23C

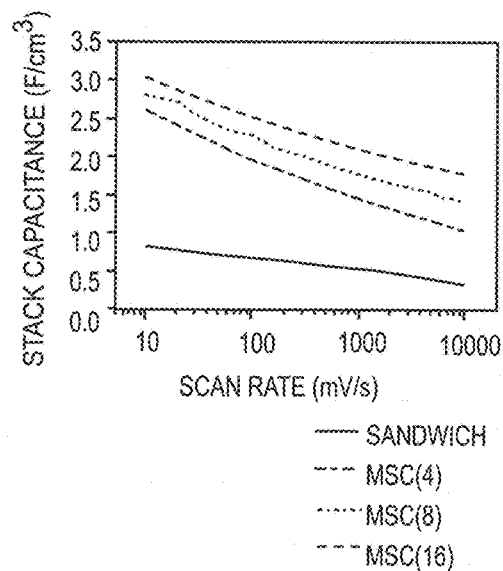


FIG. 23D

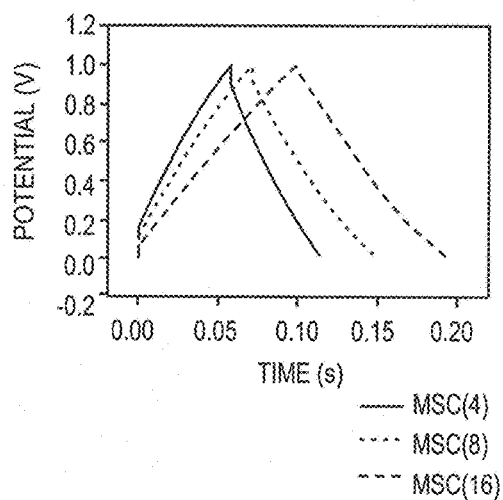


FIG. 23E

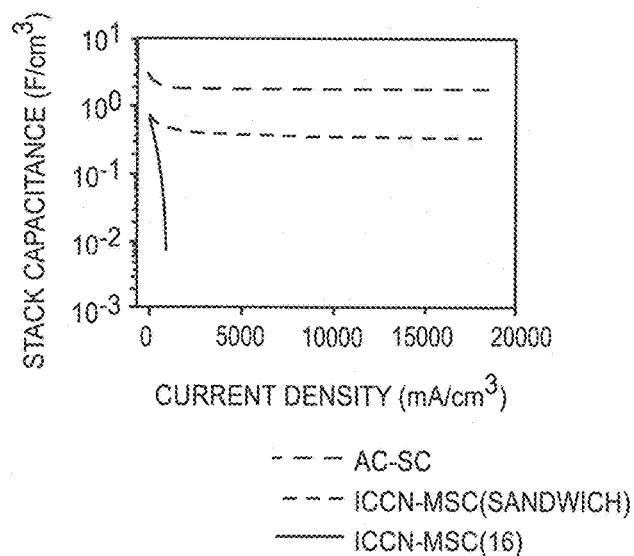


FIG. 23F

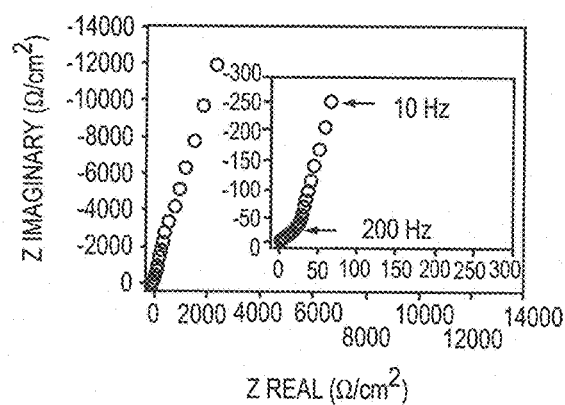


FIG. 23G

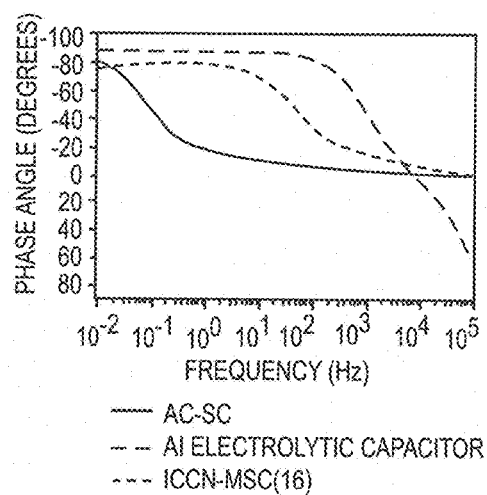


FIG. 23H

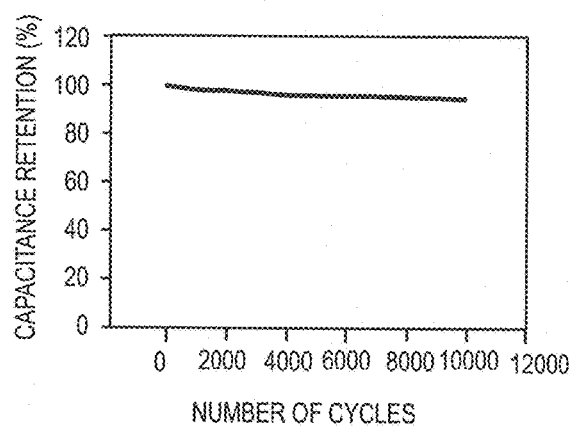


FIG. 23I

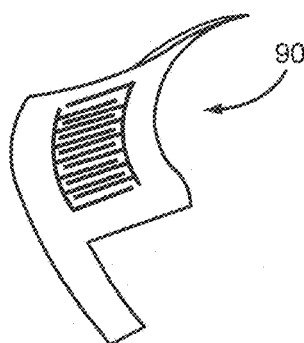


FIG. 24A

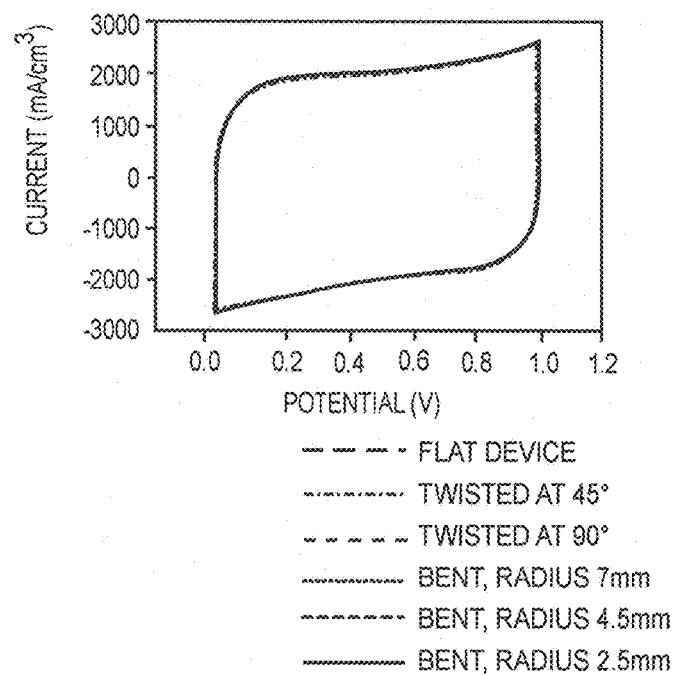


FIG. 24B

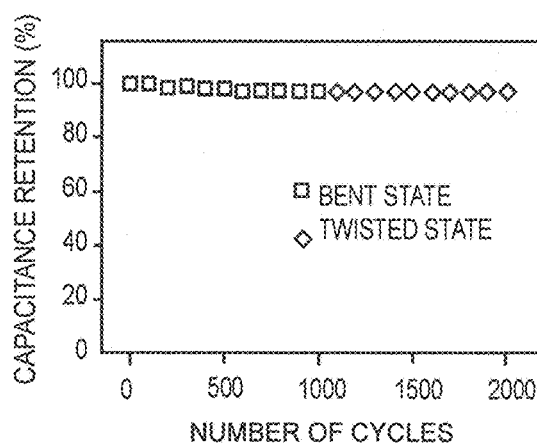


FIG. 24C

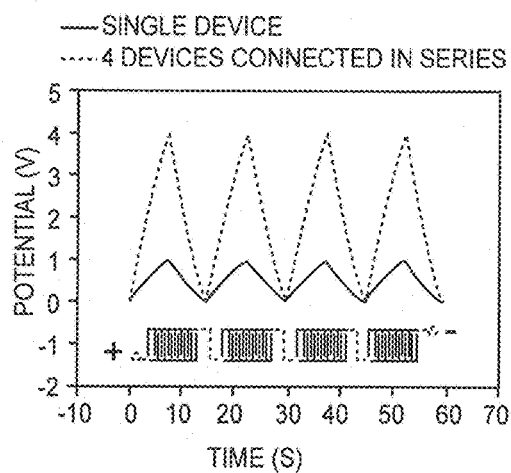


FIG. 24D

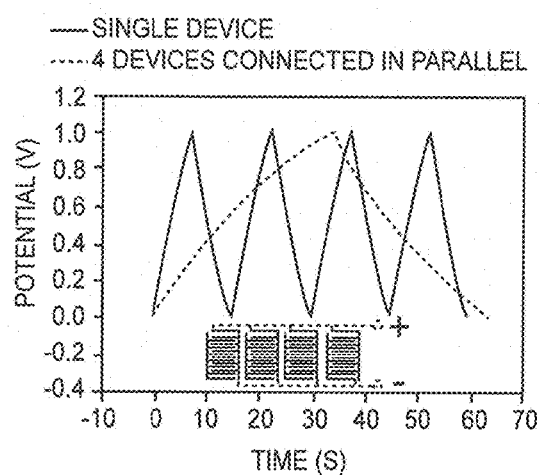


FIG. 24E

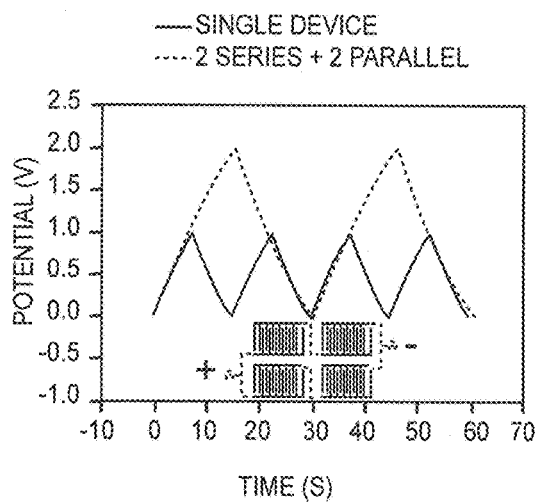


FIG. 24F

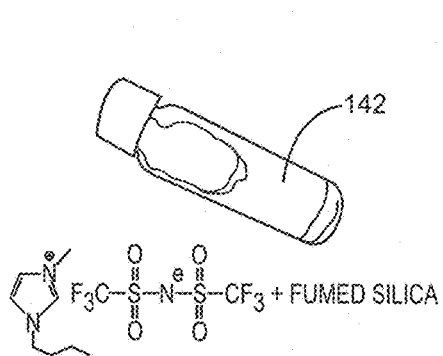


FIG. 25A

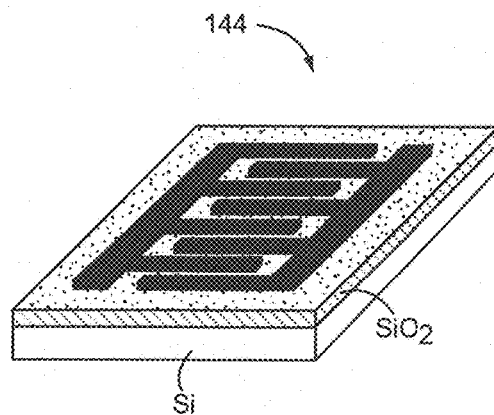


FIG. 25B

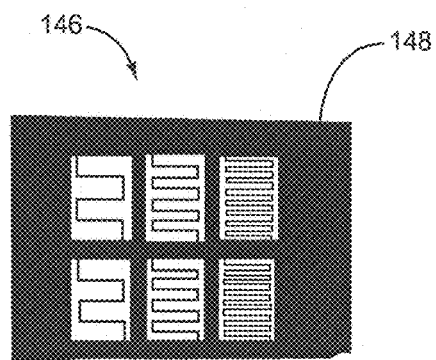


FIG. 25C

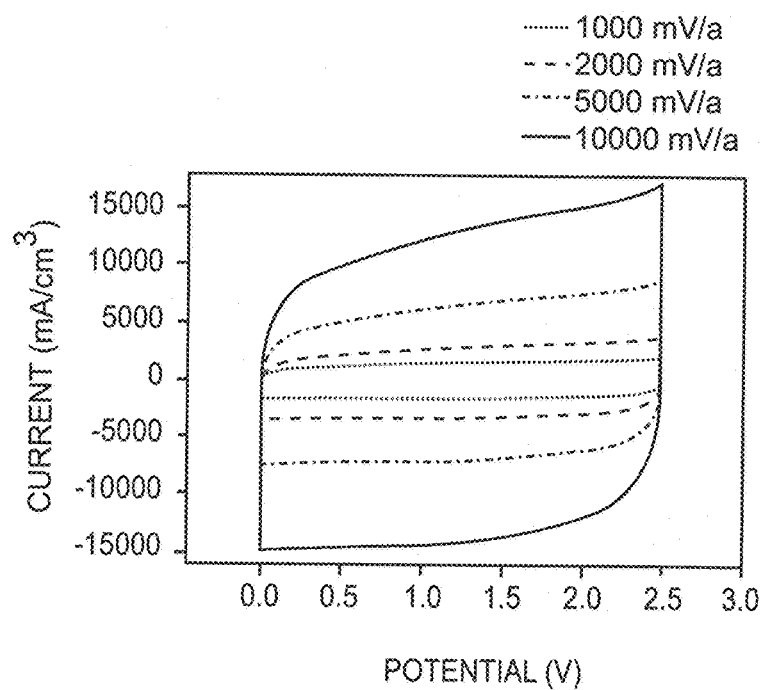


FIG. 25D

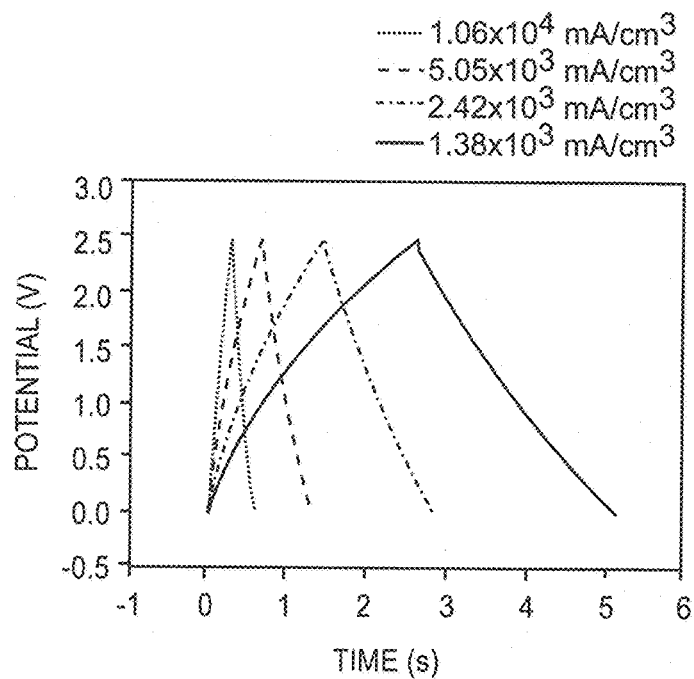


FIG. 25E

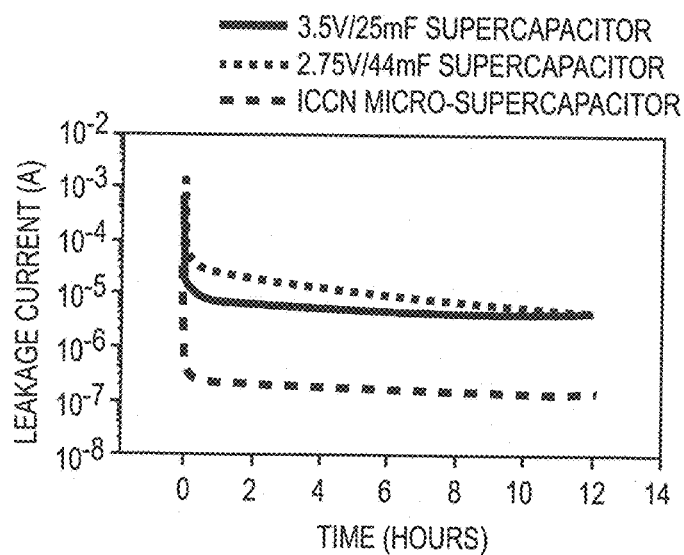


FIG. 26A

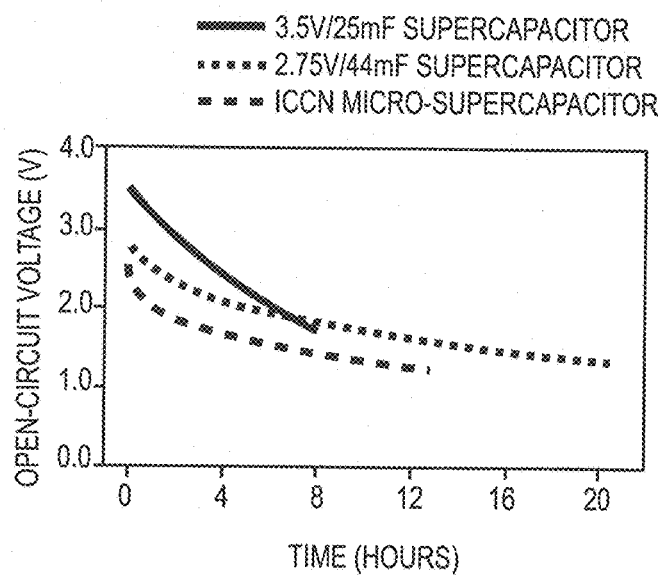


FIG. 26B

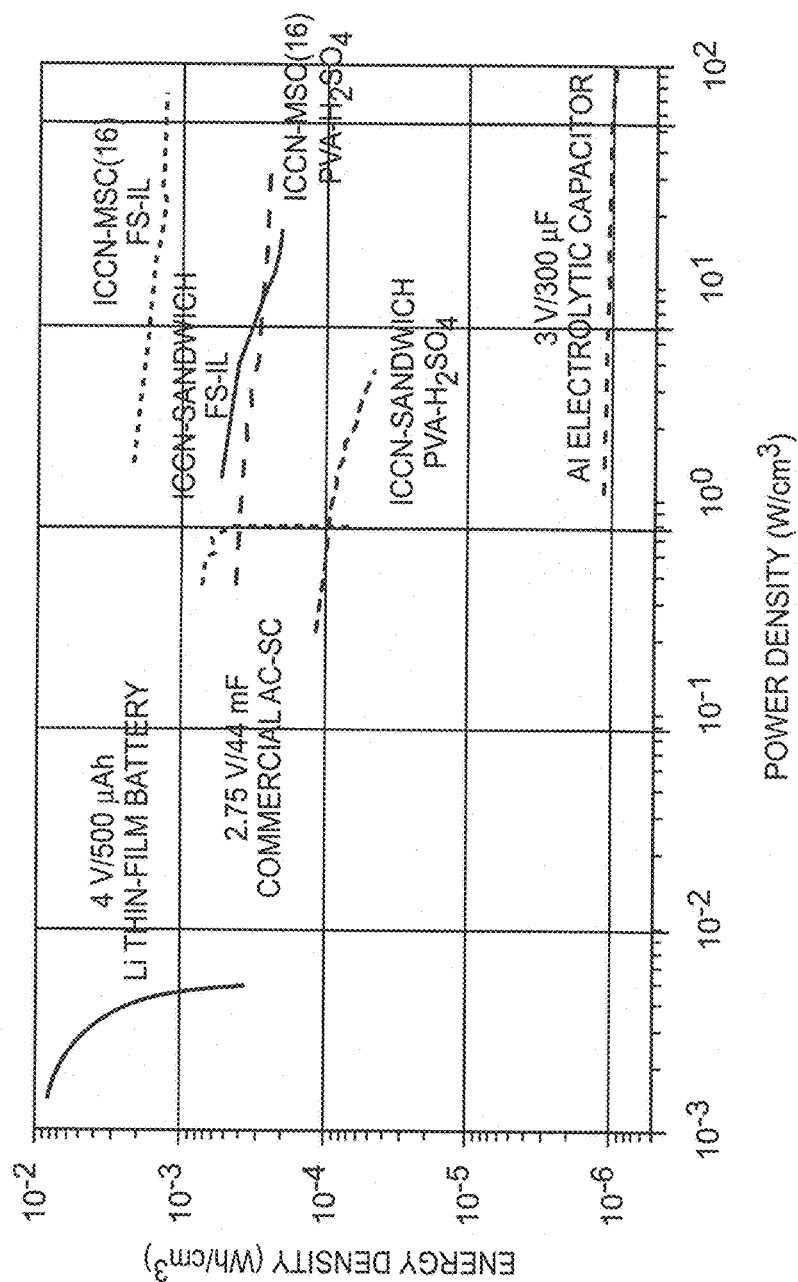


FIG. 27

CAPACITOR WITH ELECTRODES MADE OF AN INTERCONNECTED CORRUGATED CARBON-BASED NETWORK

RELATED APPLICATIONS

[0001] The present application is a continuation of U.S. patent application Ser. No. 15/612,405, filed Jun. 2, 2017, which is a continuation of U.S. patent application Ser. No. 14/382,463, filed Sep. 2, 2014, now U.S. Pat. No. 9,779,884.

[0002] U.S. patent application Ser. No. 14/382,463, filed Sep. 2, 2014, is a 35 USC 371 national phase filing of PCT/US13/29022, filed Mar. 5, 2013, which claims priority to U.S. Provisional Patent Applications No. 61/606,637, filed Mar. 5, 2012, and No. 61/757,077, filed Jan. 25, 2013.

[0003] The present application is related to U.S. patent application Ser. No. 13/725,073, filed Dec. 21, 2012, and International Patent Application No. PCT/US12/71407, filed Dec. 21, 2012, both of which claim priority to U.S. Provisional Patent Application No. 61/578,431, filed Dec. 21, 2011.

[0004] All of the applications listed above are hereby incorporated herein by reference in their entireties.

[0005] This research was supported in part by the Ministry of Higher Education of Egypt through a graduate research fellowship—the Missions Program.

FIELD OF THE DISCLOSURE

[0006] The present disclosure provides an interconnected corrugated carbon-based network (ICCN) and an inexpensive process for making, patterning, and tuning the electrical, physical and electrochemical properties of the ICCN.

BACKGROUND

[0007] Batteries and electrochemical capacitors (ECs) stand at opposite ends of the spectrum in terms of their power and energy densities. Batteries store energy through electrochemical reactions and can exhibit high energy densities (on the order of 20 to 150 Wh/kg), whereas ECs, which store charge in electrochemical double layers (EDLs), can only achieve values of 4 to 5 Wh/kg. However, because ion flow is faster than redox reactions, ECs can deliver much higher power densities. ECs are also generally maintenance free and display a longer shelf and cycle life, so they are often favored in many electronic applications.

[0008] An EC that combines the power performance of capacitors with the high energy density of batteries would represent a major advance in energy storage technology, but this requires an electrode with higher and more accessible surface area than that of conventional EC electrodes while maintaining high conductivity. Carbon-based materials are attractive in this regard because of their mechanical and electrical properties as well as exceptionally high surface area. Recently, the intrinsic capacitance of single layer graphene was reported to be $\sim 21 \mu\text{F}/\text{cm}^2$; this value now sets the upper limit for EDL capacitance for all carbon-based materials. Thus, ECs based on carbon-based materials could, in principle, achieve an EDL capacitance as high as $\sim 550 \text{ F/g}$ if their entire surface area could be used.

[0009] Currently, carbon-based materials derived from graphite oxide (GO) can be manufactured on the ton scale at low cost, making them potentially cost effective materials for charge storage devices. Although these carbon-based materials have shown excellent power density and life-cycle

stability, their specific capacitance (130 F/g in aqueous potassium hydroxide and 99 F/g in an organic electrolyte) still falls far below the theoretical value of $\sim 550 \text{ F/g}$ calculated for a single layer of carbon. A variety of other carbon-based materials derived from GO have also been used, yet the values of specific capacitance, energy density, and power density have remained lower than expected. These effects are often attributed to the restacking of carbon sheets during processing as a result of the strong sheet-to-sheet van der Waals interactions. This reduction in the specific surface area of single layer carbon accounts for the overall low capacitance. In addition, these ECs exhibited relatively low charge/discharge rates, which precludes their use for high power applications. Recently, EC devices composed of curved graphene, activated graphene, and solvated graphene have demonstrated enhanced performance in terms of energy density. However, further improvements in energy density are needed that do not sacrifice high power density. In particular, the production of mechanically robust carbon-based electrodes with large thicknesses ($\sim 10 \mu\text{m}$ or higher) and high surface-to-volume ratio in a binder free process would result in high power and high energy density ECs.

[0010] In the pursuit of producing high quality bulk carbon-based devices such as ECs and organic sensors, a variety of syntheses now incorporate graphite oxide (GO) as a precursor for the generation of large scale carbon-based materials. Inexpensive methods for producing large quantities of GO from the oxidation of graphitic powders are now available. In addition, the water dispersibility of GO combined with inexpensive production methods make GO an ideal starting material for producing carbon-based devices. In particular, GO has water dispersible properties. Unfortunately, the same oxygen species that give GO its water dispersible properties also create defects in its electronic structure, and as a result, GO is an electrically insulating material. Therefore, the development of device grade carbon-based films with superior electronic properties requires the removal of these oxygen species, re-establishment of a conjugated carbon network, as well as a method for controllably patterning carbon-based device features.

[0011] Methods for reducing graphite oxide have included chemical reduction via hydrazine, hydrazine derivatives, or other reducing agents, high temperature annealing under chemical reducing gases and/or inert atmospheres, solvothermal reduction, a combination of chemical and thermal reduction methods, flash reduction, and most recently, laser reduction of GO. Although several of these methods have demonstrated relatively high quality graphite oxide reduction, many have been limited by expensive equipment, high annealing temperatures and nitrogen impurities in the final product. As a result, of these difficulties, a combination of properties that includes high surface area and high electrical conductivity in an expanded interconnected carbon network has remained elusive. In addition, large scale film patterning via an all-encompassing step for both GO reduction and patterning has proven difficult and has typically been dependent on photo-masks to provide the most basic of patterns. Therefore, what is needed is an inexpensive process for making and patterning an interconnected corrugated carbon-based network (ICCN) having a high surface area with highly tunable electrical conductivity and electrochemical properties.

SUMMARY

[0012] The present disclosure provides a capacitor having at least one electrode made up of an interconnected corrugated carbon-based network (ICCN). The ICCN produced has a combination of properties that includes high surface area and high electrical conductivity in an expanded network of interconnected carbon layers.

[0013] In one embodiment, each of the expanded and interconnected carbon layers is made up of at least one corrugated carbon sheet that is one atom thick. In another embodiment, each of the expanded and interconnected carbon layers is made up of a plurality of corrugated carbon sheets that are each one atom thick. The interconnected corrugated carbon-based network is characterized by a high surface area with highly tunable electrical conductivity and electrochemical properties.

[0014] In one embodiment, a method produces a capacitor having electrodes made of a patterned ICCN. In that particular embodiment, an initial step receives a substrate having a carbon-based oxide film. Once the substrate is received, a next step involves generating a light beam having a power density sufficient to reduce portions of the carbon-based oxide film to an ICCN. Another step involves directing the light beam across the carbon-based oxide film in a predetermined pattern via a computerized control system while adjusting the power density of the light beam via the computerized control system according to predetermined power density data associated with the predetermined pattern.

[0015] In one embodiment, the substrate is a disc-shaped, digital versatile disc (DVD) sized thin plastic sheet removably adhered to a DVD sized plate that includes a DVD centering hole. The DVD sized plate carrying the disc-shaped substrate is loadable into a direct-to-disc labeling enabled optical disc drive. A software program executed by the computerized control system reads data that defines the predetermined pattern. The computerized control system directs a laser beam generated by the optical disc drive onto the disc-shaped substrate, thereby reducing portions of the carbon-based oxide film to an electrically conductive ICCN that matches shapes, dimensions, and conductance levels dictated by the data of the predetermined pattern.

[0016] Those skilled in the art will appreciate the scope of the disclosure and realize additional aspects thereof after reading the following detailed description in association with the accompanying drawings.

BRIEF DESCRIPTION OF THE DRAWINGS

[0017] The accompanying drawings incorporated in and forming a part of this specification illustrate several aspects of the disclosure, and together with the description serve to explain the principles of the disclosure.

[0018] FIG. 1 depicts the label side of a prior art direct-to-disc labeling type CD/DVD disc.

[0019] FIG. 2 is a schematic of a prior art direct-to-disc labeling type optical disc drive.

[0020] FIG. 3 is a process diagram for an exemplary process for providing graphite oxide (GO) films on a substrate.

[0021] FIG. 4 is a process diagram for laser scribing an interconnected corrugated carbon-based network (ICCN) and then fabricating electrical components from the ICCN.

[0022] FIG. 5 is a line drawing of a sample of the ICCN of the present embodiments.

[0023] FIG. 6A is an artwork image of a man's head covered with circuits.

[0024] FIG. 6B is a photograph of a GO film after the artwork image of FIG. 6A is directly patterned on the GO film using the laser scribing technique of the present disclosure.

[0025] FIG. 7 is a graph that provides a comparison between changes in electrical conductivity by reducing the GO film of FIG. 6B by using various grayscale levels to laser scribe the artwork of FIG. 6A to produce the patterned GO film of FIG. 6B.

[0026] FIG. 8A is a scanning electron microscope (SEM) image that illustrates an infrared laser's effect on GO film prior to laser treatment on the right side of the image in contrast to an aligned ICCN on the left side of the image.

[0027] FIG. 8B is an SEM image showing that an ICCN has a thickness that is approximately 10 times larger in comparison to that of untreated GO film.

[0028] FIG. 8C is an SEM image showing a cross-sectional view of a single laser converted ICCN.

[0029] FIG. 8D is an SEM image showing a greater magnification of a selected area within the ICCN in FIG. 8C.

[0030] FIG. 9 compares a powder X-ray diffraction (XRD) pattern of the ICCN with both graphite and graphite oxide diffraction patterns.

[0031] FIG. 10 is a plot of \log_{10} of peak current versus \log_{10} of an applied voltammetric scan rate.

[0032] FIGS. 11A-11E are graphs related to Raman spectroscopy analysis.

[0033] FIG. 12A is a graph depicting an electrical resistance change of a flexible ICCN electrode as a function of a bending radius.

[0034] FIG. 12B is a graph depicting an electrical resistance change of a flexible ICCN electrode as a function of bending cycles.

[0035] FIG. 13A is a cyclic voltammetry graph comparing a GO electrochemical capacitor (EC) with an ICCN EC.

[0036] FIG. 13B is a graph depicting galvanostatic charge/discharge (CC) curves of an ICCN EC measured at a high current density of $10 \text{ A/g}_{\text{ICCN}^{\text{electrode}}}$.

[0037] FIG. 13C is a graph of volumetric stack capacitance of an ICCN EC that is calculated from the CC curves at different charge/discharge current densities.

[0038] FIG. 13D is a graph of ICCN EC cyclic stability versus CC cycles.

[0039] FIG. 13E is a graph of a complex plane plot of the impedance of an ICCN EC, with a magnification for the high-frequency region in a graph inset.

[0040] FIG. 13F is a graph of impedance phase angle versus frequency for an ICCN EC and a commercial activated carbon EC.

[0041] FIG. 14A is a structural diagram of an assembled ICCN EC.

[0042] FIG. 14B is a graph of stack capacitance as a function of current density.

[0043] FIG. 14C is a graph of capacitance retention for the ICCN EC over a 4 month period.

[0044] FIG. 14D is a graph of cyclic voltammetry (CV) performance of the ICCN EC when tested under different bending conditions.

[0045] FIG. 14E is a graph of galvanostatic charge/discharge curves for four tandem ICCN ECs connected in series.

[0046] FIG. 14F is a graph of galvanostatic charge/discharge curves for four ICCN ECs in a series and parallel combination.

[0047] FIG. 15 is a graph of galvanostatic charge/discharge curves of the device when operated at an ultrahigh current density of $250 \text{ A/g}_{\text{ICCN/electrode}}$.

[0048] FIG. 16 is a Ragone plot comparing the performance of ICCN ECs with different energy storage devices designed for high power microelectronics.

[0049] FIG. 17A is a structural diagram showing a set of interdigitated electrodes made of ICCNs with dimensions of $6 \text{ mm} \times 6 \text{ mm}$, spaced at around about $500 \mu\text{m}$, that are directly patterned onto a thin film of GO.

[0050] FIG. 17B is a structural diagram showing the set of interdigitated electrodes transferred onto another type of substrate.

[0051] FIG. 18A shows an exploded view of a micro-supercapacitor made up of a plurality of expanded and interconnected carbon layers that are electrically conductive.

[0052] FIG. 18B shows the micro-supercapacitor of FIG. 18A after assembly.

[0053] FIG. 19A depicts a micro-supercapacitor configuration having a first electrode with two extending electrode digits that are interdigitated with two extending electrode digits of a second electrode.

[0054] FIG. 19B depicts a micro-supercapacitor configuration having a first electrode with four extending electrode digits that are interdigitated with four extending electrode digits of a second electrode.

[0055] FIG. 19C depicts a micro-supercapacitor configuration having a first electrode with eight extending electrode digits that are interdigitated with eight extending electrode digits of a second electrode.

[0056] FIG. 20 is a table listing dimensions for the micro-supercapacitors of FIGS. 19A-19C.

[0057] FIGS. 21A-21E depict the fabrication of ICCN micro-supercapacitors.

[0058] FIG. 22A depicts ICCN micro-devices with 4, 8, and 16 interdigitated electrodes.

[0059] FIG. 22B depicts an ICCN micro-device with 16 interdigitated fingers with $150\text{-}\mu\text{m}$ spacings.

[0060] FIG. 22C is a tilted view (45°) SEM image that shows the direct reduction and expansion of the GO film after exposure to the laser beam.

[0061] FIGS. 22D and 22E show I-V curves of GO and an ICCN, respectively.

[0062] FIG. 22F is a graphical comparison of electrical conductivity values for GO and an ICCN.

[0063] FIGS. 23A-23I are graphs depicting electrochemical performance of ICCN micro-supercapacitors in PVA- H_2SO_4 gelled electrolyte.

[0064] FIGS. 24A-24F are graphs depicting the behavior of ICCN micro-supercapacitors under mechanical stress in series and parallel configurations.

[0065] FIGS. 25A-25E are images depicting the fabrication of ICCN micro-supercapacitors on a chip along with graphs showing the characteristics of the micro-supercapacitors.

[0066] FIGS. 26A-26B are graphs depicting self discharge rates for ICCN micro-supercapacitors.

[0067] FIG. 27 is a Ragone plot of energy and power densities of ICCN micro-supercapacitors compared with commercially available energy storage systems.

DETAILED DESCRIPTION

[0068] The embodiments set forth below represent the necessary information to enable those skilled in the art to practice the disclosure and illustrate the best mode of practicing the disclosure. Upon reading the following description in light of the accompanying drawings, those skilled in the art will understand the concepts of the disclosure and will recognize applications of these concepts not particularly addressed herein. It should be understood that these concepts and applications fall within the scope of the disclosure and the accompanying claims.

[0069] The present disclosure provides an inexpensive process for making and patterning an ICCN having stringent requirements for a high surface area with highly tunable electrical conductivity and electrochemical properties. The embodiments described herein not only meet these stringent requirements, but provide direct control over the conductivity and patterning of an ICCN while creating flexible electronic devices in a single step process. Moreover, the production of the ICCN does not require reducing agents, or expensive equipment. The simple direct fabrication of an ICCN on flexible substrates therefore simplifies the development of lightweight electrical energy storage devices. The ICCN can be synthesized on various substrates, such as plastic, metal, and glass. Herein an electrochemical capacitor (EC), and in particular a micro-supercapacitor, is disclosed.

[0070] In at least one embodiment, the ICCNs are conducting films produced using a common and inexpensive infrared laser that fits inside a compact disc/digital versatile disc (CD/DVD) optical drive unit that provides a direct-to-disc label writing function. LightScribe (Registered Trademark of Hewlett Packard Corporation) and LabelFlash (Registered Trademark of Yamaha Corporation) are exemplary direct-to-disc labeling technologies that pattern text and graphics onto the surface of a CD/DVD disc. LightScribe DVD drives are commercially available for around \$20 and the LightScribing process is controlled using a standard desktop computer.

[0071] FIG. 1 depicts the label side of a standard direct-to-disc labeling type CD/DVD disc 10 that includes a label area 12 and a clamping area 14 that surrounds a centering hole 16. A dye film 18 covers the label area 12 and is sensitive to laser energy that is typically directed onto the label area 12 to produce a permanent visible image that may comprise graphics 20 and text 22. A position tracking indicia 24 is usable by an optical disc drive (not shown) to accurately locate an absolute angular position of the CD/DVD disc 10 within the optical disc drive so that the graphics 20 and/or text 22 can be re-written to provide increased contrast. Moreover, the position tracking indicia 24 is usable by the optical disc drive to allow additional graphics and/or text to be written without undesirably overwriting the graphics 20 and/or text 22.

[0072] FIG. 2 is a schematic of a prior art direct-to-disc labeling type optical disc drive system 26. In this exemplary case, the CD/DVD disc 10 is depicted in cross-section and loaded onto a spindle assembly 28 that is driven by a CD/DVD spindle motor 30. The label area 12 is shown facing a laser assembly 32 that includes a label writer laser

(LWL) **34**, a lens **36**, and a focus actuator **38**. The LWL **34** is typically a laser diode. Exemplary specifications for the LWL **34** includes a maximum pulse optical power of 350 mW at 780 nm emission and a maximum pulse output power of 300 mW at 660 nm emission. A laser beam **40** emitted by the LWL **34** is focused by the lens **36** that is alternately translated towards and away from the LWL **34** by the focus actuator **38** in order to maintain focus of the laser beam **40** onto the label area **12** of the CD/DVD disc **10**. The laser beam **40** is typically focused to a diameter that ranges from around 0.7 μm to around 1 μm .

[0073] The laser assembly **32** is responsive to a control system **42** that provides control signals **44** through an optical drive interface (ODI) **46**. The control system **42** further includes a central processor unit (CPU) **48** and a memory **50**. Label image data (LID) having information needed to realize a permanent image to be written onto the label area **12** of the CD/DVD disc **10** is processed by the CPU **48**, which in turn provides an LID stream signal **52** that pulses the LWL **34** on and off to heat the dye film **18** to realize the image defined by the LID.

[0074] The CPU **48** also processes the LID through the ODI **46** to provide a position control signal **54** to a radial actuator **56** that translates the laser assembly **32** in relation to the label area **12** in response to position information contained in the LID. In some versions of the present embodiments, the optical disc drive system **26** monitors the focus of the laser beam **40** with an optical receiver (not shown), so that the ODI **46** can generate a focus control signal **58** for the focus actuator **38**. The ODI **46** also provides a motor control signal **60** for the CD/DVD spindle motor **30** that maintains an appropriate rotation speed of the CD/DVD disc **10** while a label writing process is ongoing.

[0075] In some versions of the optical disc drive system **26** the LWL **34** is used exclusively for label writing directly to the label area **12** of the CD/DVD disc **10** and a separate laser diode (not shown) is used to write and/or read data to/from a data side **62** of the CD/DVD disc **10**. In other versions of the optical disc drive system **26**, the LWL **34** is used for label writing and data reading and/or writing. When the LWL **34** is used for data reading and/or writing, the CD/DVD disc **10** is flipped over to expose the data side **62** of the CD/DVD disc **10** to the laser beam **40**. In versions wherein the LWL **34** is also used as a data read/write laser, the laser assembly **32** includes optical pick-up components (not shown) such as a beam splitter and at least one optical receiver. The output power of the LWL **34** is typically around 3 mW during data read operations.

[0076] In order to use the optical disc drive system **26** to realize an inexpensive process for making and patterning an ICCN having a high surface area with highly tunable electrical conductivity and electrochemical properties, a carbon-based film is substituted for the dye film **18** (FIG. 1). In one embodiment, graphite oxide (GO) is synthesized from high purity graphite powder using a modified Hummer's method. Dispersions of GO in water (3.7 mg/mL) are then used to make GO films on various substrates. Exemplary substrates include but are not limited to polyethylene terephthalate (PET), nitrocellulose membrane (with 0.4 μm pore size), aluminum foil, carbonized aluminum, copper foil, and regular copier paper.

[0077] Referring to FIG. 3, a process **100** begins with providing graphite powder **64**. The graphite powder **64** undergoes an oxidation reaction using the modified Hum-

mer's method to become GO **66** (step **102**). However, it is to be understood that other oxidation methods for producing GO are available and such methods are within the scope of the present disclosure. An exfoliation procedure produces exfoliated GO **68** (step **104**). The exfoliation procedure may be accomplished via ultrasonication. It is to be understood that the exfoliated GO **68** results from a partial exfoliation and not a complete exfoliation to a single layer of GO. The partial exfoliation is used to create a high accessible surface area that enables a fast redox response which enables a fast sensor response. Additionally, the partial exfoliation of GO **68** provides the high surface area for growing metal nanoparticles that could then be used in catalysis. A substrate **70** carries a GO film **72** that is produced by a deposition procedure that deposits the exfoliated GO **68** onto the substrate **70** (step **106**). In at least some embodiments, a GO film **72** is made by either drop-casting or vacuum filtering GO dispersions onto the substrate **70** that is the size of a CD/DVD disc. The GO film **72** is typically allowed to dry for 24 hours under ambient conditions. However, controlling conditions to expose the GO film **72** to a relatively lower humidity and relatively higher temperature will dry the GO film **72** relatively quickly. The term GO herein refers to graphite oxide.

[0078] Referring to FIG. 4, individual ones of the GO film(s) **72** are then affixed to a substrate carrier **74**, which has dimensions similar to the CD/DVD disc **10** (FIG. 1)(step **200**). The substrate carrier **74** carrying the substrate **70** with the GO film **72** is loaded into the optical disc drive system **26** (FIG. 2) such that the GO film **72** faces the LWL **34** for laser treatment (step **202**). In this way, the present embodiments use the GO film **72** in place of the dye film **18** (FIG. 1). It is to be understood that the substrate carrier **74** can be a rigid or semi-rigid disc onto which the GO film **72** can be fabricated directly. In that case, the substrate carrier **74** replaces the function of the substrate **70**.

[0079] Images **76** for realizing electrical components **78** are patterned in concentric circles, moving outward from the center of the substrate carrier **74** (step **204**). The laser irradiation process results in the removal of oxygen species and the reestablishment of sp^2 carbons. This causes a change in the conductivity of the GO film **72** with a typical resistance of $>20 \text{ M}\Omega/\text{sq}$ to become a relatively highly conducting plurality of expanded and interconnected carbon layers that make up an ICCN **80**. The number of times the GO film **72** is laser treated results in a significant and controllable change in the conductivity of the ICCN **80**. The ICCN **80** has a combination of properties that includes high surface area and high electrical conductivity in an expanded interconnected network of carbon layers. In one embodiment, the plurality of expanded and interconnected carbon layers has a surface area of greater than around about 1400 m^2/g . In another embodiment, the plurality of expanded and interconnected carbon layers has a surface area of greater than around about 1500 m^2/g . In yet another embodiment, the surface area is around about 1520 m^2/g . In one embodiment, the plurality of expanded and interconnected carbon layers yields an electrical conductivity that is greater than around about 1500 S/m. In another embodiment, the plurality of expanded and interconnected carbon layers yields an electrical conductivity that is greater than around about 1600 S/m. In yet another embodiment, the plurality of expanded and interconnected carbon layers yields an electrical conductivity of around about 1650 S/m. In still another embodi-

ment, the plurality of expanded and interconnected carbon layers yields an electrical conductivity that is greater than around about 1700 S/m. In yet one more embodiment, the plurality of expanded and interconnected carbon layers yields an electrical conductivity of around about 1738 S/m. Moreover, in one embodiment, the plurality of expanded and interconnected carbon layers yields an electrical conductivity that is greater than around about 1700 S/m and a surface area that is greater than around about 1500 m²/g. In another embodiment, the plurality of expanded and interconnected carbon layers yields an electrical conductivity of around about 1650 S/m and a surface area of around about 1520 m²/g.

[0080] The electrical components **78** comprising electrodes **82** used in the fabrication of an electrochemical capacitor (EC) **84** are laser irradiated 6 times before reaching the relatively high conductivity of around about 1738 S/m. An exemplary laser irradiation process takes around about 20 minutes per cycle. However, it is to be understood that faster laser irradiation rates are possible depending on the power of the laser light emitted from the LWL **34** combined with an increased positioning rate of the substrate carrier. Moreover, other imaging techniques that employ photomasks and flashlamps may provide even faster fabrication of the electrical components **78**. Afterwards, the substrate **70** carrying the ICCN **80** and any remaining GO film **72** is removed from the substrate carrier **74** (step **206**). Next, the ICCN **80** is fabricated into the electrical components **78** that make up the EC **84** (step **208**). In this exemplary case, portions of the ICCN **80** on the substrate **70** are cut into rectangular sections to make the electrical components **78**, which include the electrodes **82** formed from the ICCN **80**. A separator/electrolyte **86** is sandwiched between the electrodes **82** to form the EC **84**.

[0081] The ICCN **80** possesses a very low oxygen content of only around about 3.5%, which contributes to a relatively very high charging rate. In other embodiments, the oxygen content of the expanded and interconnected carbon layers ranges from around about 1% to around about 5%. FIG. **5** is a line drawing of a sample of the ICCN **80**, which is made up of the plurality of expanded and interconnected carbon layers that include corrugated carbon layers such as a single corrugated carbon sheet **88**. In one embodiment, each of the expanded and interconnected carbon layers comprises at least one corrugated carbon sheet that is one atom thick. In another embodiment, each of the expanded and interconnected carbon layers comprises a plurality of corrugated carbon sheets **88**. The thickness of the ICCN **80**, as measured from cross-sectional scanning electron microscopy (SEM) and profilometry, was found to be around about 7.6 μm . In one embodiment, a range of thicknesses of the plurality of expanded and interconnected carbon layers making up the ICCN **80** is from around about 7 μm to 8 μm .

[0082] As an illustration of the diversity in image patterning that is possible, a complex image formed by the direct laser reduction of GO is shown in FIGS. **6A** and **6B**. FIG. **6A** is an artwork image of a man's head covered with circuits. FIG. **6B** is a photograph of a GO film after the artwork image of FIG. **6A** is directly patterned on the GO film using the laser scribing technique of the present disclosure. Essentially, any part of the GO film that comes in direct contact with the 780 nm infrared laser is effectively reduced to an ICCN, with the amount of reduction being controlled by the laser intensity; a factor that is determined by power density

of the laser beam impinging on the GO film. The resulting image of FIG. **6B** is an effective print of the original image of FIG. **6A**. However, in this case the image of FIG. **6B** is made up of various reductions of the GO film. As expected, the darkest black areas indicate exposure to the strongest laser intensities, while the lighter gray areas are only partially reduced. Since different grayscale levels directly correlate with the laser's intensity, it is possible to tune the electrical properties of the generated ICCN over five to seven orders of magnitude in sheet resistance (Q/sq) by simply changing the grayscale level used during the patterning process. As illustrated in FIG. **7**, there is a clear relationship between sheet resistance, grayscale level and the number of times the GO film is laser irradiated. Control over conductivity from a completely insulating GO film, with a typical sheet resistance value of >20 M Ω /sq, to a conducting ICCN that registers a sheet resistance value of approximately 80 Ω /sq, which translates to a conductivity of around about 1650 S/m, is possible. This method is sensitive enough to differentiate between similar grayscale levels as shown in the graph of FIG. **7**, where the sheet resistance varies significantly with only a small variation in grayscale level. In addition, the number of times a GO film is laser treated results in a significant and controllable change in sheet resistance. Each additional laser treatment lowers the sheet resistance as seen in FIG. **7**, where a film is laser irradiated once (black squares), twice (circles) and three times (triangles) with respect to the grayscale level. Therefore, the film's sheet resistance is tunable both by controlling the grayscale level used and the number of times the film is reduced by the laser, a property that has so far been difficult to control through other methods.

[0083] Scanning electron microscope (SEM) techniques are usable to understand the effects a low energy infrared laser has on the structural properties of GO film by comparing the morphological differences between an ICCN and untreated graphite oxide GO film. FIG. **8A** is an SEM image that illustrates the infrared laser's effect on GO film prior to laser treatment on the right side of the image in contrast to an aligned ICCN on the left side of the image that occurs after being reduced with the infrared laser. The image not only gives a clear definition between the ICCN and untreated GO regions, but also demonstrates the level of precision possible when using this method as a means to pattern and reduce GO. The regions of ICCN, which result from the laser treatment, can be further analyzed through cross-sectional SEM.

[0084] FIG. **8B** is an SEM image showing a cross-sectional view of a free standing film of laser treated and untreated GO film, which shows a significant difference between GO film thicknesses. As indicated by the white brackets in FIG. **8B**, an ICCN increases in thickness by approximately 10 times in comparison to that of untreated GO film. Moreover, a range of thicknesses of the plurality of expanded and interconnected carbon layers is from around about 7 μm to around 8 μm . In one embodiment, an average thickness of the plurality of expanded and interconnected carbon layers is around about 7.6 μm . The increased thickness stems from rapid degassing of gases generated and released during laser treatment, similar to thermal shock, which effectively causes the reduced GO to expand and exfoliate as these gases rapidly pass through the GO film. FIG. **8C** is an SEM image showing a cross-sectional view of

a single ICCN, which shows an expanded structure that is a characteristic of the ICCN of the present disclosure.

[0085] FIG. 8D is an SEM image showing a greater magnification of a selected area within the ICCN in FIG. 8C. The SEM image of FIG. 8D allows the thickness of the plurality of expanded and interconnected carbon layers to be calculated to be between around about 5-10 nm. However, the number of carbon layers in the plurality of expanded and interconnected carbon layers making up the ICCN is greater than around about 100. In another embodiment the number of carbon layers in the plurality of expanded and interconnected carbon layers is greater than around about 1000. In yet another embodiment the number of carbon layers in the plurality of expanded and interconnected carbon layers is greater than around about 10,000. In still another embodiment, the number of carbon layers in the plurality of expanded and interconnected carbon layers is greater than around about 100,000. The SEM analysis shows that although an infrared laser emission is only marginally absorbed by GO, enough power and focus (i.e., power density) can cause sufficient thermal energy to efficiently reduce, deoxygenate, expand, and exfoliate the GO film. Moreover, the surface area of the ICCN is greater than around about 1500 m²/g.

[0086] Since each of the carbon layers has a theoretical surface area of around about 2630 m²/g, a surface greater than around about 1500 m²/g indicates that almost all surfaces of the carbon layers are accessible. The ICCN has an electrical conductivity that is greater than around about 17 S/cm. The ICCN forms when some wavelength of light hits the surface of the GO, and is then absorbed to practically immediately convert to heat, which liberates carbon dioxide (CO₂). Exemplary light sources include but are not limited to a 780 nm laser, a green laser, and a flash lamp. The light beam emission of the light sources may range from near infrared to ultraviolet wavelengths. The typical carbon content of the ICCN is greater than around about 97% with less than around about 3% oxygen remaining. Some samples of the ICCN are greater than around about 99% carbon even though the laser reduction process is conducted in the air.

[0087] FIG. 9 compares a powder X-ray diffraction (XRD) pattern of the corrugated carbon-based network with both graphite and graphite oxide diffraction patterns. A typical XRD pattern for graphite, shown in FIG. 9 trace A, displays the characteristic peak of 2θ=27.8° with a d-spacing of 3.20 Å. An XRD pattern (FIG. 9, trace B) for GO, on the other hand, exhibits a single peak of 2θ=10.76°, which corresponds to an interlayer d-spacing of 8.22 Å. The increased d-spacing in GO is due to the oxygen containing functional groups in graphite oxide sheets, which tend to trap water molecules between the basal planes, causing the sheets to expand and separate. The XRD pattern of the corrugated carbon-based network (FIG. 9, trace C) shows the presence of both GO (10.76° 2θ) and a broad graphitic peak at 25.97° 2θ associated with a d-spacing of 3.43 Å. The GO presence in the corrugated carbon-based network is expected since the laser has a desirable penetration depth, which results in the reduction of only the top portion of the film with the bottom layer being unaffected by the laser. The small presence of GO is more prominent in thicker films, but begins to diminish in thinner films. In addition, one can also observe a partially obstructed peak at 26.66° 2θ, which shows a similar intensity to the broad 25.97° 2θ peak. Both of these

peaks are considered graphitic peaks, which are associated to two different lattice spacing between basal planes.

[0088] It has been previously shown that the immobilization of carbon nanotubes (CNTs) on glassy carbon electrodes will result in a thin CNT film, which directly affects the voltammetric behavior of the CNT modified electrodes. In a ferro/ferrocyanide redox couple, the voltammetric current measured at the CNT modified electrode will likely have two types of contributions. The thin layer effect is a significant contributor to the voltammetric current. The thin layer effect stems from the oxidation of ferrocyanide ions, which are trapped between the nanotubes. The other contribution results from the semi-infinite diffusion of ferrocyanide towards the planar electrode surface. Unfortunately, the mechanistic information is not easily de-convoluted and requires knowledge of the film thickness.

[0089] In contrast, no thin layer effect is observed in association with the interconnected corrugated carbon-based network of the present disclosure. FIG. 10 is a plot of log₁₀ of peak current versus log₁₀ of an applied voltammetric scan rate. In this case, no thin layer effect is observed since the plot has a consistent slope of 0.53 and is linear. The slope of 0.53 is relatively close to theoretical values calculated using a semi-infinite diffusion model governed by the Randles-Sevcik equation:

$$i_p = 0.3443A C_o \sqrt{\frac{D_o v (nF)^3}{RT}}$$

[0090] Raman spectroscopy is used to characterize and compare the structural changes induced by laser treating GO film. FIGS. 11A-11E are graphs related to Raman spectroscopic analysis. As can be seen in FIG. 11A, characteristic D, G, 2D and S3 peaks are observed in both GO and the ICCN. The presence of the D band in both spectra suggests that carbon sp³ centers still exist after reduction. Interestingly, the spectrum of the ICCN shows a slight increase in the D band peak at around about 1350 cm⁻¹. This unexpected increase is due to a larger presence of structural edge defects and indicates an overall increase in the amount of smaller graphite domains. The result is consistent with SEM analysis, where the generation of exfoliated accordion-like graphitic regions (FIG. 5) caused by the laser treatment creates a large number of edges. However the D band also shows a significant overall peak narrowing, suggesting a decrease in these types of defects in the ICCN. The G band experiences a narrowing and a decrease in peak intensity as well as a peak shift from around about 1585 to 1579 cm⁻¹. These results are consistent with the re-establishment of sp² carbons and a decrease in structural defects within the basal planes. The overall changes in the G band indicate a transition from an amorphous carbon state to a more crystalline carbon state. In addition, a prominent and shifted 2D peak from around about 2730 to around about 2688 cm⁻¹ is seen after GO is treated with the infrared laser, indicating a considerable reduction of the GO film and strongly points to the presence of a few-layer interconnected graphite structure. In one embodiment, the 2D Raman peak for the ICCN shifts from around about 2700 cm⁻¹ to around about 2600 cm⁻¹ after the ICCN is reduced from a carbon-based oxide. Moreover, as a result of lattice disorder, the combination of D-G generates an S3 second order peak, which appears at

around about 2927 cm^{-1} and, as expected, diminishes with decreasing disorder after infrared laser treatment. In some embodiments, the plurality of expanded and interconnected carbon layers has a range of Raman spectroscopy S3 second order peak that ranges from around about 2920 cm^{-1} to around about 2930 cm^{-1} . The Raman analysis demonstrates the effectiveness of treating GO with an infrared laser as a means to effectively and controllably produce the ICCN.

[0091] X-ray photoelectron spectroscopy (XPS) was employed to correlate the effects of laser irradiation on the oxygen functionalities and to monitor the structural changes on the GO film. Comparing the carbon to oxygen (C/O) ratios between GO and the ICCN provides an effective measurement of the extent of reduction achieved using a simple low energy infrared laser. FIG. 11B illustrates the significant disparity between the C/O ratios before and after laser treatment of the GO films. Prior to laser reduction, typical GO films have a C/O ratio of approximately 2.6:1, corresponding to a carbon/oxygen content of around about 72% and 38%. In one exemplary embodiment, the ICCN has an enhanced carbon content of around about 96.5% and a diminished oxygen content of around about 3.5%, giving an overall C/O ratio of 27.8:1. In yet another exemplary embodiment, a laser reduction of GO results in a C/O ratio of 333:1, which is around about 0.3% oxygen content. This relatively low oxygen content was measured using photoelectron spectroscopy (XPS). In other embodiments, the plurality of expanded and interconnected carbon layers has a C/O ratio that ranges from around about 333:1 to around about 25:1. Since the laser reduction process takes place under ambient conditions, it is postulated that some of the oxygen present in the ICCN film is a result of the film having a static interaction with oxygen found in the environment.

[0092] FIG. 11C shows that the C1s XPS spectrum of GO displays two broad peaks, which can be resolved into three different carbon components corresponding to the functional groups typically found on the GO surface, in addition to a small π to π^* peak at 290.4 eV. These functional groups include carboxyl, sp^3 carbons in the form of epoxide and hydroxyl, and sp^2 carbons, which are associated with the following binding energies: approximately 288.1, 286.8 and 284.6 eV, respectively.

[0093] FIG. 11D shows expected results, in that the large degree of oxidation in GO results in various oxygen components in the GO C1s XPS spectrum. These results are in contrast to the ICCN, which shows a significant decrease in oxygen containing functional groups and an overall increase in the C—C sp^2 carbon peak. This points to an efficient deoxygenating process as well as the re-establishment of C=C bonds in the ICCN. These results are consistent with the Raman analysis. Thus, an infrared laser such as the LWL 34 (FIG. 2) is powerful enough to remove a majority of the oxygen functional groups, as is evident in the XPS spectrum of the ICCN, which only shows a small disorder peak and a peak at 287.6 eV. The latter corresponds to the presence of sp^a type carbons suggesting that a small amount of carboxyl groups remain in the final product. In addition, the presence of a π to π^* satellite peak at 290.7 eV indicates that delocalized π conjugation is significantly stronger in the ICCN as this peak is miniscule in the GO XPS spectrum. The appearance of the delocalized π peak is a clear indication that conjugation in the GO film is restored during the laser reduction process and adds support that an sp^2 carbon network has been re-established. The decreased intensity of

the oxygen containing functional groups, the dominating C=C bond peak and the presence of the delocalized π conjugation all indicate that a low energy infrared laser is an effective tool in the generation of the ICCN.

[0094] FIG. 11E depicts UV-visible light absorbance spectra of GO shown in black. The inset shows a magnified view of the boxed area showing the absorbance of GO with respect to a 780 nm infrared laser in the 650 to 850 nm region.

[0095] Having established that an ICCN has an effective π conjugation, it is possible to construct devices to make use of the conducting material. In this regard, at least one embodiment of the present disclosure provides the production of ICCN ECs through a simple all-solid-state approach that avoids the restacking of carbon sheets such as the corrugated carbon sheet 88 (FIG. 5). Irradiation of the GO film 72 (FIG. 3) with an infrared laser such as the LWL 34 (FIG. 2) inside the inexpensive commercially available direct-to-disc labeling type optical disc drive system 26 (FIG. 2) which, as discussed above, reduces the GO film 72 to an ICCN, as indicated by the change in film color from golden brown to black. Analysis of cross sections of the film with scanning electron microscopy showed that the initially stacked GO sheets were converted into partially-exfoliated carbon sheets through laser irradiation (FIG. 3). The resulting ICCN showed excellent conductivity (around about 1738 S/m) as opposed to 10 to 100 S/m for activated carbons, the current state-of-the-art material used in commercial devices.

[0096] In addition, FIGS. 12A and 12B show that the ICCN made up of corrugated carbon sheets shows excellent mechanical flexibility with only around about 1% change in the electrical resistance of the film after 1000 bending cycles. Thus, ICCNs can be directly used as EC electrodes without the need for any additional binders or conductive additives. More importantly, these properties allow ICCNs to act as both an active material and current collector in the EC. The combination of both functions in a single layer leads to a simplified and lightweight architecture. Thus, a device can be readily made by sandwiching an ion porous separator [Celgard 3501 (Celgard, Charlotte, N.C.)] between two ICCN electrodes. ICCN ECs are relatively thin with a total thickness of less than around about 100 μm , making them potentially useful in microdevice applications. Other devices can be made by putting ICCNs on porous substrates such as a nitrocellulose membrane or photocopy paper or on conductive aluminum foil, which is often used in commercial devices. Therefore, ICCN ECs can be readily made into different designs, including stacked and spirally wound structures to target different applications.

[0097] The ICCN electrodes are fabricated to satisfy the critical features for high-performance ECs. First, the relatively large and accessible specific surface area of an ICCN (1520 m^2/g compared with 1000 to 2000 m^2/g for a typical activated carbon material) results in a sizeable charge storage capacity and accounts for the high areal and volumetric stack capacitances observed. Second, the LWL 34 (FIG. 2) that is typically a LightScribe or a LabelFlash laser, causes the simultaneous reduction and partial exfoliation of GO sheets and produces the ICCN 80 (FIG. 5). The novel structure of the ICCN 80 is porous, which prevents the agglomeration of carbon sheets, which has been a major barrier in achieving the full potential of carbon-based ECs. The network structure of the ICCN 80 has open pores, which

facilitates electrolyte accessibility to the electrode surfaces. This offers an opportunity to optimize ionic diffusion in the electrodes **82**, which is crucial for charging the electrochemical double layers (EDLs), and generates high power ECs. Moreover, the ICCN **80** possesses excellent electronic conductivity, which is another key factor for achieving high power. Working with these properties, three dimensional composite electrodes have been successfully used to make batteries with relatively high energy density and fast charge/discharge rates. Although activated carbons can provide high surface area, the difficulty of controlling their pore structure and pore size distribution has so far limited the energy densities and rate capabilities of commercial ECs.

[0098] In order to demonstrate the superior performance of ICCN electrodes for electrochemical energy storage, symmetric ICCN ECs were assembled using polyethylene terephthalate (PET) as a thin flexible substrate and an aqueous electrolyte of 1.0 molar (M) phosphoric acid (H_3PO_4). As shown in FIGS. **13A-13F**, the ICCN EC performance was analyzed through both cyclic voltammetry (CV) and galvanostatic charge/discharge (CC) experiments. In comparison with GO, the ICCN EC shows an enhanced electrochemical performance with a nearly rectangular CV shape at a scan rate of 1000 mV/s, which is indicative of nearly ideal capacitive behavior (FIG. **13A**) even though no metal current collectors, binders, or electroactive additives were used, as is the case in commercial ECs. Additionally, the ICCN EC is robust enough to be charged and discharged over a wide range of scan rates (100 to 10,000 mV/s) and still maintain its nearly ideal rectangular CV shape. FIG. **13B** shows the nearly triangular shape of the CC curves obtained at a high current density of 10 A/g of ICCN per electrode (abbreviated 10 A/g_{ICCN/electrode}). This is indicative of the formation of an efficient EDL and fast ion transport within the ICCN electrodes. In addition, these CC curves show only a small voltage drop of 0.018 V at the start of the discharge curve, indicating a device with a low equivalent series resistance (ESR). The specific capacitance from the CC curves was measured over a wide range of charge/discharge current densities. Here, the areal and volumetric capacitances of the stack (this includes the flexible substrate, the current collector, the active material, and the separator) were calculated and compared with a commercial activated-carbon EC (AC-EC) tested under the same dynamic conditions. Although the AC-EC shows a slightly higher volumetric capacitance at low charge/discharge rates, its capacitance falls off quickly at higher rates, whereas the ICCN EC continues to provide high capacitance even when operated at very high rates (FIG. **13C**). In addition, the areal capacitance of the ICCN EC was calculated to be 3.67 mF/cm² and 4.04 mF/cm² in 1.0 M H_2SO_4 at 1 A/g_{ICCN/electrode}. The device also shows a very high rate capability while still maintaining a capacitance of more than 1.84 mF/cm², even when the ICCN EC is operated at an ultrafast charge/discharge rate of 1000 A/g_{ICCN/electrode}. This is comparable with values reported in the literature for micro-devices and thin film ECs at much lower current charge/discharge rates (0.4 to 2 mF/cm²). These ECs can be efficiently charged/discharged on the 0.1-s time scale. Additionally, the ICCN EC retained around about 96.5% of its initial capacitance after 10,000 cycles (FIG. **13D**).

[0099] Electrochemical impedance spectroscopy (EIS) confirmed fast ion transport within the ICCN electrodes. A complex plan plot of the impedance data of the ICCN EC is

shown in FIG. **13E** with an expanded view provided in the inset. The device displays a pure capacitive behavior, even at high frequencies of up to ~158 Hz. The series resistance of the device is estimated to be ~16 ohms. This value can be attributed to the contact resistance of the device with the external circuit that could be reduced by using current collectors. The dependence of the phase angle on the frequency for the ICCN EC, AC-EC, and an aluminum electrolytic capacitor is shown in FIG. **13F**. For frequencies up to 10 Hz, the phase angle of the ICCN EC is close to -90° , which suggests that the device functionality is close to that of an ideal capacitor. The characteristic frequency f_0 for a phase angle of -45° is 30 Hz for the ICCN EC. This frequency marks the point at which the resistive and capacitive impedances are equal. The corresponding time constant τ_0 ($=1/f_0$) equals 33 ms compared with 10 seconds for the conventional AC-EC and 1 ms for the aluminum electrolytic capacitor. This rapid frequency response of the ICCN EC can be accounted for by the large and accessible surface area of the ICCN, whose exposed flat sheets enhance the ion transport rate in the device. This is consistent with results reported recently for an EC made from vertically oriented graphene nanosheets grown directly on metal current collectors and carbon nanotube electrodes made with an electrophoretic deposition technique.

[0100] The future development of multifunctional flexible electronics such as roll-up displays, photovoltaic cells, and even wearable devices presents new challenges for designing and fabricating lightweight, flexible energy storage devices. Commercially available ECs consist of a separator sandwiched between two electrodes with liquid electrolyte, which is then either spirally wound and packaged into a cylindrical container or stacked into a button cell. Unfortunately, these device architectures not only suffer from the possible harmful leakage of electrolytes, but their design makes it difficult to use them for practical flexible electronics. Referring to FIG. **14A** depicting the structure of the EC **84**, the liquid electrolyte was replaced with poly(vinyl alcohol) (PVA)- H_3PO_4 polymer gelled electrolyte, which also acts as the separator. This electrolyte reduced the device thickness and weight compared with phosphoric acid and simplified the fabrication process because it does not require any special packaging materials. As demonstrated in FIG. **14B**, at any given charge/discharge rate, the specific capacitance values for the all-solid-state device were comparable with those obtained with an aqueous electrolyte. The high-rate performance of the EC **84** can be accounted for by the porous structure of the ICCN electrodes, which can effectively absorb the gelled electrolyte and act as an electrolyte reservoir to facilitate ion transport and minimize the diffusion distance to the interior surfaces. Another key factor is that ICCN electrodes are binder free, thus enabling a reduction in interfacial resistance and enhancing the electrochemical reaction rate. As illustrated in FIG. **14C**, the device performance was completely stable over 4 months of testing. As with the aqueous ICCN EC, the flexible all-solid-state ICCN EC maintains its excellent cycling stability: >97% of the initial capacitance was maintained even after 10,000 cycles.

[0101] In order to evaluate under real conditions the potential of all-solid-state ICCN ECs, such as the EC **84**, for flexible energy storage, a device was placed under constant mechanical stress and its performance analyzed. FIG. **14D** shows the CV performance of this device when tested under

different bending conditions. The bending had almost no effect on the capacitive behavior; it can be bent arbitrarily without degrading performance. Moreover, the stability of the device was tested for more than 1000 cycles while in the bent state, with only ~5% change in the device capacitance. This performance durability can be attributed to the high mechanical flexibility of the electrodes along with the interpenetrating network structure between the ICCN electrodes and the gelled electrolyte. The electrolyte solidifies during the device assembly and acts like a glue that holds all the device components together, improving the mechanical integrity and increasing its cycle life even when tested under extreme bending conditions. Because the increased cycle life of the present EC has yet to be realized in commercial devices, the present ECs may be ideal for next-generation flexible, portable electronics.

[0102] Portable equipment often requires cells packaged either in series, in parallel, or in combinations of the two in order to meet energy and power requirements. For example, laptop batteries commonly have four 3.6-V lithium ion cells connected in series to achieve a voltage of 14.4 V, and two in parallel to increase the capacity from 2400 mAh to 4800 mAh. Thus, it would be of interest to develop an EC that could exhibit control over the operating voltage and current by using tandem serial and parallel assemblies with minimal energy losses. The performances of a set of tandem ICCN ECs were evaluated by assembling four devices both in series and in parallel configurations. Compared with a single EC, which operates at 1.0 V, the tandem series ECs exhibited a 4.0 V charge/discharge voltage window. In the parallel assembly, the output current increased by a factor of 4, and thus the discharge time was four times that of a single device when operated at the same current density. As expected, when the four ECs were combined, two in series and two in parallel, both the output voltage and the runtime (capacitive current) increased by a factor of 2 under the same charge/discharge current. As with the single devices, the tandem devices show essentially perfect triangular CC curves with a miniscule voltage drop, which again indicates excellent capacitive properties with minimal internal resistance. Thus, when used in tandem, the ICCN ECs undergo minimal energy losses. As a demonstration, a tandem EC's ability to light a red light-emitting diode (LED) that operates at a minimum voltage of 2 V is shown in the FIGS. 14E and 14F.

[0103] An organic electrolyte was also examined, and was discovered to allow the operation of the devices at higher voltages, thus achieving higher energy densities. In this case, tetraethylammonium tetrafluoroborate dissolved in acetonitrile was used because this is the most common organic electrolyte used in commercial devices. As shown in FIG. 15, the ICCN EC again exhibits enhanced performance and rate capabilities when compared with the commercial AC-EC; this is consistent with the data acquired in the aqueous and gelled electrolytes. Furthermore, the ICCN EC can be operated over a wider voltage window of 3 V. This ICCN EC offers a specific capacitance of up to 4.82 mF/cm² (265 F/g_{ICCN/electrode}) and retains a capacitance of 2.07 mF/cm² when operated at the ultrahigh current density of 1000 A/g_{ICCN/electrode}. Recently, room-temperature ionic liquids have been intensively studied as an attractive alternative to conventional electrolytes for ECs because of their high ion density, good thermal stability, and nonvolatility, as well as their wider potential window when compared with organic electrolytes. An ICCN EC was fabricated using the ionic

liquid 1-ethyl-3-methylimidazoliumtetrafluoroborate (EMIMBF₄) that exhibited a specific capacitance as high as 5.02 mF/cm² (276 F/g_{ICCN/electrode}) and at a wider potential window of 4 V. A prototype ICCN EC was made and encapsulated in the EMIMBF₄ electrolyte, charged at a constant potential of 3.5 V, and used to energize a red LED for ~24 minutes.

[0104] FIG. 16 is a Ragone plot comparing the performance of ICCN ECs with different energy storage devices designed for high power microelectronics. FIG. 16 also shows the overall performance of the ICCN ECs using various electrolytes. The Ragone plot includes a commercial 2.75 V/44 mF AC-EC and a 4 V/500-μAh thin film lithium battery and a 3 V/300 μF aluminum electrolytic capacitor, all tested under the same dynamic conditions. The plot shows the volumetric energy density and power density of the stack for all the devices tested. The ICCN EC can exhibit energy densities of up to 1.36 mWh/cm³, which is a value that is approximately two times higher than that of the AC-EC. Additionally, ICCN ECs can deliver a power density of around about 20 W/cm³, which is 20 times higher than that of the AC-EC and three orders of magnitude higher than that of the 4 V/500-μAh thin film lithium battery. Although the electrolytic capacitor delivers ultrahigh power, it has an energy density that is three orders of magnitude lower than the ICCN EC. Because of the simplicity of the device architecture and the availability of the GO precursor which is already manufactured on the ton scale, the ICCN ECs of the present embodiments hold promise for commercial applications.

[0105] Embodiments of the present disclosure also include other types of ECs, such as planar and interdigitated ECs. For example, FIG. 17A shows a set of interdigitated electrodes with dimensions of 6 mm×6 mm, spaced at around about 500 μm, that are directly patterned onto a thin film of GO. Prior to being patterned, the GO film was deposited on a thin flexible substrate, polyethylene terephthalate (PET), in order to fabricate a set of electrodes that are mechanically flexible. The top arrow points to the region of the ICCN that makes up the black interdigitated electrodes, while the bottom arrow points to the un-reduced GO film. Since the electrodes are directly patterned onto the GO film on a flexible substrate, the need for post-processing such as transferring the film to a new substrate is unnecessary. Although, if desired, a peel and stick method could be used to selectively lift-off the black interdigitated electrodes made of ICCN(s) with e.g. polydimethylsiloxane (PDMS) and transfer it onto other types of substrates (FIG. 17B). The simplicity of this method allows substantial control over pattern dimensions, substrate selectivity and electrical properties of the ICCN(s) by controlling laser intensity and thereby the amount of reduction in each film.

[0106] These interdigitated electrodes can, in turn, be used to construct supercapacitors. FIG. 18A shows an exploded view of a micro-supercapacitor 90 having a first electrode 92 and a second electrode 94 that are fabricated from ICCNs made up of a plurality of expanded and interconnected carbon layers that are electrically conductive. It is to be understood that optionally either the first electrode 92 or the second electrode 94 can be made of a metal, while the remaining one of either the first electrode 92 or the second electrode 94 is made of ICCNs. However, the first electrode 92 and the second electrode 94 are typically laser scribed from a GO film disposed onto a suitable substrate 96 such as

PET or silicon (Si) having an insulating layer **97** such as a silicon dioxide (SiO₂) layer. A first conductive strip **98** and a second conductive strip **100** are interfaced with the first electrode **92** and the second electrode **94** to provide electrically conductive terminals to couple to external circuitry (not shown). Exemplary external circuitry to be powered by the micro-supercapacitor **90** can be, but is not limited to, integrated circuits and other electrically powered micro-scale devices. A liner **102** that is non-electrically conductive covers the portions of the first electrode **92** and the second electrode **94** that are interfaced with the first conductive strip **98** and the second conductive strip **100**. The liner **102** includes a central window through which an electrolyte **104** is placed in contact with the first electrode **92** and the second electrode **94**. A polyimide tape can be used as the liner **102**. The electrolyte is preferably a gel electrolyte such as fumed silica (FS) nano-powder mixed with an ionic liquid. An exemplary ionic liquid is 1-butyl-3-methylimidazolium bis(trifluoromethylsulfonyl)imide. Another suitable gel electrolyte is a hydrogel such as poly(vinyl alcohol) (PVA)-H₂SO₄. Other electrolytes are also suitable, but the disclosed electrolytes provide a voltage window between a maximum charged voltage and a minimum discharged voltage of around about 2.5V.

[0107] FIG. 18B depicts the micro-supercapacitor **90** fully assembled. In this exemplary depiction, the first conductive strip **98** becomes a positive terminal and the second conductive strip **100** becomes a negative terminal. It is to be understood that the first conductive strip **98** and the second conductive strip **100** may be made from an electrical conductor such as copper (Cu), aluminum (Al), and/or additional ICCN structures.

[0108] FIG. 19A depicts a micro-supercapacitor configuration having a first electrode **106** with two extending electrode digits **108A** and **108B**. A second electrode **110** has two extending electrode digits **112A** and **112B** that are interdigitated with the extending electrode digits **108A** and **108B**.

[0109] FIG. 19B depicts another micro-supercapacitor configuration having a first electrode **114** with four extending electrode digits **116A** through **116D**. A second electrode **118** has four extending electrode digits **120A** through **120D** that are interdigitated with the four extending electrode digits **116A** through **116D**.

[0110] FIG. 19C depicts yet another micro-supercapacitor configuration having a first electrode **122** with eight extending electrode digits **124A** through **124H**. A second electrode **126** has eight extending electrode digits **128A** through **128H** that are interdigitated with the eight extending electrode digits **124A** through **124H**.

[0111] FIG. 20 is a table listing exemplary dimensions for the micro-supercapacitors of FIGS. 19A-19C. Referring to both FIG. 20 and FIG. 19A, the extending electrode digits **108A**, **108B**, **112A**, and **112B** are depicted with exemplary individual widths (W) of 1770 μm . The extending electrode digits **108A**, **108B**, **112A**, and **112B** are depicted with an exemplary length (L) of 4800 μm .

[0112] Referring to both FIG. 19B and FIG. 20, the width of the extending electrode digits **116A** through **116D** and the extending electrode digits **120A** through **120D** are depicted with exemplary individual widths of 810 μm . Referring to both FIG. 19C and FIG. 20, the extending electrode digits **124A** through **124H** and the extending electrode digits **128A** through **128H** are depicted with exemplary individual

widths of 330 μm . The exemplary configurations shown in FIGS. 19A, 19B, and 19C all have an exemplary edge dimension (E) of 200 μm , and an exemplary interspace dimension (I) that separates the first electrodes **106**, **114**, and **122** from the second electrodes **110**, **118**, and **126** with a serpentine gap. Moreover, the exemplary micro-supercapacitor configurations shown in FIGS. 19A, 19B, and 19C each have a total area 40 mm². In regard to the micro-supercapacitor configurations of FIGS. 19A, 19B, and 19C, it is to be understood that ranges of widths (W) are available for each of the first extending electrode digits **108A**, **108B**, **116A** through **116D**, and **124A** through **124H** and each of the second extending electrode digits **112A**, **112B**, **120A** through **120D**, and **128A** through **128H**. In various exemplary embodiments, the width (W) of each of the first extending electrode digits **108A**, **108B**, **116A** through **116D**, and **124A** through **124H** and for each of the second extending electrode digits **112A**, **112B**, **120A** through **120D**, and **128A** through **128H** are greater than around about 330 μm , or greater than around about 810 μm , or greater than around about 1770 μm in width. Moreover, ranges of interspace distance (I) between the first extending electrode digits **108A**, **108B**, **116A** through **116D**, and **124A** through **124H** and each of the second extending electrode digits **112A**, **112B**, **120A** through **120D**, and **128A** through **128H** respectively, may be less than around about 150 μm , or less than around about 100 μm , or less than around about 50 μm . The edge dimension (E) can also have multiple ranges that are around about the same dimensions as those given for the ranges of width (W). These various dimensions provide various area ranges for the micro-supercapacitor configurations of FIG. 19A. For example, in one embodiment, a total geometric area of each of the first electrodes **106**, **114**, and **122** and each of the second electrodes **110**, **118** and **126** is less than around about 50 mm². In another embodiment, a total geometric area of each of the first electrodes **106**, **114**, and **122** and each of the second electrodes **110**, **118** and **126** is less than around about 40 mm². In yet another embodiment, a total geometric area of each of the first electrodes **106**, **114**, and **122** and each of the second electrodes **110**, **118** and **126** is less than around about 30 mm².

[0113] It is to be understood that the physical size of the supercapacitors of the present disclosure is only limited by the wavelength of light that exfoliates ICCN patterns into GO. Therefore, supercapacitors produced according to the present disclosure range from the macro-scale that includes supercapacitors large enough to power electric vehicles and supply industrial electrical power grids down to nano scale nano-supercapacitors that are useable to power nano sized devices such as nanoelectromechanical (NEMS) devices.

[0114] Between the macro-scale and the nano-scale is a sub-micron scale that includes a range of micro-supercapacitors that are useable to power integrated circuits. For example, the first electrode and the second electrode have dimensions around about a sub-micron range. As such, these micro-supercapacitors can be integrated with integrated circuitry such that the integrated circuitry and micro-supercapacitors can be fabricated into a single integrated circuit package.

[0115] The ICCNs of the present disclosure are also usable to fabricate relatively large first and second electrodes separated by an electrolyte that provides enough charge storage capacity to power passenger car sized electric vehicles. Moreover, supercapacitors fabricated in accor-

dance with the present disclosure are also usable to supply electrical power to industrial electrical power grids during peak power demands. For example, the first electrode and the second electrode of a supercapacitor according to the present disclosure can be sized to supply peak power to a megawatt capacity electrical power grid.

[0116] A process for fabricating the supercapacitors of the present disclosure is schematically illustrated in FIG. 21A. Circuits designed on a computer can be patterned onto the GO film 72 on the substrate 70 which is carried by a substrate carrier such as a DVD disc. In the process GO absorbs high intensity light from a light source such as the laser beam 40 and is converted into ICCN(s). By using the precision of a laser such as the LWL 34, a direct-to-disc labeling drive renders a computer-designed pattern onto the GO film 72 to produce desired ICCN circuits. In this way, interdigitated ICCN electrodes 92 and 94 can be readily scribed on the GO film and transferred to the substrate 96 as shown in FIG. 21B. With its nearly insulating properties, GO serves as a good separator between the positive and negative ICCN interdigitated electrodes. These ICCN circuits can thus be directly used as planar micro-supercapacitors after receiving an electrolyte overcoat, as depicted in FIG. 21C. Unlike conventional micro-fabrication methods, this direct “writing” technique does not require masks, expensive materials, post-processing or clean room operations. Furthermore, the technique is cost effective and readily scalable. For example, using an exemplary design chosen for this work, 112 micro-supercapacitors 130 were produced on a single piece of GO deposited on a flexible DVD disc-shaped substrate 132 as depicted in FIG. 21D. Interdigitated electrodes can be precisely patterned with a lateral spatial resolution of around about 20 μm using direct-to-disc labeling. This technique is thus appropriate for the fabrication of high-resolution micro-supercapacitors taking into account that the interdigitated electrodes made with conventional micro-fabrication techniques are usually on the order of around about 100 μm .

[0117] The laser scribing process of the present disclosure is associated with significant changes in the optical properties, the electrical properties and the structure of the film. For example, GO changes from a golden brown color to black; a direct impact of the reduction of GO into an ICCN. FIG. 22A shows a line drawing of the as-prepared ICCN micro-supercapacitors 134. In particular, a micro-device 136 having 4 interdigitated electrodes, 2 positive and 2 negative; along with another micro device having 8 interdigitated electrodes, 4 positive and 4 negative; are shown with yet another micro-device 140 with 16 interdigitated microelectrodes, 8 positive and 8 negative. FIG. 22B is a line drawing of an optical microscope image showing a well-defined pattern with no short circuits between the microelectrodes. FIG. 22C shows the expansion of the GO film when treated with the laser, thus enabling full access to the electrode surface that is essential for charging the electrodes. Analysis of the cross-section of the micro-device reveals a thickness of 7.6 μm . For comparison, I-V tests were carried out for both GO and an ICCN as shown in FIGS. 22D and 22E, respectively. The GO film exhibits nonlinear and slightly asymmetric behavior with a differential conductivity value ranging from around about 8.07×10^{-4} through 5.42×10^{-3} S/m depending on the gate voltage. Reducing GO within the direct-to-disc labeling laser results in a linear I-V curve associated with a significant increase in the film conductivity

to around about 2.35×10^3 S/m as calculated for the ICCN as depicted in FIG. 22F. Because of its high electrical conductivity and exceptionally high surface area of over 1500 m^2/g , the ICCN can serve as both the electrode material and current collector. This simplifies the fabrication process and results in cost-effective micro-supercapacitors.

[0118] In order to understand the role of the micro-scale architecture of the device on its electrochemical properties, different configurations were designed and tested. Micro-supercapacitors with 4 (MSC4), 8 (MSC8), and 16 (MSC16) interdigitated microelectrodes were constructed and their electrochemical performance at 1,000, 5,000 and 10,000 mV/s tested, as shown in FIGS. 23A-23C. A hydrogel-polymer electrolyte, PVA- H_2SO_4 , was used to fabricate the all-solid-state micro-supercapacitors. A sandwich-type ICCN supercapacitor was also tested for comparison.

[0119] The CV profiles are all rectangular in shape, confirming the formation of an efficient electrochemical double layer (EDL) capacitor and fast charge propagation within the electrodes. Even at an ultrafast scan rate of 10,000 mV/s, the CV remains rectangular in shape indicating the high power capability of this micro-supercapacitor. Volumetric and areal capacitances give a more accurate picture of the true performance of a supercapacitor compared with gravimetric values. This is even more relevant in the case of micro-devices since the mass of the active material is very small. Therefore, calculations of the specific capacitance of the micro-devices have been made based on the volume of the stack. This includes the combined volume of the active material, current collector and the gap between the electrodes. The stack capacitances of the different micro-supercapacitors as a function of the scan rate are shown in FIG. 23D. Interestingly, the micro-devices show higher capacitance when using the interdigitated structure as opposed to the sandwich structure. Furthermore, the more interdigitated electrodes per unit area, the more power and energy can be extracted from the micro-devices. This can be explained by the unique porous network structure of the ICCN electrodes that helps minimize the pathway for ion diffusion from the electrolyte to the electrode material. Moreover, the micro-scale architecture of the devices results in a significant reduction of the mean ionic diffusion pathway between two microelectrodes. This effect becomes even more pronounced when increasing the number of interdigitated electrodes per unit area. This allows for maximizing the available electrochemical surface area and results in the increased capacitance and the fast charge/discharge rates observed with the micro-devices.

[0120] These conclusions are confirmed by the galvanostatic charge/discharge (CC) curves depicted in FIG. 23E. Note that all the micro-devices, regardless of whether they possess 4, 8 or 16 interdigitated electrodes, show nearly ideal triangular CC curves obtained at an ultrahigh current density of around about 1.684×10^4 mA/cm^2 . The voltage drop at the beginning of each discharge curve, known as the iR drop, is a measure of the overall resistance of the device and since its value is proportional to the discharge current, the small iR drop shown in FIG. 23E at a high discharge current indicates a very low resistance for all micro-supercapacitors tested.

[0121] The iR drop gradually decreases from ICCN-MSC (4) through ICCN-MSC(16), thus confirming the increase in power density of the micro-devices with an increasing number of interdigitated electrodes per unit area. FIG. 23F

shows the volumetric capacitance of the stack as a function of the current density for the ICCN micro-supercapacitor for both the interdigitated and sandwich structures. For comparison, the data for a commercial activated carbon supercapacitor obtained under the same dynamic conditions is also shown. Not only does the activated carbon supercapacitor exhibit lower capacitance, but its performance falls off very quickly at higher charge/discharge rates because of the limited diffusion of ions in the inner porous network of the activated carbon. The surface of the ICCN, on the other hand, is highly accessible to the electrolyte with very little impediment to ion transport, thus providing high capacitance even when operated at ultrahigh charge/discharge rates. For example, ICCN-MSG(16) exhibits a stack capacitance of around about 3.05 F/cm^3 at 16.8 mA/cm^2 and maintains 60% of this value when operated at an ultrahigh current density of $1.84 \times 10^4 \text{ mA/cm}^2$ (FIG. 23F). This is equivalent to the operation of the device at around about $1100 \text{ A/g}_{\text{ICCN/electrode}}$ which is around about three orders of magnitude higher than the normal discharge current densities used for testing traditional supercapacitors. This corresponds to an areal capacitance that varies only slightly from around about 2.32 mF/cm^2 at 16.8 mA/cm^2 to 1.35 mF/cm^2 at $1.84 \times 10^4 \text{ mA/cm}^2$. Moreover, in traditional supercapacitors made of activated carbon, most of the surface area resides in the micropores of the carbon; as such, this is unlikely to contribute significantly to the charge storage, especially at a high rate. This results in a poor frequency response, with the energy stored in these carbon electrode materials released only at slow rate. On the other hand, the ICCN, with its sheet-like structure, possesses a large open surface area that is readily accessible to an electrolyte with a small diffusion barrier. Thus, the ICCN has the potential for making supercapacitors with power densities that surpass any other form of activated carbon. The superior frequency response achieved with ICCN micro-devices is due to the excellent electrolyte access to the surfaces of carbon sheets through its interconnected pores. The micro-scale design of ICCN devices improves the rate capability through the reduction of the ion transport pathways. In addition, ICCN forms a highly conductive network, thus reducing the internal resistance of microelectrodes that make up micro-supercapacitors.

[0122] FIG. 23G is a graph of a complex plane plot of the impedance of an ICCN-MSG(16) with a magnification of a high frequency region shown in an inset. FIG. 23H is a graph of impedance phase angle versus frequency for an ICCN-MSG(16) compared to commercial AC-SC and aluminum electrolytic capacitors. FIG. 23I is a graph showing a relatively high amount of capacitance retention over at least 10,000 charge and discharge cycles. In particular, the graph of FIG. 23I shows only a loss of around about 4% of initial capacitance over 10,000 charge and discharge cycles.

[0123] Flexible electronics have recently attracted much attention because of their potential in providing cost-efficient solutions to large-area applications such as roll-up displays and TVs, e-paper, smart sensors, transparent RFIDs and even wearable electronics. However, the fabrication of micro-supercapacitors on flexible substrates using current micro-fabrication techniques does not appear to be feasible. Attempts to fabricate micro-supercapacitors on flexible substrates using a number of printing and electrochemical techniques have also been reported. However, none of these configurations has been shown to be suitable for flexible

energy-storage devices. In fact, the performance durability of these devices has not been examined under any strain conditions such as bending or twisting. ICCN micro-supercapacitors such as micro-supercapacitor 90 are highly flexible and can be bent and twisted without affecting the structural integrity of the device, FIG. 24A. The durability of ICCN micro-supercapacitors for flexible energy storage has been demonstrated by tests of their electrochemical performance under constant strain. FIG. 24B shows the CV performance of the micro-supercapacitor with different bending and twisting conditions at $1,000 \text{ mV/s}$. The micro-supercapacitor shows exceptional electrochemical stability regardless of the degree of bending or twisting, indicating excellent mechanical stability. The flexibility endurance of the device was tested while keeping the device under the bent or twisted state, as depicted in FIG. 24C. Remarkably, the capacitance was reversibly maintained with 97% retention of the initial capacitance after 2,000 cycles. This superior performance makes ICCN-MSG promising for flexible micro-electronics.

[0124] In general, the total energy that can be stored in a single supercapacitor is too low for most practical applications. Thus, depending on the application, supercapacitors need to be connected together in series and/or parallel combinations, just as batteries are, to form a “bank” with a specific voltage and capacitance rating. The adaptability of ICCN micro-supercapacitors for serial/parallel combinations is demonstrated by connecting four devices together both in series and in parallel configurations, as depicted in FIGS. 24D-24F. The tandem ICCN micro-supercapacitors exhibit a very good control over the operating voltage window and capacity, thus enabling them to be considered for practical applications. Like the individual micro-supercapacitors, the tandem devices exhibit essentially ideal triangular CC curves with a minute voltage drop, which again indicates excellent capacitive properties with minimal internal resistance. It is worth noting that this exceptional performance has been achieved without using a voltage balance, which is often needed with series connections to prevent any cell from going into over-voltage.

[0125] Previous research attempts to design supercapacitors in the all-solid-state form have focused mainly on using aqueous hydrogel-polymer electrolytes. Unfortunately, the operating voltage range of these devices barely exceeds 1 V, making them non-functional for many applications. Unlike water-based electrolytes, ionic liquids (IL) provide an attractive alternative to these conventional electrolytes owing to their wide electrochemical window and high ionic conductivity as well as good thermal stability and non-volatility. These interesting properties of ILs can be hybridized with another solid component (e.g. polymer, silica, etc.) to form gel-like electrolytes called ionogels.

[0126] The combination of a solid matrix with ILs preserves the main properties of ILs, while allowing easy shaping of the device without having the intrinsic leakage problems of liquid electrolytes that limit their flexible operation. Although promising, the integration of ionogels into all-solid-state micro-supercapacitors has not yet been demonstrated. Here, fumed silica (FS) nano-powder was mixed together with the ionic liquid, 1-butyl-3-methylimidazolium bis(trifluoromethylsulfonyl)imide to form a clear viscous (FS-IL) ionogel 142, as depicted in FIG. 25A.

[0127] In an exemplary embodiment, the ionogel is prepared by mixing together a fumed silica nano-powder hav-

ing an average particle size 7 nm with the ionic liquid (1-butyl-3-methylimidazolium bis(trifluoromethylsulfonyl) imide ([BMIM][NTf₂])) (0.03 g FS/1.0 g ([BMIM][NTf₂])). This mixture is then stirred under an Argon atmosphere for 5 hours to produce a clear viscous ionogel (FS-IL). The ionogel is then usable as an electrolyte for the fabrication of all-solid-state micro-supercapacitors that are capable of providing 2.5 V compared with 1 V for traditional hydrogel-polymer electrolytes. Resulting micro-supercapacitors thus have a potential for increased energy density by at least one order of magnitude. The ionogel is integrated into an all-solid-state micro-supercapacitor. Interestingly, the all-solid-state micro-supercapacitor demonstrates ultrahigh charge/discharge rates comparable to those with PVA-H₂SO₄ hydrogel electrolyte. However, as a result of the ionogel electrolyte, the all-solid-state micro-supercapacitor can be operated at a larger potential window of 2.5 V.

[0128] The almost ideal CV profiles and triangular CC curves at ultrafast charge/discharge rates verify good EDLC behavior. The ICCN-MS(16) achieved a stack capacitance of 2.35 F/cm³ at a current density of 16.8 mA/cm³. When operated at an ultrafast charge/discharge current density of 1.84×10⁴ mA/cm³, the capacitance of the device drops only slightly to 1.40 F/cm³. Since the energy density increases with the square of the operating potential window, the micro-supercapacitor employing a FS-IL ionogel promises an order of magnitude higher energy density. Furthermore, the high thermal stability of ionic liquids eliminates the fire hazards associated with commercial supercapacitors. Finally, the micro-supercapacitor shows excellent cycling stability; the capacitance remains unchanged after more than 30,000 charge/discharge cycles.

[0129] Current trends for developing miniaturized electronic devices place emphasis on achieving performance levels generally associated with integrated circuits. FIG. 25B depicts an exemplary on-chip micro-supercapacitor **144** that can be integrated with MEMS devices and CMOS in a single chip using the direct-to-disc labeling technique. A structure made up of a silicon (Si) substrate and a silicon dioxide (SiO₂) insulating layer for the on-chip micro-supercapacitor **144** is schematically illustrated in FIG. 25B; with the ionogel **142** used as the electrolyte. Other devices **146** similar to the micro-supercapacitor **144** were fabricated using the same process described earlier except for the plastic substrate which has been replaced with an oxidized silicon wafer **148**, as depicted in FIG. 25C. FIGS. 26D-26E show that the device reveals superior electrochemical performance with ultrahigh power, comparable to that demonstrated on the flexible substrate. This technique may thus present a low-cost and scalable solution for on-chip self-powered systems.

[0130] Charged supercapacitors, like charged batteries, are in a state of high free energy relative to that of the discharged state, so there is a thermodynamic driving force for them to self-discharge. The self-discharge behavior of supercapacitors is a matter of major practical significance in their operation and the types of function they may be required to fulfill. During self-discharge, a small amount of leakage current will cause the voltage decay of a charged supercapacitor over time. The leakage current can be measured by applying a rated DC voltage to the supercapacitor and measuring the current required to maintain that voltage. Typically, this is done using the voltage at which the supercapacitor is operated, V_{max}. The results are presented

in FIG. 26A which also include the data for two commercially available supercapacitors, all tested under the same dynamic conditions. The results show that the ICCN micro-supercapacitor exhibits an ultra-small leakage current of less than around about 150 nA after 12 hours compared to less than around about 5 pA for both of the commercial supercapacitors. With its low leakage current, ICCN micro-supercapacitors could be integrated with energy harvesters to create efficient self-powered systems.

[0131] The self-discharge curves obtained immediately after pre-charging to V_{max} in the previous test are shown in FIG. 26B. Basically, the voltage difference between the two terminals of the supercapacitor is recorded on open circuit as a function of time. Normally, most supercapacitors are operated in the range of V_{max} to approximately ½ V_{max}. Thus the time required for the voltage across the supercapacitor to change from V_{max} to ½ V_{max} was measured for all of the tested supercapacitors. The results show that the ICCN micro-supercapacitor self-discharges in 13 hours, a value comparable to those of commercial supercapacitors with self-discharge rates of 8 hours and 21 hours. This fine performance for the ICCN micro-supercapacitors shows promise for practical applications.

[0132] FIG. 27 shows a Ragone plot comparing the performance of ICCN micro-supercapacitors with different energy storage devices designed for high-power microelectronics. The Ragone plot shows the volumetric energy density and power density of the stack for all the devices tested. The Ragone plot reveals a significant increase in supercapacitor performance when scaling down the electrode dimensions to the micro-scale. For example, the interdigitated micro-supercapacitors deliver more energy and power than their sandwich counterparts both in the hydrogel-polymer and ionogel electrolytes. Remarkably, compared with the AC supercapacitor, the ICCN micro-device exhibits three times more energy and around about 200 times more power. Furthermore, the ICCN micro-supercapacitors demonstrate power densities comparable to those of the aluminum electrolytic capacitor, while providing more than three orders of magnitude higher energy density. Although Li-ion batteries can provide high energy density, they have limited power performance that is 4 orders of magnitude lower than the ICCN-MS. This superior energy and power performance of the ICCN micro-supercapacitors should enable them to compete with micro-batteries and electrolytic capacitors in a variety of applications. Further miniaturization of the width of the micro-electrodes and the space between them would reduce the ionic diffusion pathway, thus leading to micro-supercapacitors with even higher power density.

[0133] The single-step fabrication technique described here obviates the need for time-consuming and labor-intensive lithography, while enhancing the yield of the process and the functionality of the micro-devices produced. Remarkably, this technique allows for the fabrication of micro-devices without the use of organic binders, conductive additives or polymer separators that are often needed in commercial supercapacitors, thus leading to improved performance because of the ease with which ions can access the active material. The combination of the microscale design of the device with the ICCN whose surface is fully accessible to electrolyte ions is responsible for the high power/energy performance of the ICCN micro-supercapacitors. They combine the power density of electrolytic capacitors with the

energy density of micro-batteries that could have a significant impact on high-power microelectronics. These findings also provide a solution to microscale energy storage in numerous areas where electrolytic capacitors cannot provide sufficient volumetric energy density.

[0134] Furthermore, ICCN micro-supercapacitors show excellent cycling stability. This is relatively important when compared with micro-batteries whose finite life-time could present significant problems when embedded in permanent structures such as biomedical implants, active radio frequency identification (RFID) tags and embedded micro-sensors where no maintenance or replacement is possible. Since these micro-supercapacitors can be directly integrated on-chip, they may help to better extract the energy from solar, mechanical, and thermal sources and thus enable more efficient self-powered systems. They could also be fabricated on the backside of solar cells in both portable devices and rooftop installations, to store power generated during the day for use after sundown and thus may help to provide electricity around the clock where connection to the grid is not possible. Other applications may arise which take advantage of the flexible nature of the substrates, such as electronics embedded into clothing, large-area flexible displays, and roll-up portable displays.

[0135] Note that the electrodes made of ICCNs are fabricated on flexible PET substrates covered with GO which, when laser reduced, serves as both the electrode and the current collector, thus making this particular electrode not only lightweight and flexible, but also inexpensive. In addition, the low oxygen content in ICCNs (~3.5%) as shown through XPS analysis is quite advantageous to the electrochemical activity seen here, since a higher oxygen content at the edge plane sites have been shown to limit and slow down the electron transfer of the ferri-/ferrocyanide redox couple. As such, embodiments of the present disclosure provide methodologies for making highly electroactive electrodes for potential applications in vapor sensing, biosensing, electrocatalysis and energy storage.

[0136] The present disclosure relates to a facile, solid-state and environmentally safe method for generating, patterning, and electronic tuning of graphite-based materials at a low cost. ICCNs are shown to be successfully produced and selectively patterned from the direct laser irradiation of GO films under ambient conditions. Circuits and complex designs are directly patterned on various flexible substrates without masks, templates, post-processing, transferring techniques, or metal catalysts. In addition, by varying the laser intensity and laser irradiation treatments, the electrical properties of ICCNs are precisely tuned over at least five orders of magnitude, a feature that has proven difficult with other methods. This new mode of generating ICCNs provides a new venue for manufacturing all organic based devices such as gas sensors, and other electronics. The relatively inexpensive method for generating ICCNs on thin flexible organic substrates makes it a relatively ideal heterogeneous scaffold for the selective growth of metal nanoparticles. Moreover, the selective growth of metal nanoparticles has the potential in electrocatalysing methanol fuel cells. Further still, films made of ICCNs show exceptional electrochemical activity that surpasses other carbon-based electrodes in the electron charge transfer of ferro-/ferricyanide redox couple. The simultaneous reduction and patterning of GO through the use of an inexpensive laser is a new technique, which offers significant versatility for the fabri-

cation of electronic devices, all organic devices, asymmetric films, microfluidic devices, integrated dielectric layers, batteries, gas sensor, and electronic circuitry.

[0137] In contrast to other lithography techniques, this process uses a low-cost infrared laser in an unmodified, commercially available CD/DVD optical disc drive with LightScribe technology to pattern complex images on GO and has the additional benefit to simultaneously produce the laser converted corrugated carbon network. A LightScribe technology laser is typically operated with a 780 nm wavelength at a power output within a range of around 5 mW to around 350 mW. However, it is to be understood that as long as the carbon-based oxide absorbs within the spectrum of the laser's emission, the process is achievable at any wavelength at a given power output. This method is a simple, single step, low cost, and maskless solid-state approach to generating ICCNs that can be carried out without the necessity of any post-processing treatment on a variety of thin films. Unlike other reduction methods for generating graphite-based materials, this method is a non-chemical route and a relatively simple and environmentally safe process, which is not limited by chemical reducing agents.

[0138] The technique described herein is inexpensive, does not require bulky equipment, displays direct control over film conductivity and image patterning, can be used as a single step for fabricating flexible electronic devices, all without the necessity for sophisticated alignment or producing expensive masks. Additionally, due to the conductive nature of the materials used, it is possible to control the resulting conductivity by simply patterning at different laser intensities and power, a property that has yet to have been shown by other methods. Working circuit boards, electrodes, capacitors, and/or conducting wires are precisely patterned via a computerized program. The technique allows control over a variety of parameters, and therefore provides a venue for simplifying device fabrication and has the potential to be scaled, unlike other techniques that are limited by cost or equipment. This method is applicable to any photothermally active material, which includes but is not limited to GO, conducting polymers, and other photothermally active compounds such as carbon nanotubes.

[0139] As described above, a method has been presented for producing graphite-based materials that is not only facile, inexpensive and versatile, but is a one-step environmentally safe process for reducing and patterning graphite films in the solid state. A simple low energy, inexpensive infrared laser is used as a powerful tool for the effective reduction, subsequent expansion and exfoliation and fine patterning of GO. Aside from the ability to directly pattern and effectively produce large areas of highly reduced laser converted graphite films, this method is applicable to a variety of other thin substrates and has the potential to simplify the manufacturing process of devices made entirely from organic materials. A flexible all organic gas sensor has been fabricated directly by laser patterning of GO deposited on thin flexible PET. An ICCN is also shown to be an effective scaffold for the successful growth and size control of Pt nanoparticles via a simple electrochemical process. Finally, a flexible electrode made of ICCN was fabricated, which displays a textbook-like reversibility with an impressive increase of ~238% in electrochemical activity when compared to graphite towards the electron transfer between the ferri-/ferrocyanide redox couple. This exemplary process has the potential to effectively improve applications that

would benefit from the high electrochemical activity demonstrated here including batteries, sensors and electrocatalysis.

[0140] Those skilled in the art will recognize improvements and modifications to the embodiments of the present disclosure. All such improvements and modifications are considered within the scope of the concepts disclosed herein and the claims that follow.

What is claimed is:

1. An energy storage device comprising: a first electrode; and a second electrode separated from the first electrode by a dielectric, wherein at least one of the first electrode or the second electrode is made of an interconnected corrugated carbon-based network (ICCN) having a plurality of expanded and interconnected carbon layers comprising at least one corrugated carbon sheet that is one atom thick.

2. The energy storage device of claim 1, wherein the first electrode and the second electrode are interdigitated.

3. The energy storage device of claim 2, wherein the interdigitated first electrode and second electrode comprise digits having a width of at least about 330 μm .

4. The energy storage device of claim 2, wherein an interspace distance between the first electrode and the second electrode is less than about 150 μm .

5. The energy storage device of claim 1, wherein both the first electrode and the second electrode are made of the ICCN.

6. The energy storage device of claim 1, wherein the first electrode or the second electrode is made of a metal.

7. The energy storage device of claim 1, having a power density of greater than about 150 W/cm^3 .

8. The energy storage device of claim 1, having a time constant of less than about 20 ms.

9. The energy storage device of claim 1, further comprising an electrolyte disposed between the first electrode and the second electrode.

10. The energy storage device of claim 9, wherein the electrolyte provides a voltage window between a maximum charged voltage and a minimum discharged voltage of about 2.5 V.

11. The energy storage device of claim 9, wherein the electrolyte is an ionogel.

12. The energy storage device of claim 9, wherein the electrolyte comprises fumed silica (FS) nano-powder and an ionic liquid.

13. The energy storage device of claim 12, wherein the ionic liquid comprises 1-butyl-3-methylimidazolium bis(trifluoromethylsulfonyl)imide.

14. The energy storage device of claim 9, wherein the electrolyte is a hydrogel.

15. The energy storage device of claim 14, wherein the hydrogel comprises poly(vinyl alcohol) (PVA)- H_2SO_4 or poly(vinyl alcohol) (PVA)- H_3PO_4 .

16. The energy storage device of claim 1, wherein the plurality of expanded and interconnected carbon layers has an electrical conductivity that is greater than about 1500 S/m.

17. The energy storage device of claim 1, wherein the plurality of expanded and interconnected carbon layers has a surface area that is greater than about 1000 m^2/g .

18. The energy storage device of claim 1, wherein the plurality of expanded and interconnected carbon layers yields an electrical conductivity that is greater than about 1500 S/m and a surface area that is greater than about 1000 m^2/g .

19. The energy storage device of claim 1, wherein the plurality of expanded and interconnected carbon layers has a thickness of about 7 μm to about 8 μm .

20. The energy storage device of claim 1, wherein the plurality of expanded and interconnected carbon layers has a sheet resistance that is tunable within a range of about 20 megaohms per square to about 80 ohms per square.

21. The energy storage device of claim 1, wherein a number of carbon layers in the plurality of expanded and interconnected carbon layers is greater than about 100.

22. The energy storage device of claim 1, wherein the energy storage device comprises a capacitor, a battery, a supercapacitor, an electrochemical capacitor, or an electrochemical double layer capacitor.

* * * * *